JAEA-Conf
2010-005

Proceedings of the 2009 Annual Symposium on Nuclear Data (NDS 2009)

November 26-27, 2009, Ricotti, Tokai, Japan

(Eds.) Hiroyuki KOURA and Satoshi CHIBA

Advanced Science Research Center

December 2010

Japan Atomic Energy Agency

日本原子力研究開発機構

JAEA-Conf

独立行政法人日本原子力研究開発機構　研究技術情報部　研究技術情報課
〒319-1195　茨城県那珂郡東海村白方白根 2 番地 4
電話 029-282-6387, Fax 029-282-5920, E-mail:ird-support@jaea.go.jp

Intellectual Resources Section, Intellectual Resources Department,
Japan Atomic Energy Agency
2-4 Shirakata Shirane, Tokai-mura, Naka-gun, Ibaraki-ken 319-1195 Japan
Tel +81-29-282-6387, Fax +81-29-282-5920, E-mail:ird-support@jaea.go.jp

JAEA-Conf 2010-005

Proceedings of the 2009 Annual Symposium on Nuclear Data (NDS2009)

November 26-27, 2009, Ricotti, Tokai, Japan

(Eds.) Hiroyuki KOURA and Satoshi CHIBA

Advanced Science Research Center
Japan Atomic Energy Agency
Tokai-mura, Naka-gun, Ibaraki-ken

(Received October 22, 2010)

The annual nuclear data symposium, organized by the Nuclear Data Division of Atomic Energy Society of Japan (AESJ) was held at Ricotti, Tokai, on Nov. 26 and 27, 2009 in cooperation with Advanced Science Research Center of JAEA and under financial support from North-Kanto Branch of AESJ. The symposium was devoted for discussions and presentations of research results in wide variety of fields related to nuclear data, including 3 tutorial talks. Talks as well as posters presented at the symposium aroused lively discussions among approximately 90 participants. This report contains 21 papers submitted from the talkers and poster presenters.

Keywords: Proceedings, Annual Nuclear Data Symposium 2009, Nuclear Data, JENDL-4, Radiation Behaviour, Recent Topics

---

Organizers: S. Chiba (JAEA, Chair), Y. Watanabe (Kyushu Univ., Vice-Chair), O. Iwamoto (JAEA) K. Kato (Hokkaido Univ.), H. Koura (JAEA), C. Konno (JAEA), G. Hirano (JAEA), J. Hori (Kyoto Univ.), S. Matsufuji (NIRS), K. Yokoyama (JAEA)

2009年度核データ研究会(NDS2009)報告集

2009年11月26日〜11月27日、テクノ交流館リコッティー、東海村

日本原子力研究開発機構 先端基礎研究センター

(編) 小浦　寛之、千葉　敏

(2010 年 10 月 22 日受理)

2009年度核データ研究会は、2009年11月26日から27日にかけて、東海村のテクノ交流館リコッティーにて開催された。当研究会は日本原子力学会核データ部会の主催、日本原子力研究開発機構先端基礎研究センターの共催、及び日本原子力学会北関東支部の後援の下、核データ分野におけるJENDLを含む幅広い分野についての最新の情報交換と議論の場として多くの研究者の参加を得て行われた。初日に１件、２日目に２件の計３件のチュートリアルも行われた。参加総数は約90名で、盛況のうちに全日程を終えた。本レポートは、同研究会における講演、ポスター発表の報告集である。

原子力科学研究所（駐在）:〒319-1195 茨城県那珂郡東海村白方白根2-4

2009年核データ研究会実行委員会：千葉　敏（委員長、原子力機構)、渡辺　幸信（副委員長、九大)、岩本　修(原子力機構)、加藤　幾芳（北大)、小浦　寛之（原子力機構)、今野　力（原子力機構)、平野　豪（原子力機構)、堀　順一（京大)、松藤　成弘（放医研)、横山　賢治（原子力機構）

Contents

目 次

1. Program of 2009 Symposium on Nuclear Data

November 26, 27, 2009
Techno Plaza Ricotti (Tokai)

Host：Nuclear Data Division, Atomic Energy Society of Japan

Co-host：Japan Atomic Energy Agency

Support：North Kanto Branch of Atomic Energy Society of Japan

Nov. 26（Thur.）

10:45-10:50

1. Opening　M. Igashira（Tokyo Inst. Tech.）

10:50-12: 20

2. Status of Nuclear Data Measurement Activities　【Chair：M. Baba（Tohoku Univ.）】

2.1　Neutron Characterization of J-PARC MLF BL04 for Nuclear Data Measurements [25+5]
Y. Kiyanagi (Hokkaido Univ.)

2.2　Status and Future Perspectives of Nuclear Data Measurements at J-PARC MLF BL04 [25+5]
H. Harada (JAEA)

2.3　High-precision Measurements of Nuclear Data with Beam DT-neutrons[25+5]
I. Murata (Osaka Univ.)

12:20-13:30　Lunch

13:30-16:10

3. Status of Evaluated Nuclear Data Library and Benchmark【Chair：N. Yamano（Tokyo Inst. Tech.）】

3.1 Toward Completion of JENDL-4 [30+10]　K. Shibata (JAEA)

3.2 Status of Nuclear Structure and Decay Data - Their Impact to Decay-heat Calculation [30+10]
T. Yoshida (Tokyo City Univ.)

3.3 Benchmark of JENDL-4 for Fast Reactors[30+10]　K. Sugino (JAEA)

3.4 Benchmark of Nuclear Data for Fusion Applications [30+10]　C. Konno (JAEA)

16:10-16:20　Coffee Break

16:20-17:30

4. Topics 1: Tutorial (1)　【Chair：T. Osawa (Kinki Univ.)】

Potential Energy Surface of Heavy and Super-heavy Nuclei and Fission Dynamics [60+10]
Y. Aritomo (JAEA)

Nov. 27（Fri.）

10:20-12:00

5. Poster Session（Meeting Room 3）

12:00-13:00　Lunch

13:00-14:40

6. Topics 2：Tutorial　(2)　【Chair：T. Ito（NFI）】

6.1 Modern Apoproch to Thermal Neutron Scattering Law [60+10]　Y. Abe (Kyoto Univ.)

6.2 Requests from Backend Fields [25+5]　G. Hirano (Tepco Systems.)

14:40-15:00 Coffee Break

15:00-16:30
7. Panel Discussion on Nuclear Data and Nuclear Computation after JENDL-4/MCNP/MCNPX
 7.1 S. Chiba（JAEA）：Chair
 7.2 O. Iwamoto（JAEA）：Plans for Nuclear Data Evaluation Group
 7.3 Y. Watanabe（Kyushu Univ.）：Comments from Universities
 7.4 Y. Sakamoto（JAEA）：MCNP/MCNPX Problem
 7.5 Y. Nagaya（JAEA）：Toward Unification of JENDL-MVP-PHITS
 7.6 T. Nakata（JNES）：Nuclear Data Research from a Supporting Organization of Nuclear Regulation
 Discussion

16:30-17:00
8. Poster Awards and Closing M. Igashira（Tokyo Inst. Tech.）

Poster Presentations

1. S. Chiba (JAEA) Novel concepts of nuclear transmutation
2. K. Nishio (JAEA) Investigation of fission fragment mass distributions in the reactions involving ^{238}U target nucleus
3. G. Chiba (JAEA) Uncertainty quantification of lumped fission product cross section for fast reactor application
4. Y. Naito (Kyushu U.) Measurement of the spectral neutron flux at the ANITA facility at The Svedberg Laboratory
5. S. Hirayama (Kyushu U.) Production of protons and deuterons from silicon bombarded by 175 MeV quasi mono-energetic neutrons
6. T. Murata Resonance analysis of the ^{7}Li(p, p) reaction to estimate neutron yield by the 7Li (d, n) reaction
7. T. Togashi (Hokkaido U.) Development of Web-based User Interface for Evaluated Covariance Data Files
8. T. Mukai (Osaka U.) Development of CdTe detector for BNCT-SPECT
9. Y. Hirata (RADONET) Analysis of proton-induced reactions by using simulation
10. T. Sanami (KEK) Measurement of fragment production DDX of 72 and 144 MeV ^{12}C beam induced reaction on carbon using Bragg Curve Counter
11. K.Y. Hara (JAEA) Prompt gamma-rays emitted in the ^{74}Ge(n,gamma) ^{75}Ge
12. K. Hidaka (Kyushu U.) Measurement of Neutron Yields for 9 MeV Deuteron Incidence on Cu
13. N. Nishimura (NAOJ) Importance of nuclear data for r-process nucleosynthesis in astrophysics

2. Neutronic Characteristics of the Beam Line BL04 for Nuclear Data Measurements at J-PARC MLF

Yoshiaki KIYANAGI
Division of Quantum Science and Engineering, Graduate School of Engineering, Hokkaido University, Sapporo 060-8628, Japan
e-mail: kiyanagi@qe.eng. hokudai.ac.jp

We have been executing forward a research project on the nuclear data. The major part of this project is measurements of the neutron capture cross sections of MAs and LLFPs at J-PARC. We are now installing a neutron nucleus reaction instrument (NNRI) at the beam line 04 (BL04) at J-PARC. We designed the beam line to obtain the optimal condition for the capture cross section measurements. The neutronic characteristics of the beam line such as energy spectra, beam spot shape, and time structure of the emitted neutrons are very important since it decides the performance of the experiments. We measured the neutron beam characteristics of the beam line and found that they were consistent with those we expected. Measurements on the samples of Cm as MA, and Tc-99 and so on as LLFP are now on progress.

1. Introduction

The nuclear energy is one of the most promising energy resources after the oil shortage and have attracted lots of attention. Advanced reactor systems such as fast breeder reactors and accelerator driven systems, which are candidates for transmutation of long-lived fission products (LLFPs) and minor actinides (MAs) are now under planning, and they will become more important if we consider the increasing use of the nuclear power plants in the future. The amount of LLFP and MA produced in the existing nuclear power plants should be estimated precisely, and for the design of the advanced reactor systems, not only the produced amount but also the transmuted amount are also required to be estimated with high accuracy. Therefore, it is important to obtain accurate nuclear data of LLFPs and MAs for estimating the production and the transmutation rates in the advanced reactor systems.

J-PARC (Japan Proton Accelerator Research Complex) now under construction includes the Materials and Life Science Experimental Facility (MLF) for neutron and muon beam experiments [1]. The neutron source JSNS (Japan Spallation Neutron Source) at MLF is going to be one of the highest intensity pulsed-neutron sources in the world. A high intensity neutron source is indispensable to measure the neutron capture cross sections of LLFPs and MAs, since usually it is very difficult to obtain or handle large amount of samples of LLFPs and MAs due to its availability and high radiation.

In the nuclear data project we are performing in Japan, the first priority is neutron capture cross section measurements of MAs and LLFPs at J-PARC MLF. The samples we are now considering are Cm isotopes as MAs, and Zr-93, Tc-99 and so on as LLFPs. For the measurements, we installed a beam line for the capture cross section measurements (NNRI: Neutron Nucleus Reaction Instrument) at the beam line 04 (BL04) at J-PARC MLF. A Ge spectrometer covering a large solid angle prepared at the other project has been improved as a main detector system. The first beam was supplied successfully in 30 May in 2008.

Here, we explain the neutronic characteristics of the beam line of NNRI to provide fundamental information of this beam line.

2. Structure of the NNRI beam line

A recent photo of J-PARC taken in July of 2009 is shown in Fig. 1[2]. The proton beam from the 3GeV ring is supplied to MLF, which is in the 50 GeV synchrotron ring. A suite of instruments is shown in Fig. 2[3]. The No. 4 instrument is the one we installed and used for the measurements. The BL04 beam line looks at the coupled moderator of JSNS [2-4], which provide the highest intensity at the cold neutron region and a little bit higher intensity or almost the same intensity at higher energy region compared with other two moderators. We had to design the beam line from the moderator to the sample positions. In the measurements of the capture cross sections, we use various sizes of MA and LLFP samples, and use two detector systems, the Ge spectrometer at 21.5m position and NaI spectrometer at 26.5 m position from the moderator. For fulfill these experimental requirements, we decided the number of beams and the beam sizes of the beam spots. The sizes we chose were 3, 7 and 22 mm in diameter at 21.5 m position and also a larger beam size of 40 mm square at 26.5 m. We performed detailed simulation calculations for the design of the beam collimation system in order to minimize the background [5]. The arrangement of the collimators is shown in Fig. 3. There are five collimators to make well defined beam spots and to reduce the neutrons came from the place other than the beam line. As the last collimator a rotary collimator with four beam holes was placed.

Fig. 1 Photo of J-PARC taken in July of 2009

Figure 4 shows the structure of the beam line of the NNRI. Fundamental shields from up-stream are a pre-shield, an upstream shield, a connecting shield, a middle stream shield and down-stream shield, and behind the down-stream shield a beam stopper was placed. The materials for the shield are boric acid resin, iron and concrete. The end position of the beam stopper is about 36m from the moderator. The Ge spectrometer was installed at 21.5m from the moderator, and NaI detector was at 26.5m. The Ge spectrometer is the main detector for the capture cross section measurements and the NaI is complementary one. We are also expecting the experiment at higher energy region for the NaI spectrometer than the Ge spectrometer covers. On the beam line, placed were a T0 chopper, a filter, a disk chopper, and a rotary collimator to adjust the neutron beam in space and also in time.

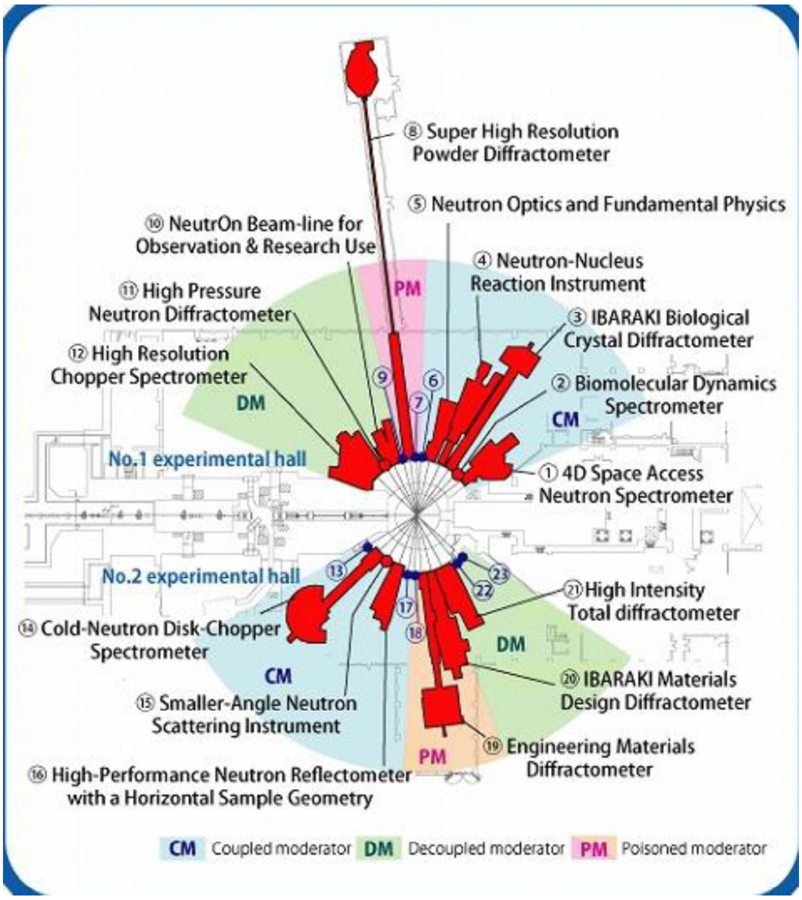

Fig. 2 Layout of the instruments in MLF at J-PARC

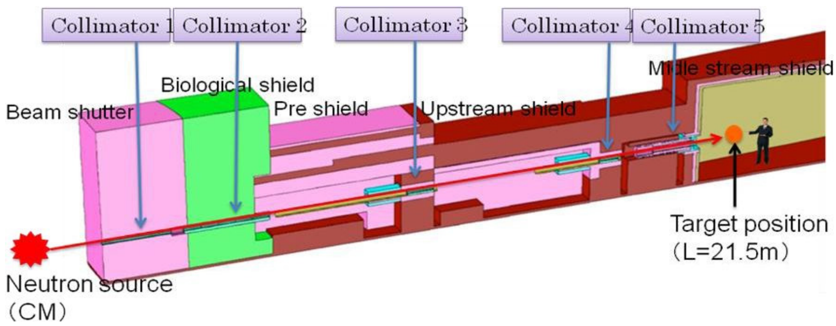

Fig. 3 Arrangement of collimators at NNRI beam line

We have measured the neutronic characteristics through the three kinds of beam sizes by selecting a beam hole in the rotary collimator, which can make a hole with 3mm, 7mm or 22 mm in diameter at the 21.5m target position, namely, the Ge spectrometer position.

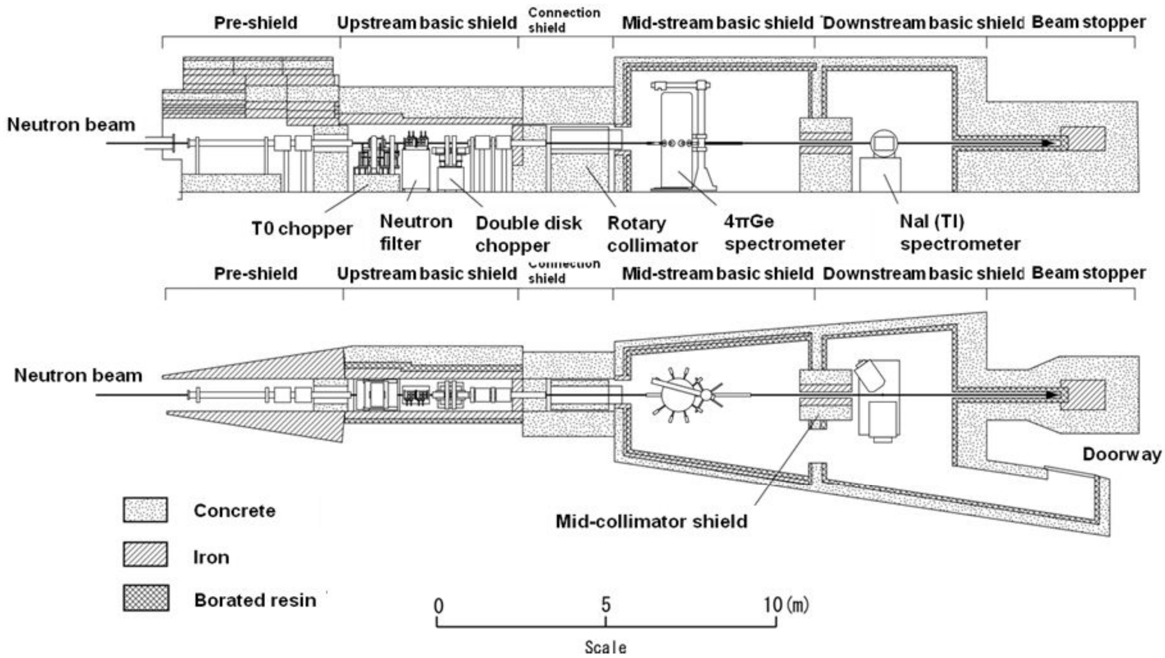

Fig. 4 Beam line structure of NNRI

3. Neutronic characteristics of the NNRI beam line

The energy spectra through the collimators were measured at 21.5m position at the beam power of about 20kW. Figure 5 shows the experimental data as well as a simulation calculation result. The experimental data give a little bit higher intensity above around 1eV, and almost the same intensity around the peak, namely, around the cold neutron region. The estimated intensities are 4.3×10^7 n/cm^2/sec (En<25meV), 9.3×10^5 n/cm^2/sec (1±0.1eV), and 6.3×10^6 n/cm^2/sec (1±0.1keV) at 1 MW. As an example the spatial distribution for the 7 mm beam is shown in Fig. 6. The data were obtained by using a 256ch-pixel type detector which consists of 16x16 Li glass scintillator matrix. The spatial resolution is about 3mm x 3mm. The data are at 10meV, 1eV and 100eV and the observed spatial distributions of the unbra are almost the same as designed ones. Other beam size data were also the same as the designed spatial distributions.

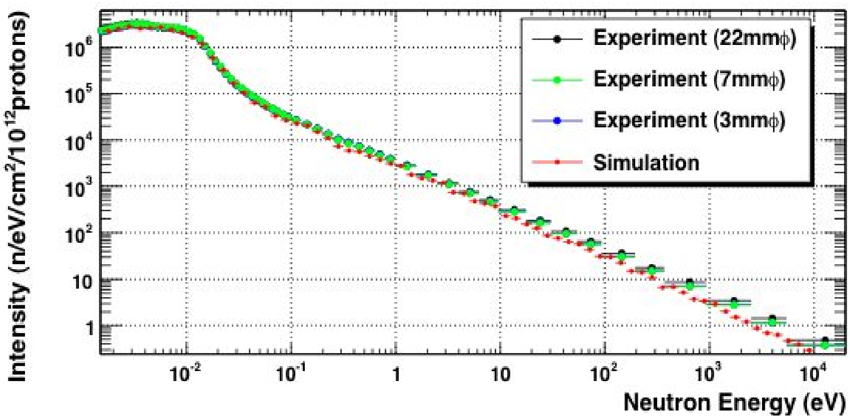

Fig. 5 Energy spectra measured through three beam collimators

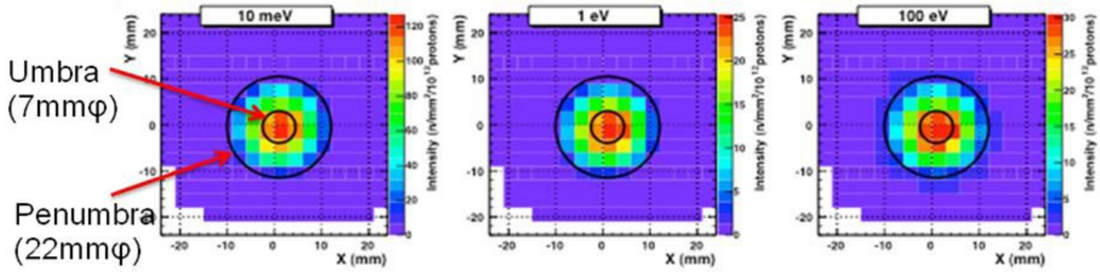

Fig. 6 Spatial distributions of beam spot at 21.5m position trough a 7mm collimator

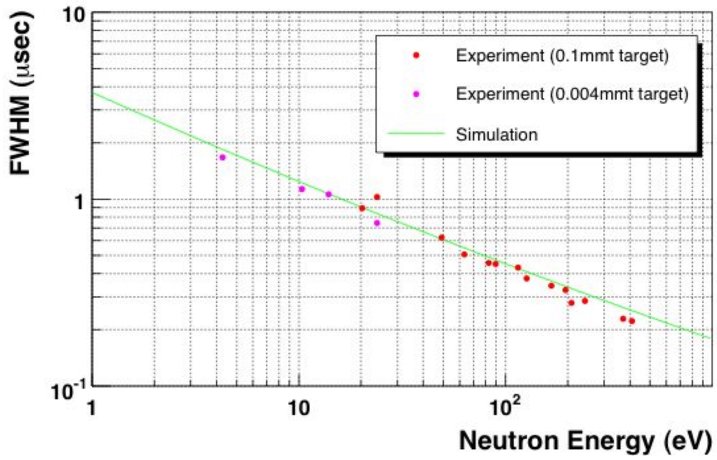

Fig. 7 FWHM of time distributions of neutrons from the moderator

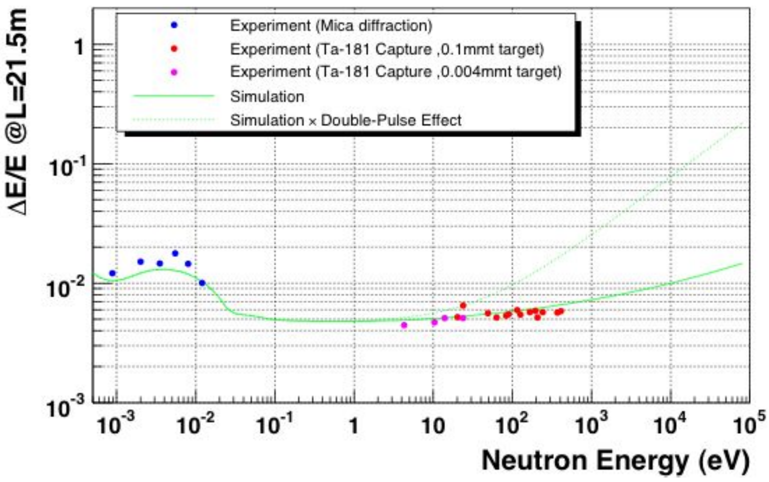

Fig. 8 Energy resolution estimated by FWHMs

We also measured the time distributions emitted from the moderator, which determine the experimental resolution. Figure 7 shows the pulse width of full width at half maximum obtained by analysis of Ta resonance peaks. In this measurement the proton pulse was single bunch. So, even at higher energy region above about 10eV, there is little effect by the proton pulse shape. The simulation result is also shown, and the experimental results and the simulation results show reasonable agreement. Figure 8 shows the energy resolution. The energy resolution is around 0.5 % from 0.02 to 1000eV, and more than 1% around 1-10meV region. The resolution at high energy region above about 10 eV becomes worse if the effect of the double pulse is taken into account. In this estimation we considered the full width of the double bunch but we get the time of flight spectra of the resonance peaks consisting of two pulses due to the double pulse. Therefore, the resolution of the single pulse is not so bad, if we want to get precise cross section data at this energy range it is required to get fine data and also detailed analysis.

4. Summary

The fundamental shields and the beam line collimation system of NNRI have been finished to install, and neutron beam was delivered to NNRI from the end of May 2008. The beam intensity and spatial distribution were almost the same as the design values. The improvement of the Ge spectrometer was completed and the commissioning of the detector systems is in progress. The capture cross section measurements of MAs and LLFPs at J-PARC are being performed.

Acknowledgement

Present study includes the result of “Study on nuclear data by using a high intensity pulsed neutron source for advanced nuclear system” entrusted to Hokkaido University by the Ministry of Education, Culture, Sports, Science and Technology of Japan (MEXT).

The author thanks very much for all collaborators at Hokkaido University, Tokyo Institute of Technology, JAEA and Kyoto University Research Reactor Institute.

References

[1] http://j-parc.jp.

[2] http://j-parc.jp/picture/2009/08/09071607-m.jpg

[3] http://j-parc.jp/MatLife/ja/news/images/080810/080810_riyou05_2.jpg

[4]Y. Kiyanagi, N. Watanabe and H. Iwasa, Nuclear Instrument and Methods in Physics Research, A312, 561-570 (1992).

[5] Y. Kiyanagi, M. Ooi, H. Ogawa and M. Furusaka, J. Neutron Research., 11, 3-11(2003).

[6] N. Watanabe, M. Harada, T. Kai, M. Teshigawara, Y. Ikeda, J. Neutron Research., 11, 13-23(2003).

[7] K. Kino, F. Hiraga, M. Furusaka, Y. Kiyanagi, M. Igashira, M. Mizumoto, T. Katabuchi, Nuclear Technology, Vol., 168, No. 2, pp. 317-321(2009).

3. Status and Future Perspectives of Nuclear Data Measurements at J-PARC MLF BL04

H. HARADA[1*], M. OSHIMA[1], A. KIMURA[1], S. GOKO[1], M. OHTA[1], K. FURUTAKA[1], T. KIN[1], F. KITATANI[1], M. KOIZUMI[1], S. NAKAMURA[1], Y. TOH[1], M. IGASHIRA[2], T. KATABUCHI[2], M. MIZUMOTO[2], Y. KIYANAGI[3], K. KINO[3], M. FURUSAKA[3], F. HIRAGA[3], T. KAMIYAMA[3], J. HORI[4], T. FUJII[4] and K. TAKAMIYA[4]

[1] *Nuclear Science and Engineering Directorate, Japan Atomic Energy Agency, Tokai-mura, Naka-gun, Ibaraki-ken 319-1195, Japan*

[2] *Research Laboratory for Nuclear Reactor, Tokyo Institute of Technology, O-okayama, Meguro-ku, Tokyo 152-8550, Japan*

[3] *Graduate School of Engineering, Hokkaido University, Kita-ku, Sapporo, Hokkaido 060-8628, Japan*

[4] *Research Reactor Institute, Kyoto University, Kumatori-cho, Sennan-gun, Osaka 590-0494, Japan*

*e-mail: harada.hideo@jaea.go.jp

A neutron-nucleus reaction instrument (NNRI) was installed at the J-PARC MLF BL04, which was designed for measuring neutron cross sections with a neutron time-of-flight technique. This includes two kinds of capture gamma-ray spectrometers : a 4π Ge spectrometer and NaI spectrometers. Measurements of neutron capture cross sections for minor actinides and fission products have been started at the NNRI using these spectrometers since 2009. In this paper, preliminary results and future perspectives are discussed.

1. Introduction

Accurate neutron cross sections of minor actinides (MAs) and long-lived fission products (LLFPs) are required for a quantitative study of a nuclear transmutation system or an innovative nuclear fuel cycle system, in which a huge amount of MAs and LLFPs is transmuted or treated [1, 2]. Over the last two decades, various efforts have been done on the measurements of cross sections for MAs and LLFPs in Japan and in the world. Through the experiments, need of high-intensity pulsed-neutron beam facility was recognized for the measurements of nuclear data for radioactive samples. The n_TOF facility at CERN was constructed along this line, where a high-energy proton beam with 9 kW was used to produce neutrons. A series of measurements has been performed since 2001 [3]. They published result of the measurement for the neutron capture cross section of ^{151}Sm (the weight is 200mg and the activity is 200 GBq) with a set of C_6D_6-based liquid scintillation detectors [4]. The 4π array of BaF_2 detectors (DANCE) was installed in a beam line of the Lujan Center at the Los Alamos Neutron Science Center. Proton beam power is about 100 kW. They published results of the measurements for the neutron capture cross sections of ^{237}Np [5] and ^{241}Am [6] in 2008.

The neutron-nucleus reaction instrument (NNRI) was installed at the J-PARC MLF BL04 as shown in **Figure 1**, which was designed for measuring neutron cross sections with a neutron time-of-flight technique. This includes two kinds of capture gamma-ray spectrometers : the 4π Ge spectrometer and the NaI spectrometers. The preliminary measurements have been performed during the commissioning phase since June 2009. The beam power has been increased step-by-step from 4 kW, and reached 120 kW in November 2009. The measurements of neutron capture cross sections for minor actinides and fission products have been performed at the NNRI using these spectrometers since November 2009. In this paper, the preliminary results obtained mainly during the commissioning phase and future perspectives are discussed.

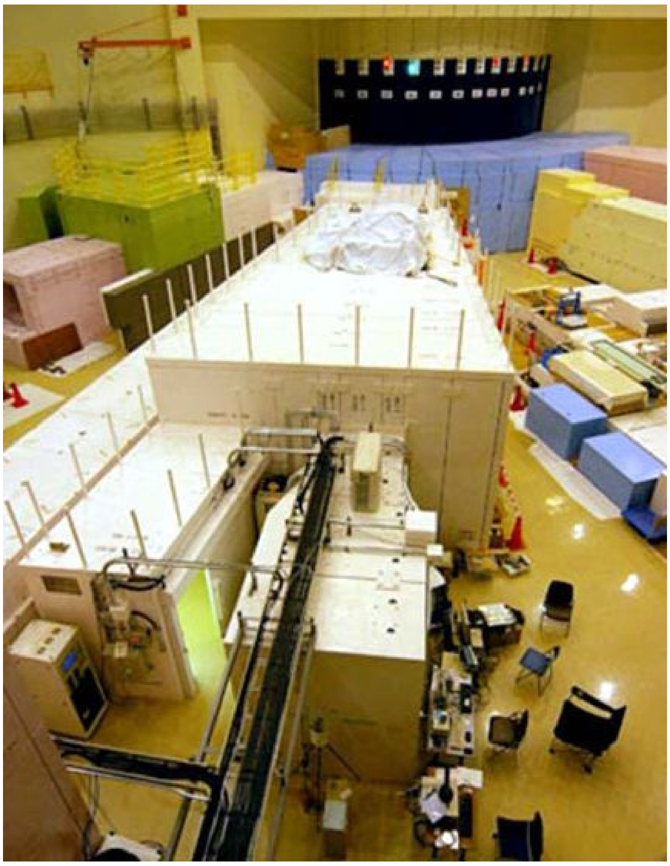

Figure 1. The neutron-nucleus reaction instrument (NNRI) installed at the J-PARC MLF BL04

2. Measurements using Ge detectors

The 4π Ge spectrometer is composed of two cluster Ge detectors and eight coaxial Ge detectors surrownded by BGO anti-coincidence shields [7]. **Figure 2** shows the two cluster Ge detectors with the BGO anti-coincidence shields set in the beam line BL04. The distance between the neutron source and the spectrometer is 21.5 m. A high-performance data aquisition system based on Flash-ADC was developed and utilized [8]. Samples were set in the neutron beam tube. Air in the tube was replaced by He gas during measurements of radioactive samples, since the scattering cross section of ^{4}He is much smaller than that of air mainly composed of ^{14}N and ^{16}O.

The energy dependence of the incident neutron flux was measured using the ^{10}B(n, $\alpha_1\gamma$)^{7}Li reaction. A ^{nat}B sample was set at the sample position in the beam line. By selecting events by gating at γ-ray energy 478 keV produced by the ^{10}B(n, $\alpha_1\gamma$)^{7}Li reaction, a TOF spectrum was deduced with a high S/N ratio. The effectiveness of the neutron flux determination method was reported in ref. [9].

A gold sample (6.2 mg in weight and 6 mm in diameter) was used during the commissioning phase, where the beam power was 20 kW and the repetition rate was 25 Hz. Resolved resonances of ^{197}Au were observed up to keV region. The resonance peaks above about 100 eV were observed as doublet peaks, since the pulse beam was operated under a double-bunch mode (an interval of the double pulse is about 600 nsec). Nevertherless, high-statistical data was obtained during a short measurement period even at the power of 20 kW [7, 8].

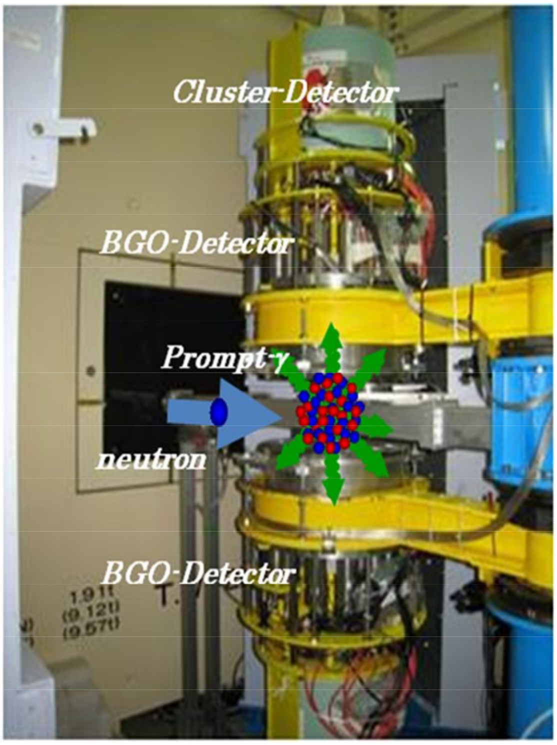

Figure 2 A photograph of the 4π Ge spectrometer

A ^{244}Cm sample (1.8 GBq in activity, CmO_2 in chemical form, 0.6 mg in weight and 5 mm in diameter) encapsulated by an aluminum sample holder was used for the measurement at the beam power 20 kW and 120 kW. The resonance peaks of ^{244}Cm were observed clearly up to about 100 eV. In off-line analyses, a gamma-ray pulse-height spectrum gated at a resonance peak of ^{244}Cm was created. Some discreate γ rays from excited states of ^{245}Cm were assigned in the spectrum. These results demonstrated the effectiveness of the 4π Ge spectrometer for neutron capture study [10].

3. Measurements using NaI detectors

The NaI spectrometers are composed of large NaI crystals (13"Φ×8" and 8"Φ×8") surrownded by NaI anti-coincidence shields [11]. **Figure 3** shows the NaI spectrometers set in the beam line BL04. The distance between the neutron source and the detectors is 26 m. The energy dependence of the incident neutron flux was measured using a C_6D_6 detector and a ^{6}Li glass detector [12]. The NaI spectrometer including a 13"Φ×8" NaI detector was set at 90 degree to the neutron beam direction, and the other at 125 degree. A multi-stop TDC was used as a data aquisition system. A gold sample (0.05 mm in thickness) was used during the commissioning phase, as well as a carbon sample and blank used to evaluate background levels. From the obtained TOF spectrum, the neutron capture cross section are expected to be obtained in the case of gold up to about 100 keV [13].

The data obtained by the NaI spectrometers will be used to cross-check the results deduced by the Ge detectors in the energy range of thermal-keV, and also to deduce the cross sections above keV.

Figure 3 A photo of the NaI spectrometers

4. Conclusions and Future Perspectives

The 4π Ge spectrometer and the NaI spectrometers were set in the NNRI, and measurements of neutron capture cross sections have been started for MAs and LLFPs using an intense pulsed neutron beam. Test experiments during a commissioning phase have shown effectiveness of the installed instruments for measuring neutron capture cross sections. For an example, it was shown that a measurement of a neutron capture cross section for a small sample less than 1 mg (0.6 mg in the case of ^{244}Cm) is possible up to 100 eV - keV region.

In the campaign of 2009 JFY, the neutron capture cross sections are planned to be measured for MAs (^{244}Cm, ^{246}Cm, ^{237}Np, ^{241}Am) and LLFPs (^{99}Tc, ^{129}I, ^{93}Zr, ^{107}Pd) for a neutron energy from thermal to keV region, together with some stable isotopes for estimating backgrounds. Detailed analyses are anticipated to supply accurate neutron capture cross sections of these radioactive nuclei. The results will be presented for each sample in near future [14].

Acknowledgements

Present study includes the result of "Study on nuclear data by using a high intensity pulsed neutron source for advanced nuclear system" entrusted to Hokkaido University by the Ministry of Education, Culture, Sports, Science and Technology of Japan (MEXT).

References

1) OECD/NEA, "Accelerator-driven systems (ADS) and fast reactors (FR) in advanced nuclear fuel cycles, a comparative study," (2002).
2) M. Salvatores, "Nuclear fuel cycle strategies including Partitioning and Transmutation", Nuclear Engineering and Design, **235** [7] 805 (2005).
3) F. Gunsing *et al.*, "Neutron resonance spectroscopy at n_TOF at CERN", Proc. Int. Conf. on Nuclear Data for Science and Technology 2007, Nice, France, p.537 (2008).
4) S. Marrone *et al.*, "Measurement of the ^{151}Sm(n, γ) cross section from 0.6 eV to 1 MeV via the neutron time-of-flight technique at the CERN n_TOF facility", *Phys. Rev.*, **C73**, 034604 (2006).
5) E.-I. Esch, *et al.*, "Measurement of the ^{237}Np(n, γ) cross section from 20 meV to 500 keV with a high efficiency, highly segmented 4π BaF_2 detector", Phys. Rev. **C77**, 034309 (2008).
6) M. Jandel, *et al.*, "Neutron capture cross section of ^{241}Am", Phys. Rev. **C78**, 034609 (2008).
7) T. Kin, *et al.*, "Development of a 4π Germanium Spectrometer for Nuclear Data Measurements at J-PARC", to be published in Conf. Record on 2009 IEEE Nuclear

Science Symposium and Medical Imaging Conference, Florida, USA.

8) A. Kimura, *et al.*, "A Dead-Time Correction Method for Multiple Gamma-ray Detection", to be published in 2009 IEEE Nuclear Science Symposium Conference Records, Florida, USA, October 2009.

9) M. Ohta, *et al.*, "Measurement of Neutron Spectrum at BL04 of J-PARC/MLF", 2009 Fall Meeting of the Atomic Energy Society of Japan, Sendai, September 2009, **J15**.

10) H. Harada, *et al.*, "Measurements of neutron capture cross sections using a 4π Ge spectrometer at the J-PARC/MLF/NNRI", Bulletin of the American Physical Society, vol. **54**, No. 10, p.190, **LC7** (2009).

11) T. Katabuchi, *et al.*, "Neutron capture gamma-ray measurement with NaI(Tl) detector at BL04 of J-PARC/MLF", 2009 Fall Meeting of the Atomic Energy Society of Japan, Sendai, September 2009, **J16**.

12) M. Mizumoto, *et al.*, "The characteristic experiments of neutron flux and neutron and gamma-ray fields with gamma-ray detectors at the BL04 of J-PARC MLF", 2009 Fall Meeting of the Atomic Energy Society of Japan, Sendai, September 2009, **J14**.

13) T. Katabuchi, *et al.*, "Measurements of neutron capture cross sections using a NaI(Tl) detector at the J-PARC MLF neutron nucleus reaction instrument", Bulletin of the American Physical Society, vol. **54**, No. 10, p.190, **LC8** (2009).

14) To be published in 2010 Annual Meeting of the Atomic Energy Society of Japan, and also in Int. Conf. on Nuclear Data for Science and Technology 2010.

4. High-precision Measurements of Nuclear Data with Beam DT-Neutrons

Isao Murata*
Division of Electrical, Electronic and Information Engineering, Osaka University
Yamada-oka 2-1, Suita, Osaka, 565-0871 Japan
*E-mail: murata@eei.eng.osaka-u.ac.jp

For about last 10 years the author's group of Osaka University has carried out development of new experimental techniques to measure high-precision nuclear data for the fusion reactor under the collaboration with the FNS group of JAEA. This could be realized using a pencil-beam DT neutron source implemented in the FNS facility. Up to now the author's group measured charged-particle emission double differential cross sections for beryllium, carbon and fluorine, and lithium under measurement, and angle correlated neutron spectrum of (n,2n) reaction for beryllium and zirconium. In the present report, summarized descriptions of the measuring techniques, measured results and future plans and perspectives are given.

1. Introduction

The authors' group of Osaka University has carried out fusion neutronics studies for more than 20 years. Especially differential and integral experiments regarding fusion(-reactor) related nuclear data have been performed at the Intense 14 MeV Neutron Source Facility (OKTAVIAN) of Osaka University and at the Fusion Neutronics Source (FNS) facility of JAEA partly under the collaboration between Osaka University and JAEA. Those include particle (neutron, charged-particle and gamma-ray) emission double differential cross sections (DDX) measurements, integral experiments with spherical and slab assemblies, tritium production rate (TPR) measurements with a lithium sphere and slab, and so on. The obtained data played an important role in the research field of the fusion related nuclear data. Since 15 years ago, the OKTAVIAN's maintenance budget began to decrease, and we had to move to the FNS facility to continue our fusion neutronics activities.

Surely, it seems or it is sometimes said by the nuclear data community members that fusion related nuclear data were measured almost completely, meaning the measured data covered more-or-less the whole elements, whole energies and angles. However, of course, nuclear data at 14 MeV are the most crucial information for development of the fusion reactor even at the moment. Nuclear data around 14 MeV have been measured with several parties so far, i.e., Tohoku University, Nagoya University, JAEA and so on, as well as Osaka University. However, there still exist elements, the nuclear data of which have not yet been accurately and perfectly measured. Highly accurate data are always very important for a good engineering design. Especially for light elements the data are sometimes obtained partly for energies and angles. Systematical measurements are required for such elements. These data are quite valuable for evaluation of the nuclear data and establishment of the nuclear models for evaluation as well.

In the author's group, taking into account such circumstances, development of new high-precision nuclear data measuring systems started about 10 years ago with a quite unique pencil-beam DT neutron source implemented in the FNS facility of JAEA. This report describes details of the two new reaction cross section measurement techniques established recently by Osaka University group under the collaboration with the FNS group, together with a part of the obtained results for the last few years. Meanwhile more details of the techniques and measured results are found elsewhere[1-6].

2. Pencil-beam DT neutron source

The whole experiments were carried out using a pencil-beam DT neutron source implemented in the FNS facility of JAEA[7]. It should be said that the pencil-beam source could realize the present measurements. This neutron source was developed by making a narrow (2cm ϕ) hole (collimator) through a very thick shield (～2m) positioned between the DT neutron source (2nd target room) and the measuring room (1st target room), as shown in **Fig. 1**. The average neutron flux intensity of ～1×10^6 n/sec/cm^2 was utilized at the exit of the collimator. The neutron flux rapidly decreases as it leaves the beam region. Neutron detectors can therefore be arranged near the beam line without any radiation shield. With the present neutron source, scattering angle-correlated neutron energy spectra of two neutrons emitted by a (n,2n) reaction and spectra of charged particles emitted from a very thin film sample could be measured successfully with a high accuracy as detailed in the following sections.

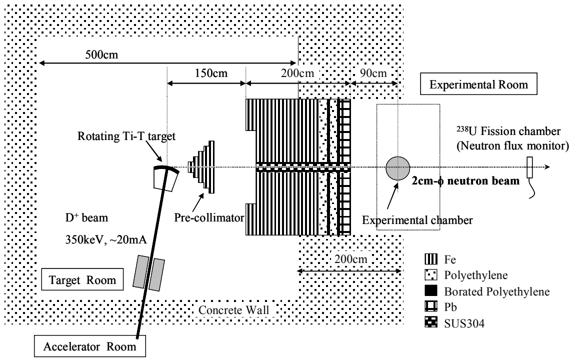

Fig. 1 Schematic description of the pencil-beam DT neutron source.

3. Charged-particle emission DDX[1,2,5]

Charged-particle emission data are quite crucial especially for evaluation of KERMA, DPA, GPA and so on. However, not so many experimental data were obtained so far for light elements. In the present study, we aimed at a system as shown in **Fig. 2** to measure high-precision charged-particle emission double differential cross section (CP-DDX). The system includes a ΔE-E counter telescope with two Si-SSDs which has an ability to distinguish kinds of charged particles. **Figure 3** shows an example of a measured energy deposition spectrum by two SSDs. The main features include a high signal-to-noise(S/N) ratio and excellent energy resolution. These are indebted to use of a pencil beam source, and as a result the SSDs, which are commonly known to be very weak for neutron irradiation, can be placed very close to a sample. Surprisingly, the spectrum in **Fig. 3** is the case of without subtracting the background spectrum. This example is for fluorine which shows several groups of points corresponding to excited states of the residual nuclides made by nuclear reactions. This quite low-level background successfully realizes spectrum measurement of lower energy alpha particles down to about 1 MeV by estimating it from a measured anti-coincidence spectrum by the ΔE detector, which means alphas not passing through the ΔE detector.

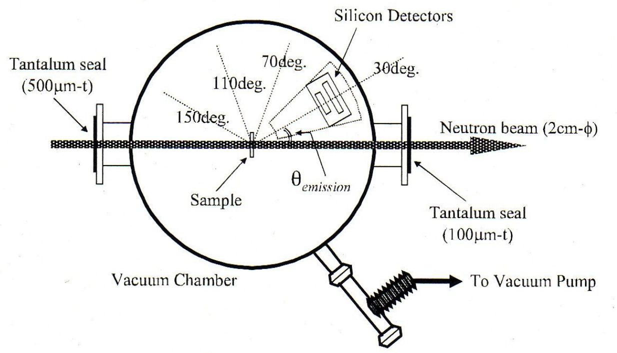

Fig. 2 High-precision CP-DDX measuring system.

Up to now, we have measured CP-DDXs for beryllium, carbon and fluorine. In 2009, preliminary measurement of ^{7}Li has started. Every CP-DDX data have been measured for the first time with the highest accuracy in the world. In this report, measured results of beryllium having a breakup process and of fluorine being a typical light nuclide not having a breakup process are described.

3.1 Beryllium

Figure 4 shows the CP-DDX of beryllium. Measurements were done at 9 angles. In the forward angles, peaks corresponding to the ground and first excited states of residual nuclide, ^{6}He, are clearly seen. It is found that the peak intensity of the ground state varies drastically with increase of the emission angle. **Figure 5** shows the alpha emission ADX. ENDF/B-VI underestimates in the forward angles and JENDL-3.3 underestimates in the backward angles.

Because beryllium decays mostly through a breakup process by nuclear reactions induced by a neutron, there exist various paths (channels) to reach the final state of 2 alphas and 2 neutrons. Kinematics analysis was thus carried out to experimentally determine the branching

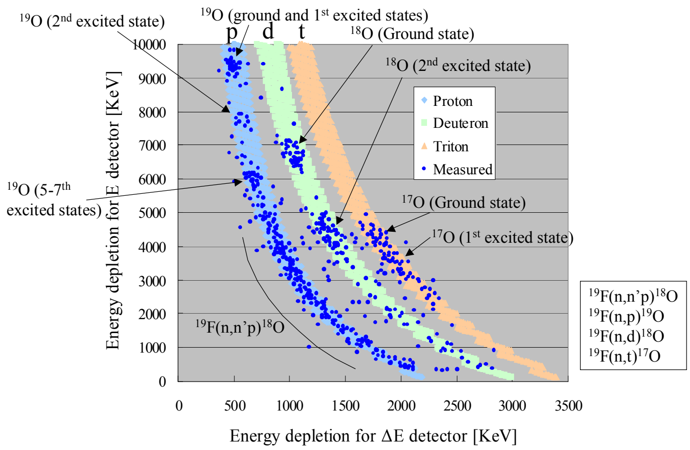

Fig. 3 Measured 2-d energy deposition spectra of ΔE(20 μm)-E detectors for ^{19}F(n,CP) reaction at scattering angle of 30 deg. The sample (CF_2) thickness is 50 μm.

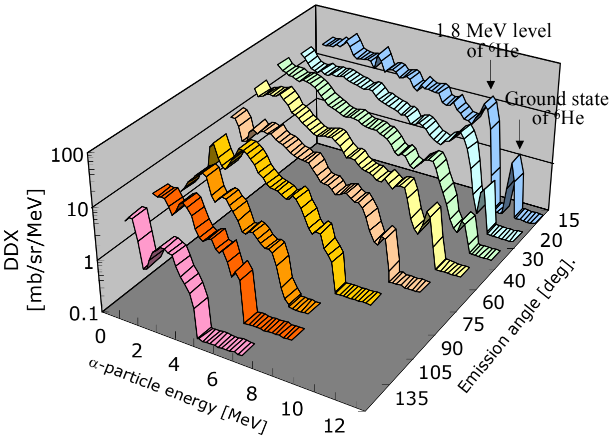

Fig. 4 Measured DDX for ^{9}Be(n,x α) reaction. The sample thickness is 20 μ m.

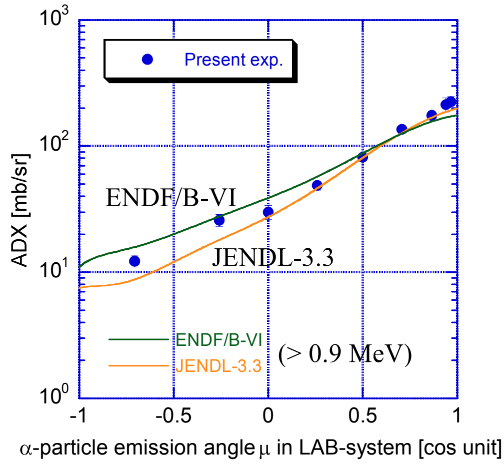

Fig. 5 Measured ADX for ^{9}Be(n,x α) reaction.

ratio of each reaction channel. We took into account the following reaction channels, i.e., decay from ^{9}Be via (n,n') reaction, decay from ^{6}He via (n,alpha) reaction, and 3-body breakups into n, alpha and ^{5}He and n, n and ^{8}Be. After estimating energy distribution of each particle for each reaction channel, the branching ratio of each channel was determined by fitting the previously obtained neutron DDX and the present CP-DDX with the obtained energy distributions of all the reaction channels. **Figure 6** shows the obtained branching ratio, in which it is confirmed that reaction channels via 3-body breakup and (n,alpha) reactions are dominant. Especially contribution via a higher excited state of ^{6}He seems to be quite crucial in this reaction. The TOX is estimated to be 1021 mb through this analysis. The evaluations of JENDL-3.3 (971 mb at 14.2 MeV) and ENDF/B-VII (976 mb at 14.2 MeV) underestimate the present value by several %.

3.2 Fluorine

Fluorine reaction does not include a breakup process. Thus in this study DDXs of p, d, t and alpha particles were measured at the same time. It should be noted that the following results are still preliminary. **Figure 7** shows the proton emission DDX at 30 deg., including (n,p) and (n,np) channels. The agreement is not good for both ENDF/B-VI and JENDL-3.3. In JENDL-3.3 transition to the ground state of ^{19}O is clearly overestimated. **Figure 8** shows an example of alpha particle emission DDX at 30 deg. JENDL-3.3 does not reproduce the experiment at all, and in addition the energy range to be obtained theoretically seems to be not correct. **Figure 9** is the ADX of proton emission. As seen similarly in other particles, consideration of forward orientation is more-or-less insufficient in the evaluations. As for the TOX, discrepancy of JENDL-3.3 to the measured result was quite large, while that of ENDF/B-VI is acceptable. For proton

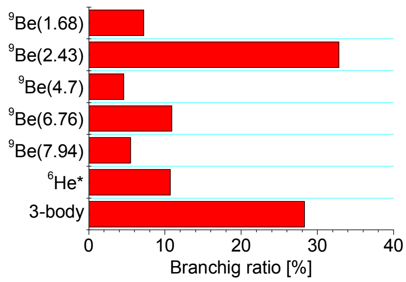

Fig. 6 Obtained branching ratio for ^{9}Be(n,2n+2 α) reaction.

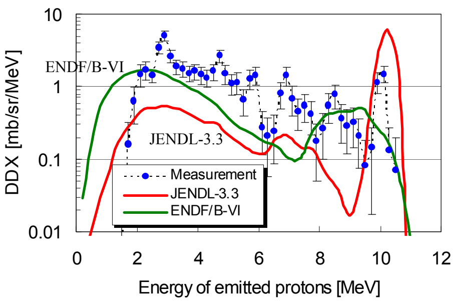

Fig. 7 Proton emission DDX of ^{19}F at 30 deg.

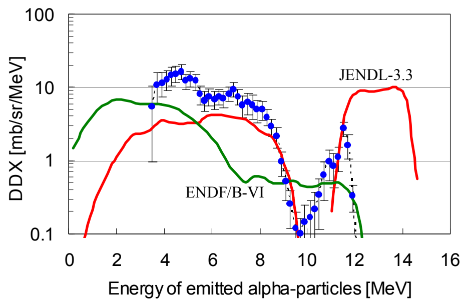

Fig. 8 α emission DDX of ^{19}F at 30 deg.

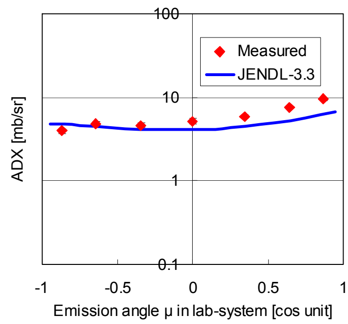

Fig. 9 Proton emission ADX of ^{19}F

emission JENDL-3.3 shows a large underestimation, and it shows overestimation for other particles. Substantial examination is required for the fluorine nuclear data.

4. Angle-correlated emitted-neutron spectrum for (n,2n) reaction[3,4,6)]

There is no doubt that (n,2n) reaction is crucial in a fusion reactor development, because this is a neutron multiplication reaction and has a large cross section value at around 14 MeV. However, the measurement is not straightforward except for use of the foil activation method. Hence, if the activation method is not available, the (n,2n) reaction cross section is not known in principle. This is typically the case that stable isotopes are produced via (n,2n) reaction. In the present study, two neutrons emitted from the (n,2n) reaction are detected by two NE213 detectors in a coincidence mode. **Figure 10** shows the schematic experimental arrangement. With the pencil-beam DT neutron source the two detectors could be arranged very close to the sample without any shields, so that the coincidence detection of the two neutrons is easily realized. However, as a troublesome background, an inter-detector scattering event was found during the developing phase of the present technique. This is a sequential detection of a neutron by the two detectors, which makes a coincident signal. To prevent this as much as possible, a small polyethylene shield is positioned between the two detectors. **Figure 11** shows the raw flight time difference spectrum between the two detectors. The peak observed is the coincidence events of interest.

In the author's group, measurements for beryllium and zirconium have been completed. The results are briefly described in the following sections.

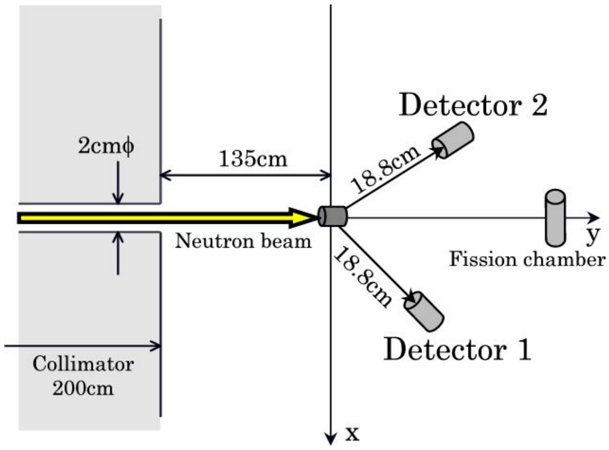

Fig. 10 Schematic experimental arrangement for (n,2n) reaction cross section measurement.

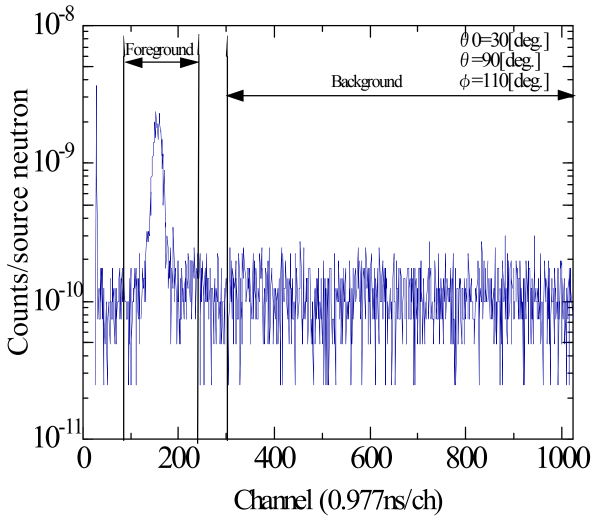

Fig. 11 Typical flight time difference spectrum between the two detectors. A delay is artificially added to one detector to make a peak in the measured spectrum.

4.1 Beryllium

Figure 12 shows the result of beryllium. This is a so-called triple (one-energy and two-angle) differential cross section (TDX), because two detectors are used to take a coincidence signal. Since beryllium is a typical light nuclide having a breakup process as mentioned in Sec. 3.1, the obtained spectrum is expected to have a complicated structure. The measurements were therefore performed at as many angle points (18 in this case) as possible. Definition of angle variables in **Fig. 12** is depicted in **Fig. 13**. In the TDX spectra a peak corresponding to 2.4 MeV level of ^{9}Be is seen. This sort of spectrum was first obtained worldwide. By integrating the TDX in energy and angle, the ADX spectrum is obtained as shown in **Fig. 14**. Agreement of JENDL-3.3 is acceptable. ENDF-B-VI shows underestimation in backward angles. For energies over 1.2 MeV, the TOX is 387±11 mb, which is underestimated by JENDL-3.3 (344 mb) and ENDF/B-VI (340 mb). This result is consistent with the alpha particle DDX measurement in Sec. 3.1.

4.2 Zirconium

Figure 15 shows the TDX of zirconium. It is found that the spectrum is like an evaporation spectrum as expected because zirconium is a medium heavy element, which is expected to show an evaporation spectrum in the neutron DDX (but, exactly speaking, not in the TDX). As pointed out in the previous benchmark experiments, it seemed that the evaluations showed a little overestimation. Especially

ENDF/B-VI showed overestimation in higher energy region, while JENDL-3.2 showed overestimation in lower energy region. To examine these discrepancies a series experiments were carried out with a natural zirconium sample. As a result, comparing the ADX with the evaluation in **Fig. 16** the opposite trend is seen interestingly. To solve this, a spectrum below the lowest measurable energy of 800 keV is estimated by extrapolation with an evaporation spectrum and appropriate nuclear temperature, in order to derive the total cross section of the (n,2n) reaction. From the analysis results with three nuclear temperatures, (1) The nuclear temperature used in ENDF/B-VI, 1.73 MeV, is confirmed to be a little too large, because the fitting is not smoothly carried out. Consequently, the estimated TOX is fairly smaller than the only existing measured data by Frehaut et al.[8] (2) Inversely, in the lower energy region a large peak is made in case of using a lower nuclear temperature of 0.65 MeV adopted in JENDL-3.3. As a result, the TOX is getting larger than Frehaut. And (3) for the nuclear temperature of 1 MeV proposed by the author's group, the agreement with Frehaut is sufficient. Moreover, several causes of the previous discrepancies between experiment and analysis pointed out by Ichihara et al. have been removed by this nuclear temperature. In conclusion, not the absolute value but the spectrum shape depending on the nuclear temperature is quite crucial, and it is suggested that inappropriate nuclear temperatures given in the nuclear data should be examined substantially.

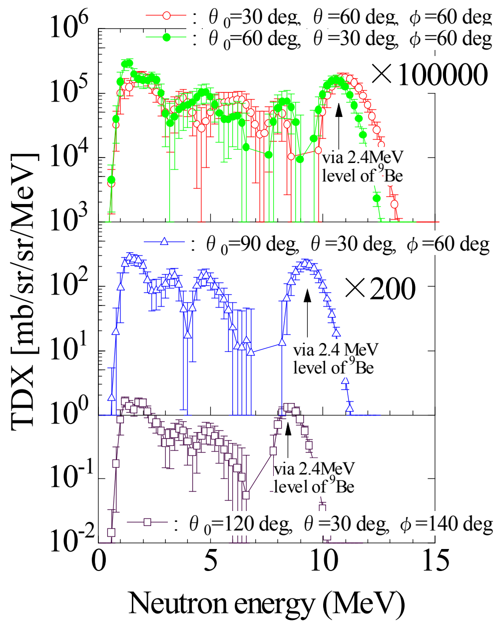

Fig. 12 Triple (one-energy and two -angle) differential cross section (TDX) of neutron emitted via ^{9}Be(n,2n) reaction.

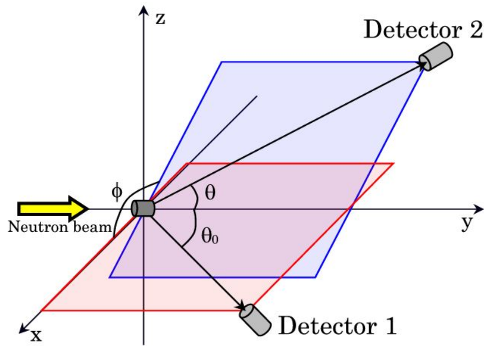

Fig. 13 Definition of angle variables in Fig. 12.

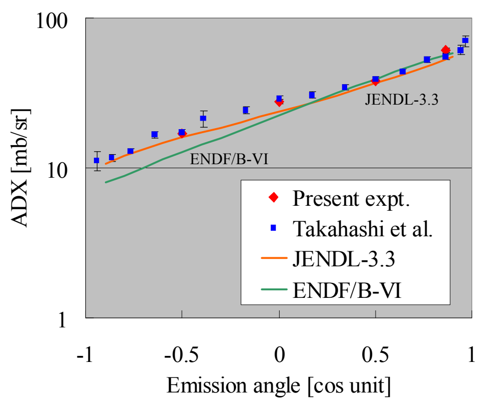

Fig. 14 Neutron emission ADX via ^{9}Be(n,2n) reaction.

5. Conclusion

For about last 10 years the author's group of Osaka University has carried out development of new experimental techniques to measure high-precision nuclear data for the fusion reactor under the collaboration with the FNS group of JAEA. This was realized by using a pencil-beam DT neutron source of the FNS facility. Obtained data so far are quite high-precision data, which would be utilized not only for nuclear data evaluation but also for development of the nuclear model theory. The present techniques are quite suitable for a pencil-beam neutron field formed by using a very strong collimator. Other possibilities should be considered, i.e., reaction cross section measurement with a white pulsed neutron source.

From the next fiscal year, 2010, CP-DDX measurements for lithium and oxygen followed by important fusion reactor materials and (n,2n) reaction cross section measurements for silicon, titanium, tin, tungsten and so on being crucial for the fusion reactor are planned in the framework of the coordination research with JAEA.

Finally, for the nuclear data community especially for the fusion reactor, we think of and are doing at the moment the following activities; (1) Release of the measured data through EXFOR, NDC of JAEA, JCPRG of Hokkaido University and so on., (2) Succession of the measuring techniques, thus, including education of young specialists of nuclear data and enlightening the nuclear data, and (3) Maintenance of neutron source with a sufficient financial support as well as education of accelerator engineers including specialists to treat tritium target and tritium itself.

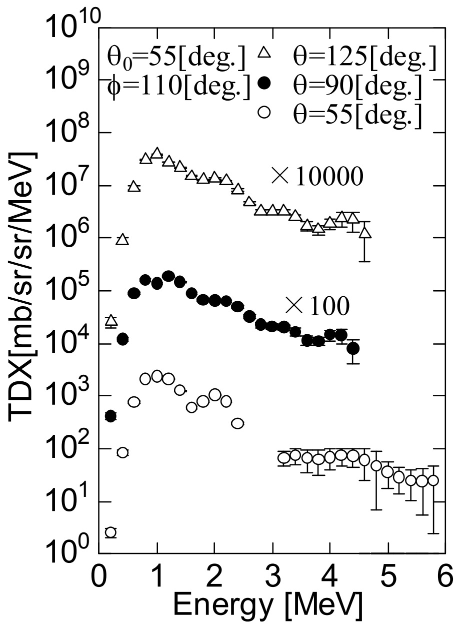

Fig. 15 Triple (one-energy and two -angle) differential cross section (TDX) of neutron emitted via ^{nat}Zr(n,2n) reaction.

Acknowledgement

The author would like to express his sincere appreciation to Dr. Keitaro Kondo for his excellent contribution to the present series study. The CP-DDX experiments and their theoretical studies were carried out by him. The author wishes to acknowledge the FNS staffs of JAEA for their excellent operation of the FNS accelerator.

References

1) K. Kondo, I. Murata et al., “Charged-particle spectrometry using a pencil-beam DT neutron source for double-differential cross section measurement,” *Nucl. Instrum. Meth.*, A568, 723 (2006).

2) K. Kondo, I. Murata et al., “Experimental study on breakup reaction of beryllium and carbon induced with 14-MeV neutrons based on emitted charged-particle measurements,” *Proc. Int. Conf. Nucl. Data on Sci. and Technol.*(ND2007), April 22-27, 2007, Nice, 407 (2008).

3) I. Murata, S. Takaki et al., “Measurement of Angle-correlated Neutron Spectrum for ^{9}Be(n,2n) Reaction with A Pencil-beam DT Neutron Source,” *Proc. Int. Conf. Nucl. Data on Sci. and Technol.*(ND2007), April 22-27, 2007, Nice, 999 (2008).

4) I. Murata, S. Takagi et al., “Angle-Correlated Spectrum Measurement for Two Neutrons Emitted from (n,2n) Reaction with the Coincidence Detection Technique Using A Pencil-Beam DT Neutron Source,” *Nucl. Instrum. Meth. in Phys. Res.* A595, 439 (2008).

5) K. Kondo, I. Murata et al., “Measurement and Analysis of Neutron Induced Alpha-Particle Emission Double-Differential Cross-Section of Carbon at 14.2-MeV,” *J. Nucl. Sci. Technol.*, 45, 103 (2008).

6) I. Murata, K. Shiken et al., “Direct Neutron Spectrum Measurement To Validate ^{nat}Zr(n,2n) Reaction Cross section at 14 MeV,” *Fusion Eng. Des.*, 84, 1376 (2009).

7) H. Sakane, Y. Uno et al., Reactor Dosimetry: Radiation Metrology and Assessment, ASTM-STP-1398, 475 (2001).

8) W. Frehaut et al., “Measurement of (n,2n) and (n,3n) cross sections at incident energies between 8 and 15 MeV,“ *Proc. 5th Int. Sym. on the Interactions of Fast Neutrons with Nuclei,* Nov. 17-21, 1975, Gaussig, GDR, (1976) 17-21. see also EXFOR (http://www.nndc.bnl.gov/exfor/exfor00.htm) to get the latest issue.

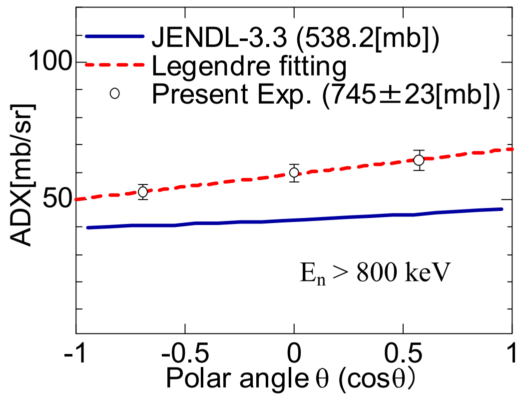

Fig. 16 Neutron emission ADX via ^{nat}Zr(n,2n) reaction.

5. Towards JENDL-4

Keiichi SHIBATA
Nuclear Data Center
Japan Atomic Energy Agency
Tokai-mura, Naka-gun, Ibaraki-ken 319-1195
e-mail: shibata.keiichi@jaea.go.jp

The fourth version of Japanese Evaluated Nuclear Data Library is being developed at the JAEA Nuclear Data Center in cooperation with the Japanese Nuclear Data Committee. After the release of JENDL Actinoid File 2008, we have continued to revise actinide data. The data on fission products have been evaluated. Covariances of actinide cross sections were estimated on the basis of experimental data and nuclear model calculations. The new library JENDL-4.0 will be made available by the end of March 2010.

1. Introduction

We are developing the fourth version of Japanese Evaluated Nuclear Data Library (JENDL-4) in cooperation with the Japanese Nuclear Data Committee. As we mentioned in the previous seminars, much emphasis is placed on the improvements of minor actinide and fission product data in JENDL-4. Therefore, we first developed nuclear model codes, since experimental data are scarce for those nuclei. After the release of JENDL Actinoid File 2008 (JENDL/AC-2008)[1)], we continued to revise actinide data by considering the results of the benchmark analyses[2)]. As for fission products, the data have been evaluated in cooperation with the Japanese Nuclear Data Committee, the members of which are in charge of resolved resonance parameters. The cross sections were updated in the resonance and fast regions for many nuclides. Covariances of actinide cross sections were estimated on the basis of experimental data and nuclear model calculations. This paper deals with the JENDL-4 evaluations and the features of the evaluated data.

2. Actinide Data

We already released JENDL/AC-2008, which contained the evaluated data for 79 nuclides. This file reveals a good performance for the thermal and fast reactor benchmarks. Concerning ^{235}U, the resolved resonance region was modified in order to improve the predicted criticalities of fast neutron cores with U fuels. The capture cross sections of ^{235}U , which are given in the existing major libraries, seem larger than available experimental data at 500 eV – 2 keV. Thus, we changed the upper limit of the resolved resonance region to 500 eV from 2.25 keV, and then reduced the capture cross sections in the energy region concerned. The capture cross section of ^{235}U is illustrated in Fig. 1.

In the fast region, we adopted the calculations using the CCONE code[3]. As an example, the ^{238}U(n,2n) cross section, which was calculated with the code, is shown in Fig. 2.

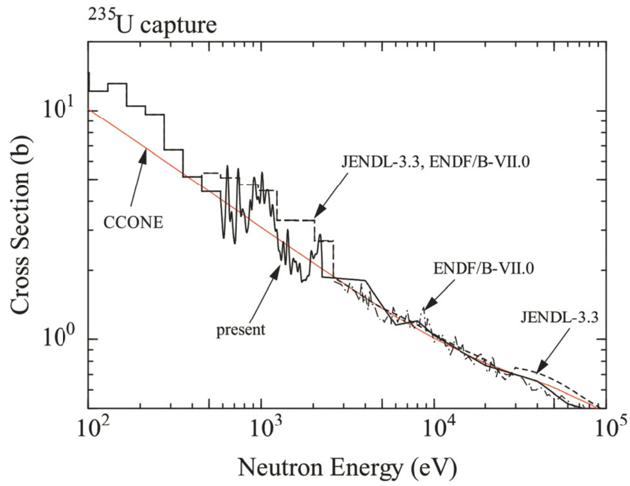

Fig. 1 Capture cross section of ^{235}U.

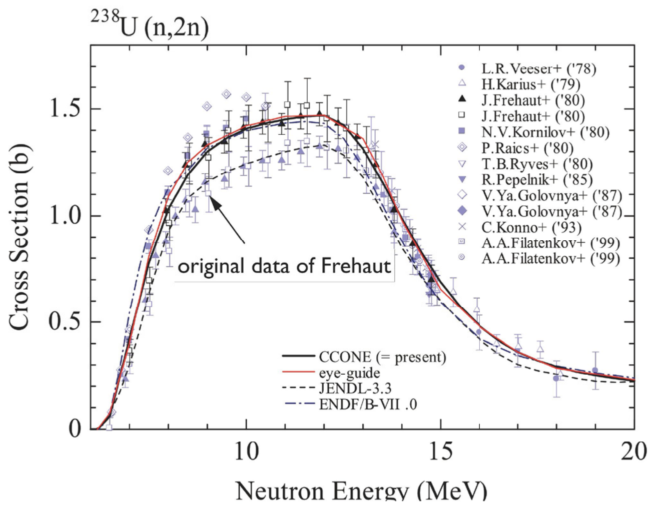

Fig. 2 (n,2n) cross section of ^{238}U.

In the final stage of the compilation for JENDL/AC-2008, small data corrections were made systematically for ^{233,235,238}U, ^{239,240,241}Pu and ^{237}Np by considering the fast-reactor benchmarks. Using the corrected data, the criticalities were well reproduced for not only the referenced reactors but also other ones that were not considered in the data correction. Unfortunately, with this procedure, we are unable to produce the covariances which are strictly consistent with both differential and integral data. The users, who were involved in the fast reactor development, did not prefer to use the JENDL/AC-2008 for the reactor design. We finally gave up the systematic corrections for JENDL-4. Of course, small data correction is required to reproduce highly accurate integral measurements. Alternatively, old-fashioned independent manual correction is being performed for JENDL-4.

3. Fission Product Data

A total of 215 nuclei are categorized as fission products. The resolved resonance parameters were updated or newly evaluated for 123 nuclei by considering the measurements that were made available after JENDL-3.3 had been released.

The smooth cross sections were evaluated using the CCONE[3] and POD[4] statistical model codes for 161 nuclei as of Nov. 24, 2009. We often used the coupled-channel optical model parameters obtained by Kunieda *et al.*[5] for neutrons. For example, Figs. 3 and 4 show the evaluated capture cross sections of ^{76}Se and ^{80}Se, respectively.

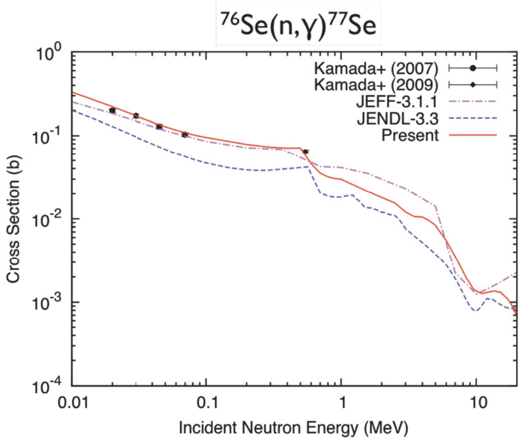

Fig. 3 Capture cross section of ^{76}Se.

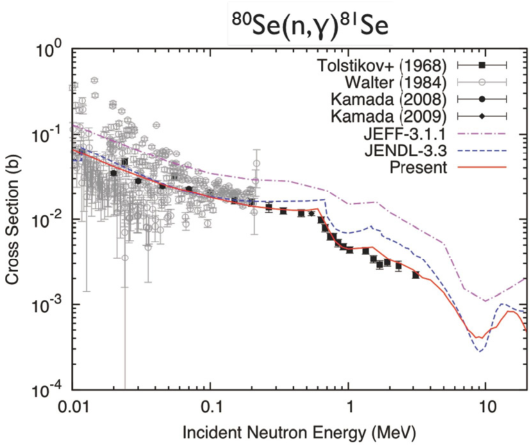

Fig. 4 Capture cross section of ^{80}Se.

One of the issues in the FP mass region is the thermal capture cross section of ^{157}Gd. The use of the new resonance parameters of Leinweber *et al.*[6] leads to about 10 percent reduction of the capture cross section, being better agreement with the benchmarks with Gd_2O_3-UO_2 fuels. However, the same parameters predict higher criticalities for the systems having Gd in water than the JENDL-3.3 data. It was almost impossible to solve the puzzle by changing the resonance parameters. Finally, we added background cross sections to the capture cross sections calculated from the new resonance parameters below 0.1 eV. Addition of background cross sections is not preferable in the modern evaluation. We should return to the resonance parameters sometime later.

4. Data on Other Nuclides

As for light nuclei, we revised the data on $^{1,2}H$, ^{9}Be, ^{10}B, ^{nat}C and ^{16}O. Based on the experimental data of Firestone et al.[7], the thermal capture cross section of ^{nat}C was changed to 3.86 mb from 3.53 mb. This small change influences the calculations for the thermal reactors having a large amount of graphite such as HTTR. Concerning the structural materials, the data on chromium, iron, and copper isotopes were modified. The evaluation of ^{59}Ni was performed for the estimate of helium production for the reactor vessels.

As medium-heavy nuclei, the re-evaluation was done for W and Hf isotopes. The cross sections of $^{181,182}Hf$ were newly evaluated in order to estimate the activation of control rods for BWR. Figure 5 shows the Maxwellian averaged capture cross section of ^{182}Hf. Moreover, we newly evaluated Os isotopes, ^{197}Au and ^{169}Tm. So far, we did not have ^{197}Au in JENDL, although the capture cross section of ^{197}Au is used as standard.

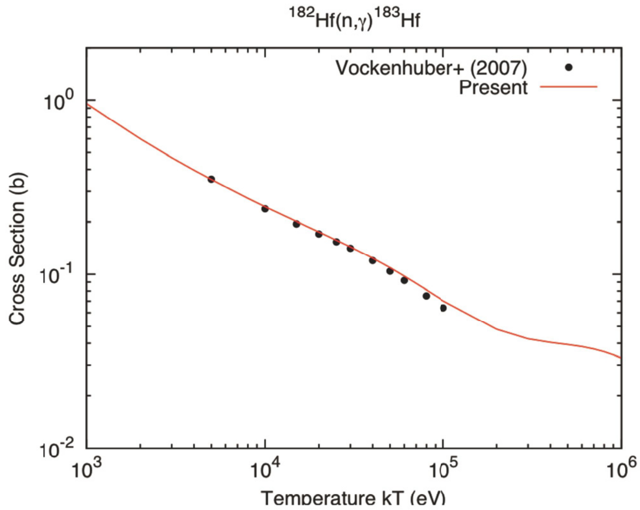

Fig. 5 Maxwellian-averaged capture cross section of ^{182}Hf.

5. Fission Product Yield Data

Fission product yields were taken from ENDF/B-VII.0 with some modifications. We considered ternary fission producing light nuclei from H to Li. The number of FP nuclides coincides with that of JENDL FP Decay Data File 2000[8]. Neutron-induced fission yield data are given for 31 nuclides, while the number of nuclides is 12 in JENDL-3.3. Moreover, the present evaluation includes the data of 9 nuclides for spontaneous fission.

6. Covariances for Actinides

Concerning the resonance parameters, their covariances were taken mainly from the SAMMY analyses on major actinides performed by the ORNL group. Only variances are given for minor actinides by considering the measurements and the parameter uncertainties given in the literature. As for the fission cross sections of major actinides, the covariances were obtained by the simultaneous evaluation[1]. Figure 6 shows the standard deviations thus obtained. For the fission cross sections of other nuclei, the least-squares method was used to estimate covariances for each nuclide. The covariances of the capture cross sections were estimated from the error propagation of the uncertainties in nuclear model parameters by using the CCONE code on the KALMAN system[9].

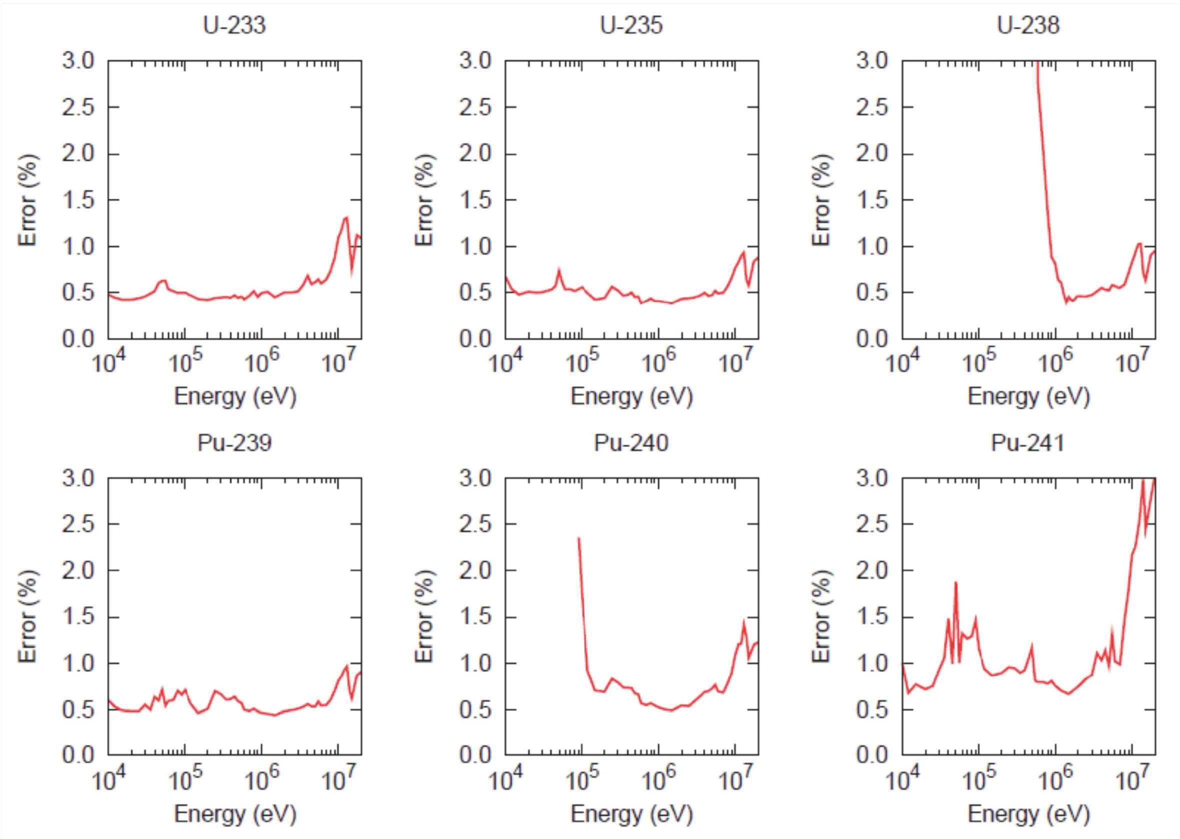

Fig. 6 Relative standard deviation of the fission cross sections.

7. JENDL-4.0 Package and Related Libraries

The package includes the following sub-libraries:

(1) Neutron sub-library including about 390 nuclides,

(2) FP yield sub-library including 31 nuclides for neutron-induced fission and 9 nuclides for spontaneous fission,

(3) Thermal scattering sub-library including 15 materials selected from ENDF/B-VI.8 and ENDF/B-VII.0,

(4) Photo-atomic sub-library including 100 atoms taken from EPDL97[10].

The package does not contain the decay data sub-library. However, the decay data sub-library might be made available at the next release of JENDL-4, namely, the version 4.1.

JAEA should take the responsibility of producing the libraries for reactor and shielding calculations, which include the continuous-energy cross section data for Monte Carlo calculations, multi-group cross sections for thermal and fast reactor calculations, MATXS-format data for shielding calculations, and the library for burn-up calculations. These libraries are expected to disseminate after the release of JENDL-4.0.

8. Conclusions

Evaluation and compilation for JENDL-4 are now in the final stage. The compilation will be certainly finished by the end of March 2010. The library will be released as JENDL-4.0. This project is being carried out in collaboration with many people. We would like to take this opportunity to thank all of them for their work almost on a voluntary basis.

References

1) O. Iwamoto et al.: *J. Nucl. Sci. Technol.*, **46**, 510 (2008).
2) K. Okumura, G. Chiba: Private communication (2009).
3) O. Iwamoto: *J. Nucl. Sci. Technol.*, **44**, 687 (2007).
4) A. Ichihara et al.: JAEA-Data/Code 2007-012 (2007).
5) S. Kunieda *et al.*: *J. Nucl. Sci. Technol.*, **44**, 838 (2007).
6) G. Leinweber *et al.*: *Nucl. Sci. Eng.*, **154**, 261 (2006).
7) R.B. Firestone et al.: Proc. The 2007 International Workshop on Compound-Nucleus Reactions and Related Topics – CNR*2007, Yosemite, Oct 22-26, 2007, 26 (2007).
8) J. Katakura *et al.*: JAERI 1343 (2001).
9) T. Kawano, K. Shibata: JAERI-Data/Code 97-037 (1997) [in Japanese].
10) D.E. Cullen et al.: http://iaea-nds.iaea.org/epdl97/

6. Status of Nuclear Structure and Decay Data – From the View Point of Decay-Heat Calculation –

Tadashi YOSHIDA
Faculty of Engineering, Tokyo City University
Tamazutsumi 1-28-1, Setagaya-ku, Tokyo 158-8557
e-mail: tyoshida@tcu.ac.jp

Abstract

The TAGS measurement seems to have resolved the long-standing pandemonium problem inherent to β-decay of short-lived nuclides. It showed that not a little amount of β-feeding to high-lying unknown levels is left unidentified in the current decay schemes based on the high-resolution γ-ray spectroscopy. The newly found β-feeding to high energy region in the daughter nuclides should not be ignored any longer. It gave rise to, however, new problems. The first one is that the β-feeding rate is given not to individual energy levels but to energy bins with finite width in this method. In other words, the individual energy levels can not be identified. Further, it tells us nothing about the γ-ray cascade which follows the β-feeding. These facts mean that the TAGS results do not help us with constructing the decay schemes such as those given in Nuclear Data Sheets or ENSDF (Evaluated Nuclear Structure Data File). The current JENDL FP Decay Data File gives the β- and the γ-ray energy spectra for all the unstable FP nuclides applying the theoretical calculation where it is needed. If we adopt the E_β and E_γ values from TAGSmeasurements in near future, how we keep the consistency between the energies (E_β and E_γ) and their spectra? This remains as an open question for future revision of the JENDL FP Decay Data File.

1. Introcuction

Summation calculation is a versatile tool to deal with the aggregate behavior of the fission product (FP) nuclides, which are generated and depleted in nuclear fuels not only during the reactor operation but also after the reactor shudown. The FP decay heat is one of the most important quantities obtained from the summation calculation. This method needs an extensive nuclear data library composed of the fission yield, the decay constant, the neutron cross-section and the energies released in the form of the beta-particle (E_β) and the gamma-ray (E_γ) for each FP nuclide. The essential part of this kind of library, which consists of the decay data, is often called the FP decay data file.

2. Brief History

The core-melt accident in the Three Mile Island Nuclear Plant Unit 2 in 1979 spotlighted the importance of the accurate prediction of the FP decay heat and accelerated the efforts for making the extensive FP decay data files using the up-to-date decay schemes at that time in Japan, in the US and in

Europe. By the early 1980s, three major FP decay data files had been completed: these include the JNDC FP Decay Data File Version 0, the decay data file of the ENDF-B/IV and the UKFPDD File. The JNDC FP Decay Data File was the direct ancestor of the extensive FP decay data library elaborated by Tasaka[1], which contained the decay and the yeild data for more than 1000 FP nuclids. All of these new files, generated on the basis of the newest FP decay schemes, were expected to reproduce the results of the sample-irradiation experiments on FP decay heat which had been conducted over the world[2] by that time. The summation calculation using these new decay-data files resulted, however, in a disertrous disagreement with the sample-irradiation results in spite of the strong expectation among the peole involved in these decay-data file projects. Then, it was pointed out[3] that this disagreement was caused by the *pandemonium* effect which had been suggested by a computer simulation by Hardy *et al.*[4]. In the case of the JNDC FP Decay Data File Version 1 released in 1983[5], the pandemonium problem was circumvented by the aid of the nuclear theory, viz, the gross theory of β-decay[6]. The brief history of the decay-heat summation calculations mentioned above is illustrated in the upper part of Fig. 1.

3. Pandemonium Problem

The pandemonium problem is essentially a missing of the β-feeding rate to unknown high-lying levels of the daughter nuclide in the evaluated β- and γ-decay schemes, which are usually constructed not from β-rays itself but from the de-excitation γ-rays immediately following the β-transitions to an excited level. The γ-ray energy and intensity are obtained from the high-resolution γ-ray measurements by using the Ge-detectors. In reality, most of the published β- and γ-decay schemes of short-lives nuclides with high-Q_β values suffer from this troublesome problem. The missing of the β-feeding to unknown high-lying levels inevitably leads to the overestimation of E_β and the underestimation of E_γ. As a result, the γ-ray component of the FP decay heat is underestimated when calculated on the basis of a decay data file suffering from the pandenonium problem. An example is given in the left-hand side of Fig. 2. The FP decay data included in the European JEF-JEFF series of the evalutaed nuclear data are fully based on the published β- and γ-decay schemes derived from the high-resolution experiments when they are available. For the rest, the nuclides without any experimentar information, the 1/3-rule ($E_\beta = Q_\beta/3$, $E_\gamma = Q_\beta/3$) were applied. It is easy to see that inrtoduction of the new decay schemes became available between 1994 ~ 2006 remarkably decreased the γ-ray component of the FP decay heat. This fact indicates that even the modern decay-schemes based on the high resolution method suffer heavily from the pandemonium problem. This decrease (Fig.1; left-side) inevitably accompanies an increase of the β-ray component (right-side). It is worthy to add that the broken curves, viz, the summation calculation results based on the JENDL[7] reproduce the sample-irradiation experiments satisfactorily.

4. TAGS measurement

In the early 1990s, Greenwood et al. started a new type of measurements on the β-decay of short-lived FP nuclides using the total absorption gamma-ray spectrometer (TAGS)[8]. In this series of experiments, the US group measured the β-feeding rate for 45 FP nuclides and 3 meta-stable states as a function of the excitation energy of their daughter nuclides[9]. The introduction of the E_β and E_γ values derived from their β-feeding data remarkablly improved the consistency between the sample-irradiation experiments and the summation calculation based on JEFF-3.1[10]. In the case of JENDL, there left some problem concerning the theoretical correction applied there[10] but this was resolved later[11]. Sonzogni confirmed that the TAGS data leads to improved consistency between the sample-irradiation experiments and the summation calculation and, then, introduced the TAGS E_β and E_γ values to the latest version of ENDF/-B, viz, ENDF/B-VII[12].

These results lead to a very important consequence that the TAGS measurements are free from the pandemonium problem. The US TAGS, however, does not cover evenly both the light and the heavy peaks of FP yields and there left many important FP nuclides to be measured from the view point of the FP decay heat calculations[13]. In this respect, it is very fortunate that a new series of TAGS measurement was initiated by an European group[14] and their measurement was carefully programed based on a close cooperation between the experimenters and the data-users in the framework of the OECD/NEA WPEC[15]. The process of this cooperative work including two IAEA meetings at Vienna and Paris is illustrated in the lower part of Fig. 1. The first results from the Polar Project, so called as the mesaurements are being carried out at University of Jyvaskyla (Finland), was presented at Cologne in 2008[16]. Their results on Tc-104 and -105 applied very well to improve a long-standing discrepancy between the sample-irradiation measurement and the calculation based on JENDL in the cooling-time range from 300-3000 sec after a fission burst[17].

5. Concluding Remarks

The success of the TAGS measurement in resolving the pandemonium problem will make a large impact on evaluation, expression and utilization of the decay data of short-lived nuclides. The newly found β-feeding to unknown high-lying levels in the daughter nuclides should not be ignored any longer. It also, however, gives rise to new problems. The first one is that the β-feeding rate is given not to individual energy levels but to energy bins with finite width in the TAGS data. In other words, the individual energy levels can not be identified by the TAGS measurement. This is because the TAGS is a low resolution detector by the nature. Further, it tells us nothing about the γ-ray cascade which follows the β-feeding. These facts mean that the TAGS results do not help with constructing the decay schemes such as those given in Nuclear Data Sheets or ENSDF (Evaluated Nuclear Structure Data File). JENDL FP Decay Data File gives the β- and γ-ray energy spectra for all the unstable FP nuclides applying the theoretical calculation where it is needed. If we adopt the E_β and E_γ values from TAGS in near future, how do we keep the consistency between the energies (E_β and E_γ) and their spectra? This remains as an open problem for future revision of the JENDL FP Decay Data File.

References

[1] K. Tasaka and N.Sasamoto: Nucl. Sci. and Engn, **54**, 117 (1974)

[2] Summarized by A. Tobias: Progr. Nucl. Energy, **5**, 1 (1980)

[3] T. Yoshida and R. Nakasima: J. Nucl. Sci. and Technol., **18**, 393 (1981)

[4] J.C. Hardy, C. Carrez, B.Jonson and P.G. Hansen: Phy. Lett., **71B**, 307 (1977)

[5] K. Tasaka, H.Ihara, M.Akiyama et al.: *JNDC Nuclear Data Library of Fission Products*, JAERI 1287 (1983)

[6] for example, K. Takahashi, M. Yamada and T. Kondoh: Atom Data and Nucl. Data Tables, **12**, 101 (1973)

[7] J.Katakura, T.Yoshida, K.Oyamatsu and T.Tachibana :*JENDL FP Decay Data File 2000*, JAERI 1343 (2001)

[8] R.C.Greenwood, R.G.Helmer, M.A.Lee et al.: Nucl. Instrum. Methods, **A314**, 514 (1992)

[9] R.C.Greenwood, R.G.Helmer, M.H.Putnam and K.D.Watts: Nucl. Instrum. Methods, **A390**, 95 (1997)

[10] N.Hagura, T.Yoshida and T.Tachibana: J. Nucl. Sci. and Technol., **43**, 497 (2006)

[11] N.Hagura, T.Tachibana and T.Yoshida: J. Nucl. Sci. and Technol., accepted for publication

[12] A.Sonzogni: Nuclear Data Sheets, 107, 3001 (2006)

[13] N.Hagura, PhD Thesis, Musashi Institute of Thchnology (2010)

[14] J.L.Tain: *Beta decay toal absorption measurements for nuclear technology and astrophysics*, Proc. Int. Conf. on Nucl. Data for Sci. and Technol., Nice (2008) pp.43-46

[15] OECD/NEA Working Party on International Evaluation Cooperation, Subgroup 25 with T.Yoshida as coordinator and A.L.Nichols as monitor; http://www.nea.fr/html/science/wpec/index.html

[16] A.Algora, D.Jordan, J.L.Tain et al.:Application of the total absorption technique to improve reactor decay heat calculations, Proc. Int. Symp. on Capture Gamm-ray Spectroscopy and Related Topics, Cologne (2009) pp.207-214

[17] T.Yoshida, Y.Wakasugi and N.Hagura: J. Nucl. Sci. and Technol., **45**, 713 (2008)

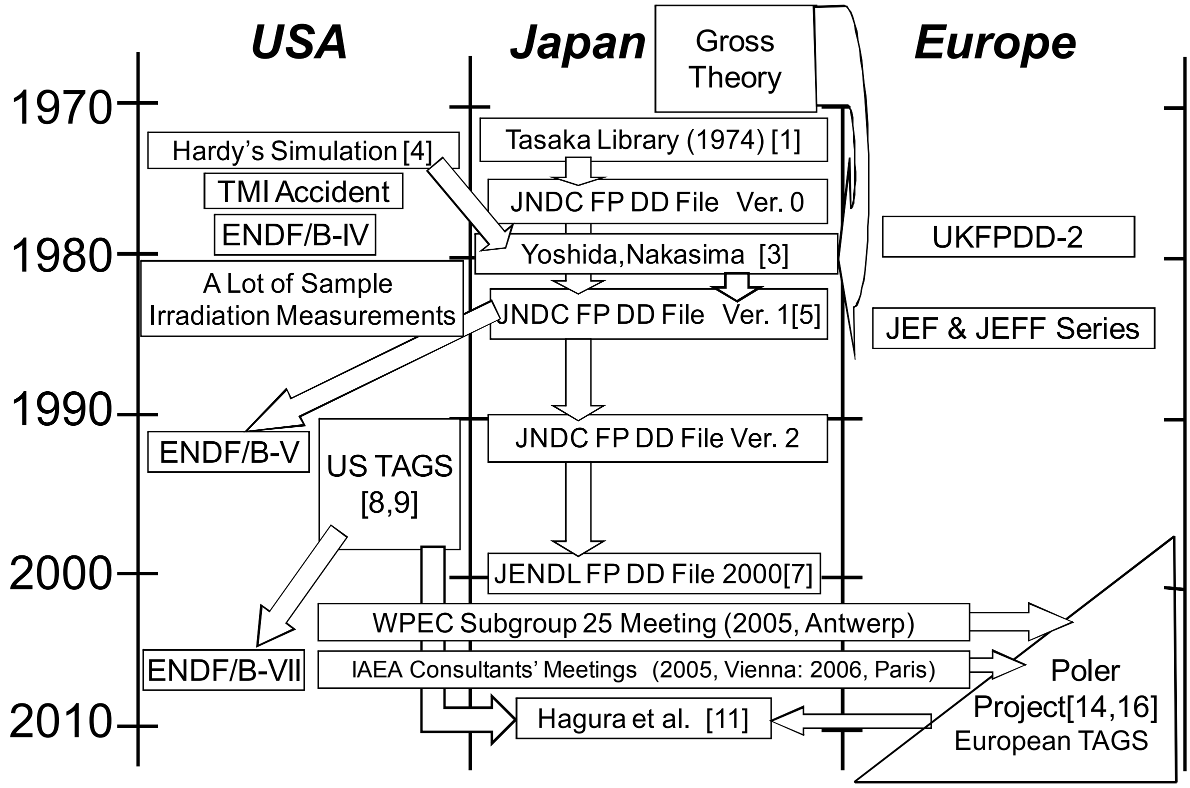

Fig.1 Brief History of Struggle against the Pandenonium Problem

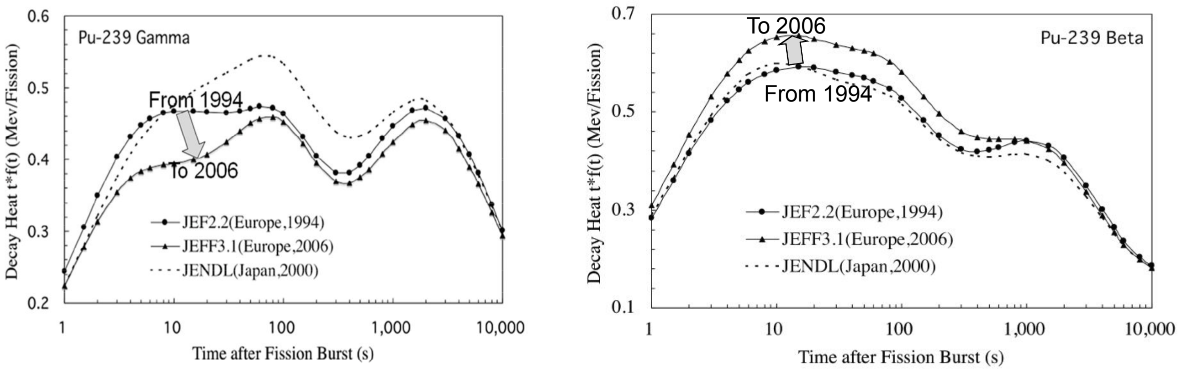

Fig.2 Pandemonium Problem Seen in Summation Calculations using European Decay Data Files (Decay Heat after a Burst Fission in Pu-239)

7. Plan of the JENDL-4 Benchmark for Fast Reactors

Kazuteru SUGINO and Go CHIBA
Nuclear Science and Engineering Directorate, Japan Atomic Energy Agency (JAEA)
2-4 Shirane, Shirakata, Tokai-mura, Naka-gun, Ibaraki 319-1195, Japan
E-mail: sugino.kazuteru@jaea.go.jp

In order to examine the reliability of the JENDL-4 data in application to fast reactor core characteristics analyses, benchmark calculations are planned. As a demonstration test, preliminary benchmark calculations with JENDL/AC-2008 were performed in order to check the effectiveness of some of selected core data in benchmark.

From the preliminary benchmark, it is found that validation of cross sections can be effectively carried out with selected core data.

1. Introduction

Nuclear data is evaluated on the basis of measured cross section data and calculation results based on the nuclear theory. On the other hand, core characteristics and their prediction accuracy strongly depend on the nuclear data used for their analyses. Therefore, it is quite important to reflect the measured core characteristics data to the evaluation of nuclear data. For this purpose, benchmark calculations are planned.

The present paper describes the benchmark items to be used for validation of JENDL-4 in terms of application to fast reactor core analyses. A variety of experiments on critical facilities and reactor physics tests on power reactors are selected to check the performance of JENDL-4 from the viewpoints of the fast reactor core design.

2. Benchmark Items

A variety of critical facilities and power reactors are selected. Their details and selected core characteristics or properties are described in the following.

(1) ZPPR (JUPITER program)

The JUPITER critical experiment was a joint research program between US DOE and PNC (the former of JAEA), using the ZPPR facility at ANL-Idaho (the former of Idaho National Laboratory (INL)) from 1978 to 1988 [1]. The JUPITER experiment is considered as one of the most important data source in

FBR reactor physics study. In JUPITER, experiments on middle-size and large-size cores were performed.

In the benchmark, criticality, control rod worth, reaction rate distribution, reaction rate ratio, Na void reactivity, sample Doppler reactivity and Pu-vector zone substitution reactivity are planned to be analyzed.

(2) FCA

FCA is a fast critical assembly in JAEA to evaluate the core characteristics of various fast reactor cores [2]. Experimental data of FCA is particularly useful for covering the core characteristics of small-sized core.

Criticality and reaction rate ratio on small-size cores with various neutron spectra are planned to be calculated.

(3) ZEBRA (MOZART program)

The MOZART program was carried out by a joint Japanese-UK team using the ZEBRA fast critical facility at the Atomic Energy Establishment, Winfrith, in the UK, between 1971 and 1973 [1]. The program was in support of the design of the Monju sodium cooled plutonium-uranium fueled fast reactor.

Criticality is planned to be analyzed for the benchmark.

(4) BFS

A series of critical experiments was performed by using the BFS-2 facility in a collaboration work between JNC (the former of JAEA) and the Institute of Physics and Power Engineering (IPPE) of Russia to dispose Russian surplus weapons plutonium, focusing on the effect of the introduction of uranium-plutonium mixed-dioxide fuel and stainless steel reflector into the current BN-600 core that is comprised of UO_2 fuel and blanket [3].

Criticality, control rod worth, reaction rate distribution and Na void reactivity are selected for the benchmark.

(5) MASURCA (CIRANO Program)

The French CIRANO experiments provide an integral database for plutonium burning fast reactor physics [4]. In the CIRANO experiment, fuel with considerable ratio of high-order Pu was loaded in the core.

A series of fuel substitution reactivity measurements parameterized by plutonium isotopic vector and enrichment is planned to be analyzed.

(6) LANL Small Cores

Experiments with small cores were performed in 1950s in Los Alamos National Laboratory, USA [5]. The sphere-shaped metallic fuel was composed with ^{239}Pu, or ^{240}Pu-riched plutonium, or ^{233}U or

^{235}U-riched uranium with diameters of about 10cm.

Criticality and reaction rate ratio are planned to be calculated for each core.

(7) Joyo

Joyo is the experimental FBR in JAEA which started its operation in 1977 [1]. Since Joyo is a power reactor, it has some special features differed from critical experiments, such as the ability of burnup characteristics measurement and the double heterogeneity configuration with fuel pins and wrapper tube. In addition, ^{241}Am, ^{243}Am and ^{244}Cm (MA) samples encapsulated in a small vanadium capsule were irradiated in Joyo MK-II for 275 effective full power days by the neutron fluence of 8×10^{22} n/cm^2 [6]. After dissolution of these samples, Am, Cm, and Pu were chemically separated and the isotopic composition was determined by alpha and gamma-ray spectrometries and mass spectroscopy. By calculating the irradiated sample composition data, capture cross sections of ^{238}Pu, ^{241,243}Am, and ^{242,244,245,246}Cm can be effectively validated.

For the benchmark, criticality, burnup reactivity coefficient and irradiated MA sample compositions are planned to be analyzed.

(8) SEFOR

SEFOR (South-West Experimental Fast Oxide Reactor) is a fast reactor fueled with mixed PuO_2-UO_2 and cooled with sodium. The experimental program was conducted by the American General Electric Company (GE) and the West German Karlsruhe Laboratory (KfK) (the former of Forschungszentrum Karlsruhe (FZK)) from 1969 to 1972. The SEFOR Doppler experiments have unique and valuable features of measuring whole core Doppler reactivity induced in various situations, such as steady-state at power levels up to 20MW (isothermal temperature coefficient) and prompt critical transients (power coefficient) [7].

Power coefficient is planned to be analyzed with higher priority than isothermal temperature coefficient because of its little core expansion component.

(9) Monju

Monju is the proto-type fast reactor in JAEA. Initial criticality was achieved in April of 1994 and the first start-up core was assembled in May of 1994. A series of reactor physics parameters on the initial core was measured by November of 1994 as a part of the system start-up tests [8].

Criticality and control rod worth are planned to be calculated for the benchmark.

(10) PFR

Actinide samples were irradiated in the 600-MW Dounreay Prototype Fast Reactor (PFR) in the UK under a cooperative agreement between the US and the UK [9]. Small amounts of enriched isotopes of U, Np, Pu, Am, Cm, and so on were encapsulated and assembled in the fuel pin. The fuel pin was irradiated for 492 effective full power days by the neutron fluence of 2×10^{23} n/cm^2. Under the Japan/U.S. Actinides Program, portions of the dissolved samples were transferred to JAERI (the former of JAEA) to determine the compositions of the irradiated samples with radiochemical analyses. By evaluating the irradiated sample composition data, capture cross sections of ^{233,234,236}U, ^{237}Np, ^{238,242}Pu, ^{241,243}Am, ^{242,244,245,246,247,248}Cm, ^{249}Bk, and ^{250,251}Cf can be validated.

For the benchmark, irradiated MA samples compositions are planned to be calculated.

3. Preliminary Benchmark Calculation

As a demonstration of effectiveness of selected cores in benchmark, preliminary benchmark calculations on criticality and MA sample irradiation tests were carried out with JENDL Actinoid File 2008 (JENDL/AC-2008) [10].

Figure 1 presents the calculation to experiment (C/E) values on criticality for various cores. Significant improvement is observed by replacing JENDL-3.3 with JENDL/AC-2008 as not only systematic underestimation but also dependency on core types is considerably eliminated. Thus, reliability of JENDL/AC-2008 for criticality analysis was confirmed by selecting a variety of core types (Cell structure, Fuel composition, and so on).

Figure 2 shows the C/E values on composition ratios of ^{241}Am and ^{243}Am samples irradiated in Joyo MK-II. Results with sensitivity to the capture cross sections of ^{241}Am and ^{243}Am are satisfactory for both JENDL-3.3 and JENDL/AC-2008. Concerning the capture cross sections of ^{242}Cm and ^{244}Cm, considerable improvement is observed for JENDL/AC-2008. Thus, MA cross sections in JENDL/AC-2008 were validated by utilizing the MA sample irradiation tests data.

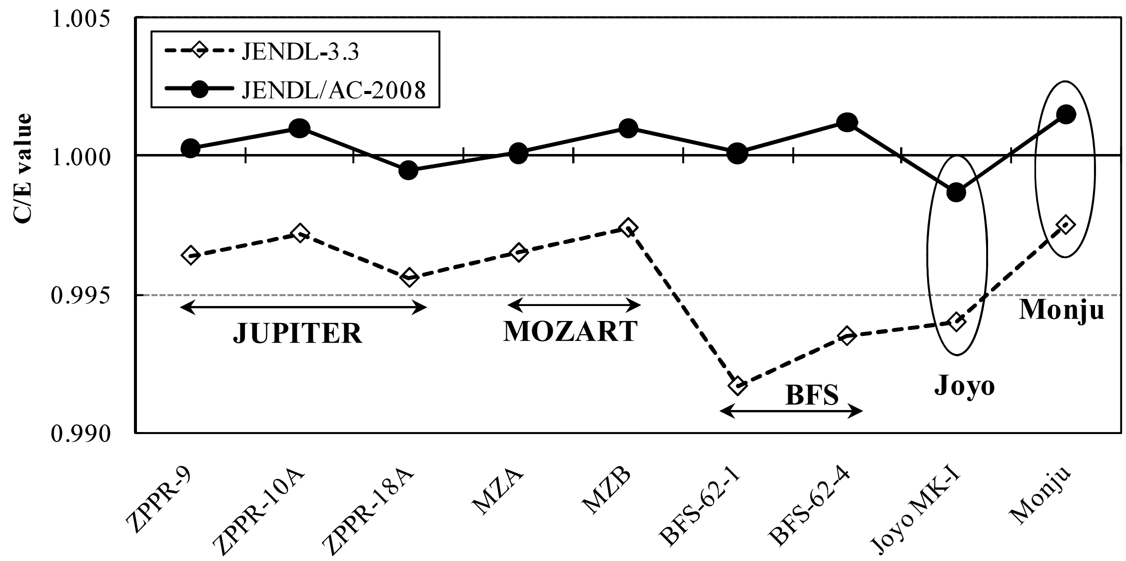

Fig.1 Results on criticality

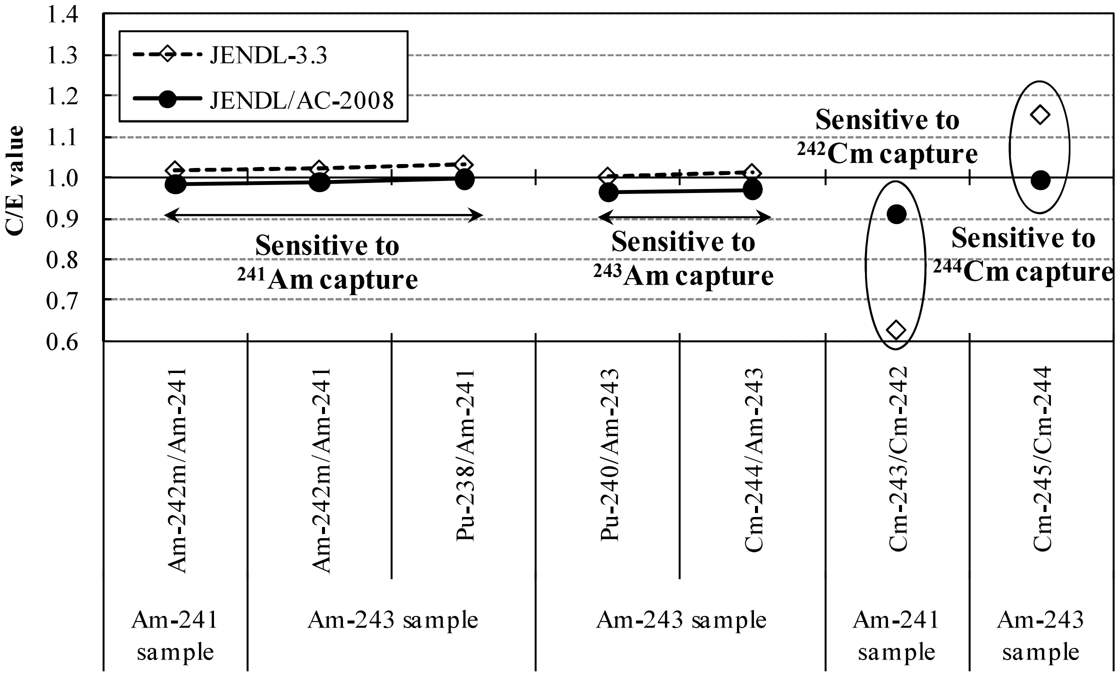

Fig.2 Results on composition ratios of MA samples irradiated in Joyo MK-II

4. Conclusion

In order to examine the applicability of the JENDL-4 data for fast reactor core characteristics analyses, benchmark calculations are planned.

Prior to the benchmark tests for JENDL-4, preliminary benchmark calculations with JENDL/AC-2008 cross section data were performed in order to check the effectiveness of some of selected core data in benchmark. From the preliminary benchmark, it is found that validation of major nuclide (U, Pu, Fe, Na, and so on) cross sections can be effectively carried out. In addition, minor actinide (MA) cross section data can be validated by evaluating MA sample irradiation tests on power reactors.

To improve the quality of benchmark and demonstrate the reliability of JENDL-4, more variety of experiments on critical facilities and reactor physics tests on power reactors are selected. By utilizing these critical experiments and reactor physics tests, the reliability of JENDL-4 will highly be reinforced.

It is desired that the present benchmark work will be of great use for gathering world-wide interests to JENDL-4.

References

[1] NEA Nuclear Science Committee, "International Handbook of Evaluated Reactor Physics Benchmark Experiments," *NEA/NSC/DOC(2006)1.*

[2] M. Andoh, S. Iijima, et al., "Benchmark Experiments of MOX Fueled LMFBR Using FCA-XVII-1 Core," *JAEA-Data/Code 2006-006* (2006).

[3] T. Hazama, A. Shono, et al., "Verification of a Nuclear Analysis System for Fast Reactors using BFS-62

Critical Experiment," *J. Nucl. Sci. Eng.*, Vol. 41, No. 12, pp.1145-1154 (2004).

[4] S. Ohki and T. Iwai, "Analysis of the CIRANO Experiment for Plutonium Burning Fast Reactor using JNS's Calculation Scheme," *J. Nucl. Sci. Eng.*, Supplement 2, p.888-891 (2002).

[5] NEA Nuclear Science Committee, "International Handbook of Evaluated Criticality Safety Benchmark Experiments," *NEA/NSC/DOC(95)03*.

[6] K. Sugino, "Improvement on the Prediction Accuracy of Transmutation Properties for Fast Reactor Core Using the Minor Actinides Irradiation Test Data on the JOYO MK-II Core," *Proc. of International Conference on the Advanced Nuclear Fuel Cycles and Systems GLOBAL2007*, Boise, ID (2007).

[7] T. Hazama and J. Tommasi, "Re-Evaluation of SEFOR Doppler Experiments and Analyses with JNC and ERANOS system," *Proc. of International Conference on the Physics of Fuel Cycles and Advanced Nuclear Systems: Global Developments PHYSOR 2004*, Lagrange Park, IL (2004).

[8] K. Sugino and T. Iwai, "MONJU Experimental Data Analysis and its Feasibility Evaluation to Build up the Standard Data Base for Large FBR Nuclear Core Design," *Proc. of ANS Topical Meeting on Reactor Physics PHYSOR 2006*, Vancouver, BC, Canada (2006).

[9] K. Tsujimoto, N. Kohno, et al., "Validation of Minor Actinide Cross Sections by Studying Samples Irradiated for 492 Days at the Dounreay Prototype Fast Reactor-II: Burnup Calculations," *Nucl. Sci. Eng.* 144, pp129-141 (2003).

[10] O. Iwamoto, T. Nakagawa, et al., "JENDL Actinoid File 2008," *J. Nucl. Sci. Eng.*, Vol. 46, No. 5, pp.510-528 (2009).

8. Novel Concept of Nuclear Transmutation

Satoshi Chiba and Futoshi Minato
Japan Atomic Energy Agency
Tokai, Naka, Ibaraki 319-1195, Japan
e-mail : chiba.satoshi@jaea.go.jp

A new concept of nuclear transmutation by using fission of heavy Λ hypernuclei is proposed. Other possibility of using K^- induced reactions for application purposes such as detection of nuclear matter inside materials is also proposed.

1. Introduction

Recently, Minato et al. have shown via a constrained-Skyrme-Hartree-Fock-BCS calculation that the Λ-particle dominantly sticks to heavier fragments if heavy nuclei containing Λ-particle in the s-state make fission[1], as shown in Fig. 1. This is due to the reason that the attractive nuclear force that a Λ feels is stronger in the heavier fragments than in the lighter ones. The phenomena predicted by them imply that there is a possibility to generate many kinds of neutron-rich hypernuclei as the Λ-hyper-fission-fragments as shown in Fig. 2, which shows a contour plot of fission fragment distribution for the case of thermal neutron induced fission of ^{235}U.

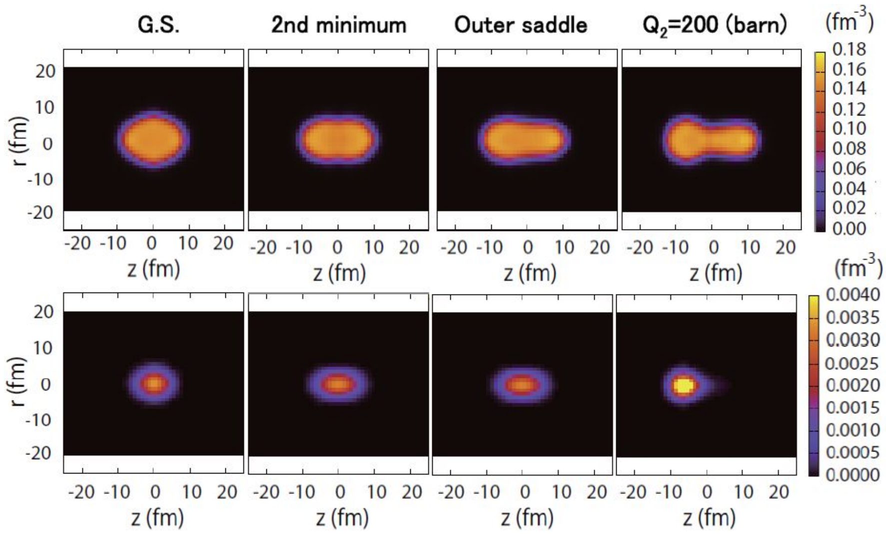

Fig. 1 Change of density distributions of nucleon (above panels) and Λ-particle (lower panels) of $^{237}{}_{\Lambda}U$ during modification of nuclear shape toward fission, starting from the ground state (leftmost panels), at the 2nd minimum, at the outer saddle and at the quadrupole moment (Q_2) of 200 barn (rightmost panels). At Q_2=200 barn, the Λ-particle density is localized to the heavier fragment.

2. New concept of nuclear transmutation

Fission of heavy Λ hypernuclei will open a new possibility for nuclear transmutation as well. Namely, fission of heavy hyper nuclei produced by absorption of stopped K^- can be utilized in the following way: 1) the K^- will be absorbed by nucleon (N) via $K^- + N \rightarrow \Lambda + \pi$ reaction which generate excitation energy of about 160 MeV , 2) the Λ-particle makes a transition to the lowest s-state, 3) heavy nuclei will make fission by the excitation brought by the Λ production and/or the transition of Λ to the lowest single-particle state, 4) the Λ-particle sticks to the heavier fission fragment, and 5) Λ+ N > N + N reaction inside the heavier fragment makes spallation or even fission of the heavier fragments (with Q-value of 190 MeV). There is enough time for the Λ to survive during fission because the life time of Λ-particle (10^{-10} sec) is much larger than the typical timescale of fission (~10^{-18} sec). By means of this sequence of reactions, a total energy of about 350MeV will be released due to the mass difference between K^- and π. It will bring to a possibility that the long-lived fission product (LLFP) such as ^{126}Sn and ^{129}I originated from the heavier fragments may not be produced at all (see Fig. 2).

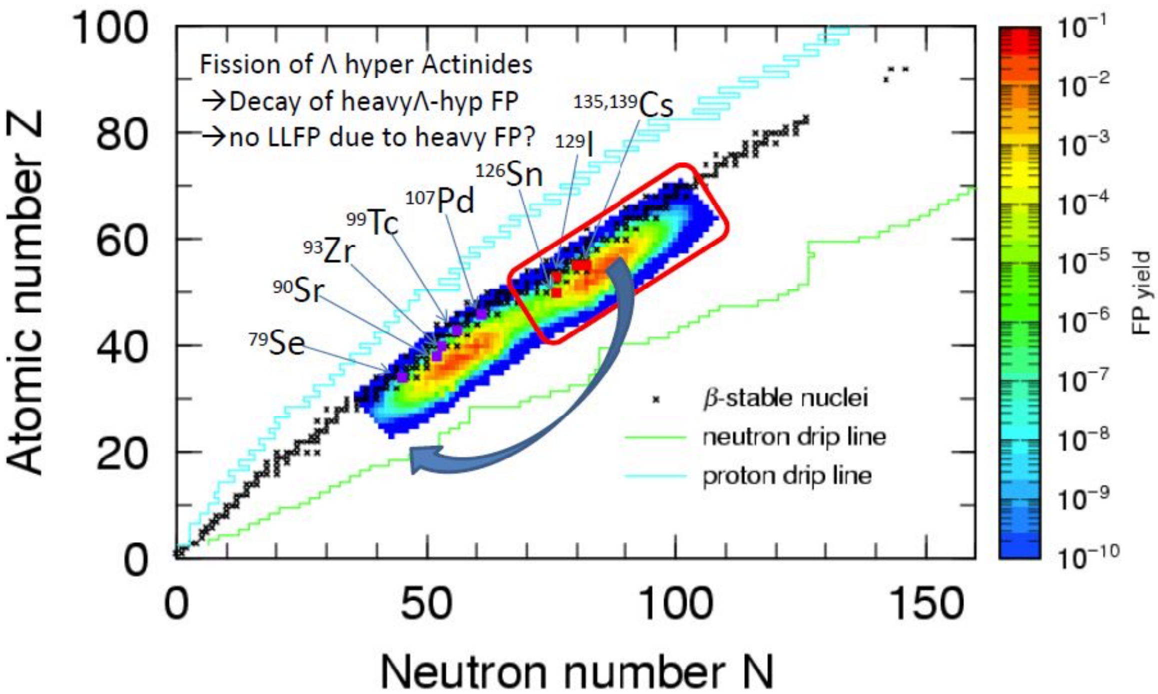

Fig. 2 Contour plot of fission fragment distribution (independent yield) for the case of thermal neutron induced fission of ^{235}U. If the heavy Λ hypernuclei make fission, the Λ-particle will stick to the heavier fragment (enclosed by the round square), then the heavier fragments will make spallation and/or fission when the Λ-particle in them decay via Λ+ N > N + N process (non-mesic decay) which generates excitation of about 190 MeV at the center of them.

3. Other possibility of using K^- for applications

There is also a possibility that K^- is used to transmute LLFP directly, or detect nuclear matter hidden in other material. The first possibility is brought by the fact that stopped K^- would be absorbed in the material consisting of LLFP and the excitation energy of 350 MeV brought by the production and decay of Λ-particle by K^- will be used to transmute LLFP directly. The second possibility is based on the reactions induced by stopped K^-. Let us consider a simple case in which 1 GeV proton and K^- is incident on a block of cylindrical ^{238}U as shown in Fig. 3.

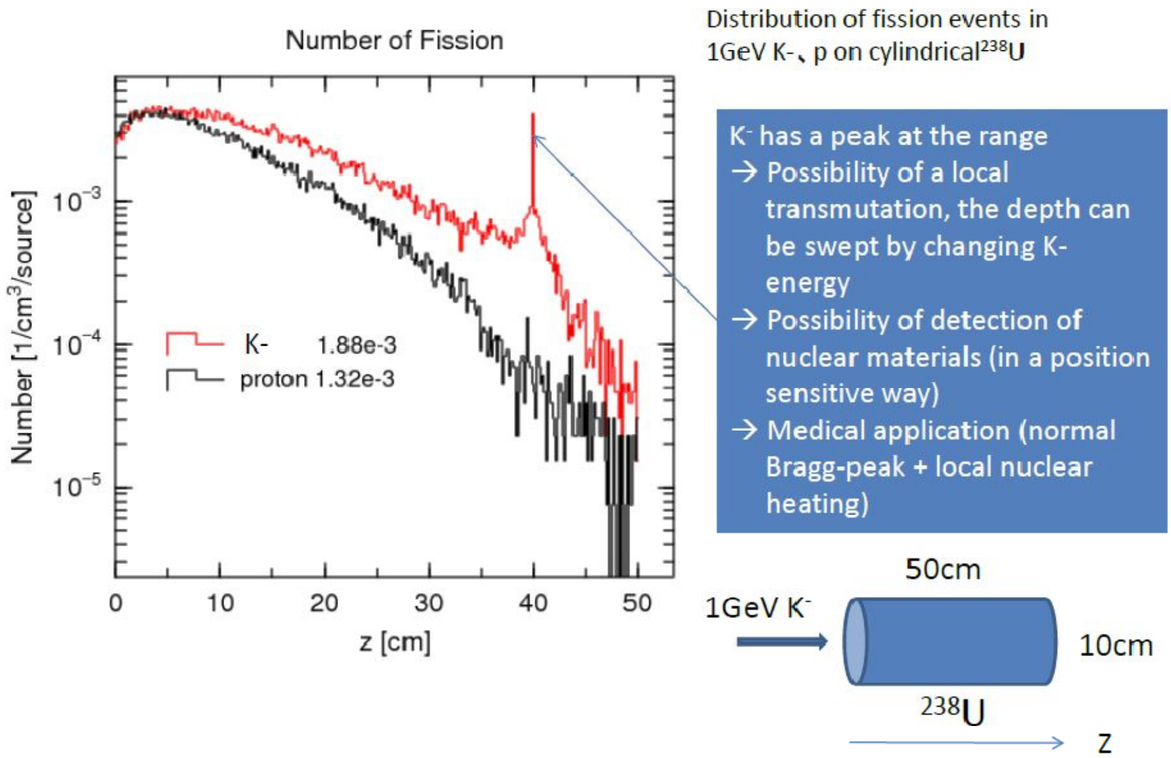

Fig. 3 Distribution of fission events along the beam axis of incident proton and K^- of 1GeV inside a block of ^{238}U.

Compared to the gradual decrease of fission events induced by proton, those of K^- has a sharp peak at the range position (stopping length) where the stopped K^- is absorbed by ^{238}U, Λ hypernuclei is produced and total of 350 MeV is released there. This fact can be used in 2 ways. Firstly, it can be used as a method to transmute materials predominantly at the region of range, namely, position-selective method of transmutation. The position can be changed by varying the K^- beam energy. Secondly, it can be used to detect what kind of material exists at the range. For example, we can think of a material consisting of ^{238}U inside Iron as in Fig. 4. Here, a cylindrical ^{238}U with 10cm in radius and 20cm in length is embedded in Iron of 10cm in thickness. Let us impinge K^- of various energy from the left, and let us measure the distribution of heat deposition along the beam axis. The result is shown in Fig. 5. When the K^- energy is less than 250 MeV which is the energy with stopping length of less than 10 cm in Iron, the heat deposition has a peak at the range. However, the distribution of the heat deposition has a discontinuity at 10 cm when K^- energy is larger, which is enough for K^- to penetrate 10-cm Iron intruding into the region of ^{238}U which gives extra heat generation by fission.

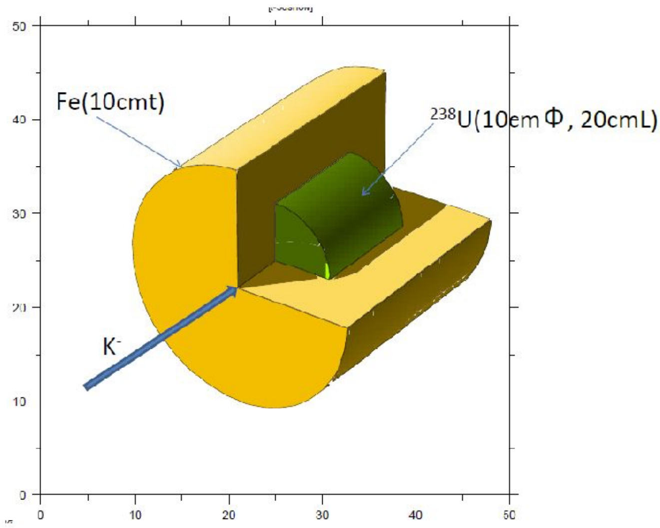

Fig. 4 Cross-cut view of considered geometry

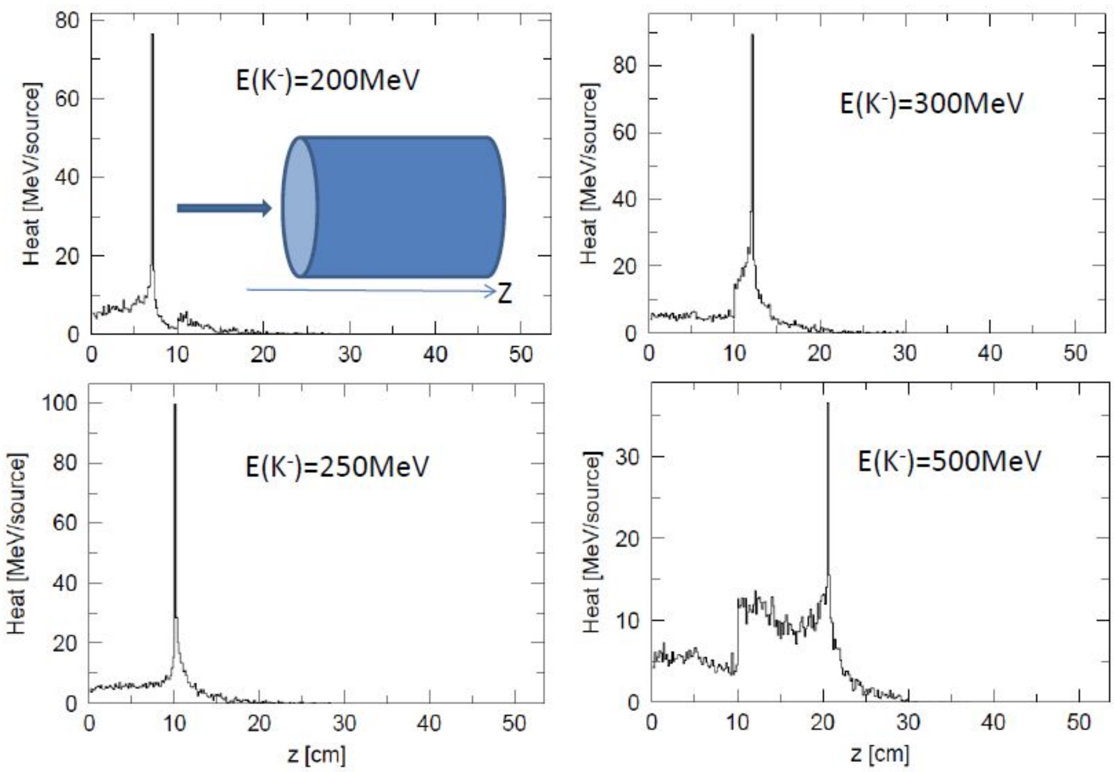

Fig. 5 Distribution of heat deposition along the beam axis in the geometry shown in Fig. 4

Similar discontinuity can be seen in the particle flux ejected perpendicular to the beam. Figure 6 shows a case with 1-GeV K^- incident on the material of Fig. 4. Various particles, mostly neutrons, emitted perpendicular to the K^- beam, are assumed to be detected by a collimated detector, and distribution of the particle yields along the beam axis is displayed. As in the previous examples, the particle yields exhibits a sudden jump at 10 cm, where hidden layer of ^{238}U comes to give more neutrons than the layer of Iron in front of it. In the same way, radial distribution of ^{238}U can be also detected by offsetting the incident K^- beam. By combining several observables, we expect that nuclear materials hidden even in a thick metallic container can be detected including how it is distributed in the container.

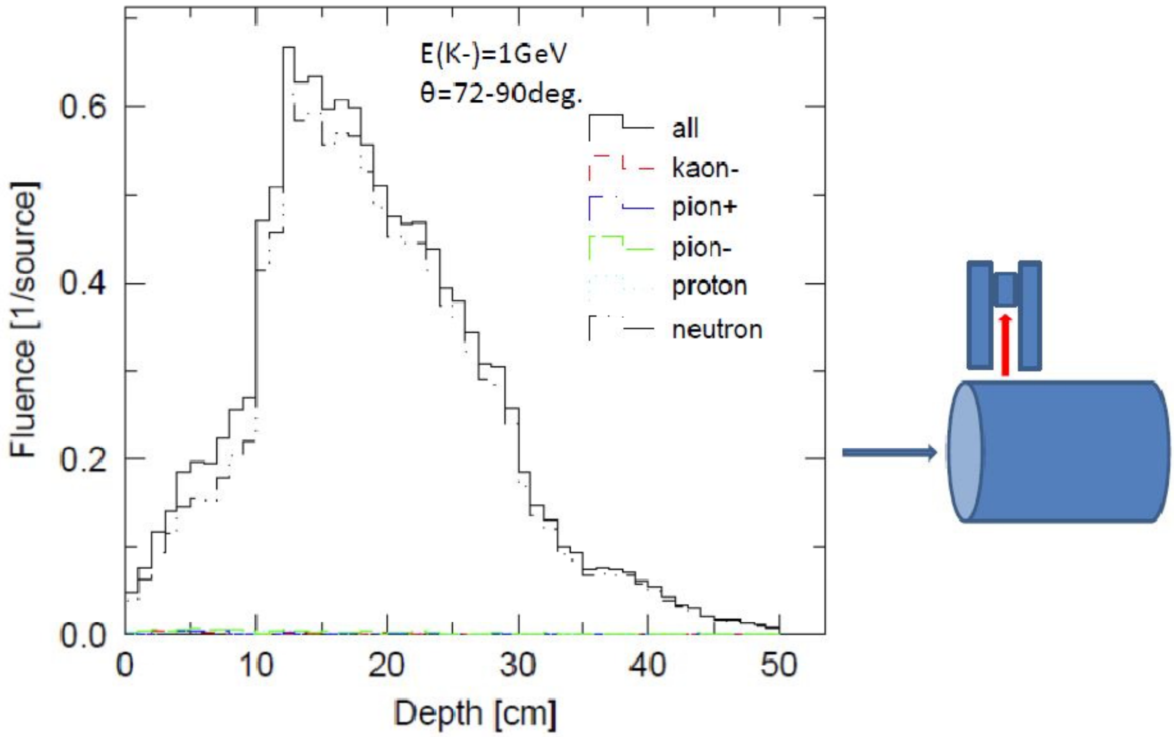

Fig. 6 Fluence of various particles (mostly neutrons) emitted perpendicular to the K^- beam as a position along the beam.

4. Summary

We propose a new method to use strangeness, namely, K^- beam and Λ-particles produced by it inside nuclei, for various application purposes. Firstly, we point out that many neutron-rich hypernuclei can be produced by fission of heavy Λ hypernuclei, mostly in the heavier fission fragment region. Secondly, production and decay of Λ-particles in (minor) actinides and LLFP can be used to transmute them to much lighter fragments. Especially, there is a possibility that LLFP originating from the heavier fission fragments may not be produced at all since Λ-particles stick to the heavier fragment, then decay of them transmute the heavier fragments by spallation and/or fission to much lighter nuclei. This itself is a new mode of fission. Thirdly, such a transmutation can be carried out in a position-selective way by varying the K^- beam energy. Finally, K^- beam may be used to detect hidden nuclear materials inside thick containers including how nuclear materials distribute in the container.

At present, we have to admit that using K^- for these applications are the most expensive (and may not be most effective) way to do any of the things proposed here. However, it is academically interesting to exploit such possibilities since accelerator technologies may progress more than the speed we can think of, which makes the cost of producing K^- less and flux of K^- much more than they are now. As a matter of fact, some basic experiment of the matters proposed in this paper can be carried out at the hadron physics hall of J-PARC.

References

[1] F. Minato, S. Chiba and K. Hagino, Nucl. Phys. A 831, 150-162(2009).

9. Uncertainty Quantification of Lumped Fission Product Cross Section for Fast Reactor Application

Go CHIBA
Reactor Physics Group, Japan Atomic Energy Agency
Tokai-mura, Naka-gun, Ibaraki-ken 319-1195
e-mail: chiba.go@jaea.go.jp

The uncertainty of the lumped fission product (FP) cross section is quantified by using the covariance data given in TENDL-2008 and the low-fidelity covariance (Low-Fi). The relative standard deviations of the one-group capture cross section of the lumped FP are calculated as 4.7% with TENDL-2008 and as 1.5% with Low-Fi. It is found that TENDL-2008 gives larger uncertainty to the FP nuclear data than Low-Fi. In addition, the lumped FP cross sections are calculated with various nuclear data libraries including JENDL and it is found that the largest difference in the one-group capture cross sections among these libraries is 3.8%.

1. Introduction

Fission product (FP) nuclides are accumulated through burn-up of fast reactors, and that results in a reactivity loss. For example, the burn-up reactivity loss per a cycle of the reactor simulating Japanese proto-type fast reactor [1] is about -2.7%dk/kk'. This is due to the reduction of fissile materials and the FP accumulation, and the latter component is calculated as about -0.7%dk/kk'. In addition, the FP accumulation usually increases a coolant density coefficient of fast reactors. Though the FP nuclear data are less important than the nuclear data of other fissile and structure materials, these errors should be properly considered in a reactor core design by setting a proper margin.

Impact of the FP nuclear data uncertainty on reactor performance parameters has been roughly estimated through the experimental analyses of the integral data. While such estimation is quite useful for a fast reactor design, it is desirable to estimate the FP nuclear data uncertainty also from a differential side to complement the information obtained from the integral side.

Recently, two projects yield the "differential" uncertainty information on the FP nuclear data; TENDL-2008 [2] and the low-fidelity covariance (Low-Fi) [3]. TENDL-2008 is an evaluated nuclear data library based on the TALYS nuclear data evaluation code and Low-Fi is a product of a joint project of several US laboratories. Both have already been open to public.

In the present study, we will quantify the uncertainty of the FP nuclear data by using the covariance data given in TENDL-2008 and Low-Fi. In usual fast reactor calculations, all the FP nuclides are treated as a "lumped" nuclide. Hence, we estimate the cross section uncertainties of the lumped FP in the present study.

2. Processing of covariance data with NJOY/ERRORJ

Since the FP accumulation affects the reactor performance parameters through the neutron capture reaction, we estimate the uncertainty of the lumped FP capture cross sections.

Firstly, the covariance data given in the nuclear data files are processed into the multi-group form for each FP nuclide. This processing is performed with the NJOY code [4], into which the ERRORJ code [5] is incorporated, under the following conditions; the number of energy groups is set to be 18 and the NJOY-implemented weighting function simulating a fast reactor neutron energy spectrum (iwt=8) is used. The processed FP nuclides, which have large contributions to capture rate of the lumped FP [6], are listed in **Table 1**. These chosen FP nuclides cover more than 90 percent of the total capture rate of the lumped FP [6].

With the obtained 18-group cross sections and their covariance data, we calculate a one-group capture cross section and its relative standard deviation for each FP. The same weighting function to the preceding section's one is used. **Table 2** shows the result. Large differences are observed in the standard deviations between TENDL-2008 and Low-Fi, and TENDL-2008 gives much larger uncertainties than Low-Fi. Here, we compare the covariance data of Ru-101 in which a significantly large difference is observed and which has a large contribution to capture rate of the lumped FP. **Table 3** shows group-wise relative standard deviations. We can find that uncertainties given to the TENDL-2008 data are much larger than those of Low-Fi above 1keV. **Figures 1 and 2** show the correlation matrices. Above 1keV, a correlation between energy groups of the TENDL-2008 data is stronger than that of Low-Fi. This difference in correlation matrices is similarly observed in other FP nuclides. This is one of the reasons why TENDL-2008 gives larger uncertainties to the one-group cross sections than Low-Fi.

3. Generation of lumped fission product nuclear data covariance

With the multi-group covariance data obtained in the preceding section, we calculate the covariance data for the lumped FP cross section.

The lumped FP cross section of group i, $\overline{\sigma}_i$, is calculated as

$$\overline{\sigma}_i = \frac{\sum_n R_n \sigma_{n,i}}{\sum_n R_n},$$

in which R_n corresponds to the number density ratio of nuclide n in the lumped FP.

Covariance between $\overline{\sigma}_i$ and $\overline{\sigma}_j$ is given as

$$\left(d\overline{\sigma}_i\right)\cdot\left(d\overline{\sigma}_j\right) = \sum_n \sum_g \sum_{n'} \sum_{g'} \frac{\partial \overline{\sigma}_i}{\partial \sigma_{n,g}} \cdot \frac{\partial \overline{\sigma}_j}{\partial \sigma_{n',g'}} \cdot \left(d\sigma_{n,g}\right)\cdot\left(d\sigma_{n',g'}\right), \qquad (1)$$

in which the subscripts g, g' denote the energy groups. Since correlations between different FP nuclides are not provided in both TENDL-2008 and Low-Fi, Eq. (1) can be simply written as

$$\left(d\overline{\sigma}_i\right)\cdot\left(d\overline{\sigma}_j\right) = \sum_n \left(\frac{R_n}{\sum_{n'} R_{n'}}\right)^2 \cdot \left(d\sigma_{n,i}\right)\cdot\left(d\sigma_{n,j}\right). \qquad (2)$$

With Eq. (2), we calculate the covariance matrix of the lumped FP cross section. In this calculation, we use the number density ratio of FP nuclides for Pu-239 fission reaction reported in Ref. [6]. **Figure 3** shows the relative standard deviations of the lumped FP cross section. We can find that the one of TENDL-2008 is larger than the one of Low-Fi above 1keV. While the correlation matrices of the lumped FP cross section are not shown in the present paper, a similar result to the Ru-101 case is obtained.

Finally, the relative standard deviations of the one-group capture cross section of the lumped FP are calculated. Results of TENDL-2008 and Low-Fi are 4.7% and 1.5%, respectively. It is confirmed by an additional calculation that the uncertainty of Low-Fi does not change if we exclude the FP nuclides shown as the bolded character in Table 1.

4. Comparison of lumped FP cross section among various nuclear data files

In order to obtain more information on the lumped FP cross section uncertainty, we calculate the lumped FP cross sections with various nuclear data files such as JENDL-3.2, -3.3, JEFF-3.1, ENDF/B-VII.0 and TENDL-2008. Eighteen-group FP cross sections are obtained with NJOY and the lumped FP cross section is generated with the same weighting function. In this calculation, FP nuclides listed in Table 1 (without bolded ones) are considered. We compare the one-group capture cross sections of the lumped FP. **Table 4** shows the one-group capture cross sections with their relative differences to the JENDL-3.2 value. The largest difference between different nuclear data libraries is 3.8%. This result is not so different to the lumped FP cross section uncertainty obtained in the preceding section.

5. Conclusion

We have quantified the uncertainty of the lumped FP cross section by using the covariance data given in TENDL-2008 and Low-Fi. The relative standard deviations of the one-group capture cross sections of the lumped FP have been calculated as 4.7% with TENDL-2008 and as 1.5% with Low-Fi. It has been observed that TENDL-2008 gives larger uncertainty to the FP nuclear data than Low-Fi. In addition, the lumped FP cross sections have been calculated with various nuclear data libraries including JENDL. The largest difference in the one-group capture cross sections among these libraries is 3.8%. This result is not so different to the lumped FP cross section uncertainty obtained with the covariance data of TENDL-2008 and Low-Fi.

Acknowledgment

The author wishes to express his gratitude to M. Ishikawa and S. Okajima of Japan Atomic Energy Agency for providing useful comments on this manuscript.

References

[1] H. Takashita, et al.: "Report on neutronic design calculational methods," JNC TN8410 2000-011, Japan Nuclear Cycle Development Institute (2000).

[2] A. J. Koning, D. Rochman: "TENDL-2008: Consistent TALYS-based evaluated nuclear data library including covariance data," JEFF-DOC 1262 (2008).

[3] R. C. Littile, et al.: "Low-fidelity covariance project," Nucl. Data Sheets, 109, p.2828 (2008).

[4] R. E. MacFarlane, D. W. Muir: "The NJOY Nuclear Data Processing System, Version 91", LA-12740-M, Los Alamos National Laboratory (1994).

[5] G. Chiba: "ERRORJ: A code to process neutron-nuclide reaction cross section covariance, version 2.3," JAEA-Data/Code 2007-007 (2007).

[6] G. Chiba, K. Numata: "Development of the fast reactor group constant set JFS-3-J3.2R based on JENDL-3.2," JNC TN9400 2001-124, Japan Nuclear Cycle Development Institute (2002).

Table 1 Processed FP nuclides

Kr-83, -84, Rb-85, Y-89, -91, Zr-91, -92, -93, -94, **-95**, -96, Nb-95,
Mo-95, -97, -98, -100, Tc-99, Ru-100, -101, -102, **-103**, -104, -106,
Rh-103, Pd-105, -106, **-107**, -108, Ag-109, Cd-111, I-127,-129,
Xe-131, -132, -134, Cs-133, -134, -135, -137, La-139, Ce**-141**, -142, -144,
Pr-141, Nd-143, -144, -145, -146, -148, -150, Pm-147,
Sm-147, -149, -150, -151, -152, Eu-153, **-154**, Gd-157

*Only the low-fidelity covariance is processed for bolded nuclides

Table 2 One-group capture cross section (b) with standard deviation (%)

	TENDL-2008		Low-fidelity Cov.			TENDL-2008		Low-fidelity Cov.	
Kr-83	0.304	(28.9)	0.353	(17.7)	I-127	0.613	(23.6)	0.708	(7.1)
Kr-84	0.060	(12.7)	0.057	(9.5)	I-129	0.257	(29.0)	0.413	(12.7)
Rb-85	0.251	(16.5)	0.282	(14.4)	Xe-131	0.418	(15.9)	0.386	(6.0)
Y-89	0.023	(8.3)	0.023	(3.0)	Xe-132	0.054	(28.9)	0.050	(15.0)
Y-91	0.068	(31.9)	0.103	(14.0)	Xe-134	0.026	(30.9)	0.020	(15.8)
Zr-91	0.096	(13.5)	0.095	(9.1)	Cs-133	0.530	(19.1)	0.579	(7.8)
Zr-92	0.049	(14.2)	0.052	(10.8)	Cs-134	0.881	(20.4)	1.326	(12.8)
Zr-93	0.111	(19.1)	0.129	(10.8)	Cs-135	0.177	(14.7)	0.251	(13.7)
Zr-94	0.027	(10.7)	0.029	(13.6)	Cs-137	0.030	(12.8)	0.021	(14.5)
Zr-95			0.169	(11.2)	La-139	0.041	(9.8)	0.042	(8.9)
Zr-96	0.034	(10.8)	0.032	(3.0)	Ce-141			0.330	(11.4)
Nb-95	0.593	(13.0)	0.414	(13.5)	Ce-142	0.027	(21.6)	0.026	(12.1)
Mo-95	0.329	(26.7)	0.378	(11.4)	Ce-144	0.083	(38.4)	0.026	(12.9)
Mo-97	0.317	(26.4)	0.394	(11.6)	Pr-141			0.161	(8.4)
Mo-98	0.113	(8.2)	0.123	(6.4)	Nd-143	0.379	(13.4)	0.379	(12.5)
Mo-100	0.101	(11.1)	0.103	(5.8)	Nd-144	0.083	(17.0)	0.086	(9.4)
Tc-99	1.043	(22.8)	0.792	(4.8)	Nd-145	0.501	(21.2)	0.576	(10.5)
Ru-100	0.151	(9.4)	0.174	(16.0)	Nd-146	0.108	(21.4)	0.098	(5.7)
Ru-101	0.904	(23.5)	0.873	(6.5)	Nd-148	0.142	(14.6)	0.146	(6.5)
Ru-102	0.169	(14.7)	0.183	(10.0)	Nb-150	0.164	(15.0)	0.161	(5.4)
Ru-103			0.576	(36.4)	Pm-147	1.468	(27.8)	1.558	(8.7)
Ru-104	0.155	(17.1)	0.182	(4.7)	Sm-147	1.428	(24.5)	1.352	(9.7)
Ru-106	0.103	(16.4)	0.107	(17.6)	Sm-149	12.244	(6.1)	12.227	(2.6)
Rh-103	0.857	(24.2)	0.827	(4.7)	Sm-150	0.568	(27.4)	0.513	(8.7)
Pd-105	0.992	(25.6)	1.031	(7.8)	Sm-151	5.469	(28.1)	4.840	(11.6)
Pd-106	0.239	(22.1)	0.239	(13.5)	Sm-152	0.773	(11.7)	0.754	(4.4)
Pd-107			1.171	(8.4)	Eu-153	2.701	(21.8)	2.922	(12.9)
Pd-108	0.251	(19.1)	0.248	(11.3)	Eu-154			4.068	(16.6)
Ag-109	0.817	(22.1)	0.839	(9.1)	Gd-157	17.346	(2.9)	17.709	(0.6)
Cd-111	0.596	(27.2)	0.751	(13.9)					

Table 3 Group-wise relative standard deviation of Ru-101

Energy group	Upper energy	Relative standard deviation	
		TENDL-2008	Low-fidelity Cov.
1	10 (MeV)	0.66	0.44
2	6.07	0.79	0.25
3	3.68	0.72	0.17
4	2.23	0.67	0.15
5	1.35	0.61	0.13
6	820850 (eV)	0.47	0.08
7	387740	0.39	0.08
8	183160	0.38	0.08
9	86517	0.34	0.08
10	40868	0.31	0.09
11	19305	0.25	0.10
12	9118.8	0.21	0.08
13	4307.4	0.19	0.09
14	2034.7	0.17	0.09
15	961.12	0.05	0.09
16	454	0.07	0.09
17	214.45	0.02	0.09
18	101.3	0.03	0.09

Table 4 Relative difference in lumped FP one-group capture cross section (reference: JENDL-3.2)

	One-group capture cross section (b)	Relative difference
JENDL-3.2	0.43335	(Ref.)
JENDL-3.3	0.43453	0.003
TENDL-2008	0.42825	-0.012
ENDF/B-VII.0	0.43011	-0.007
JEFF-3.1	0.44444	0.026

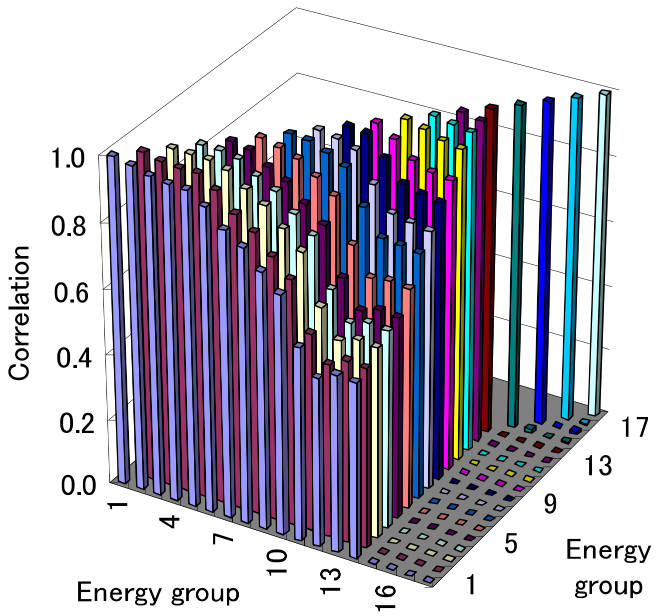

Fig. 1 Correlation matrix of Ru-101 of TENDL-2008

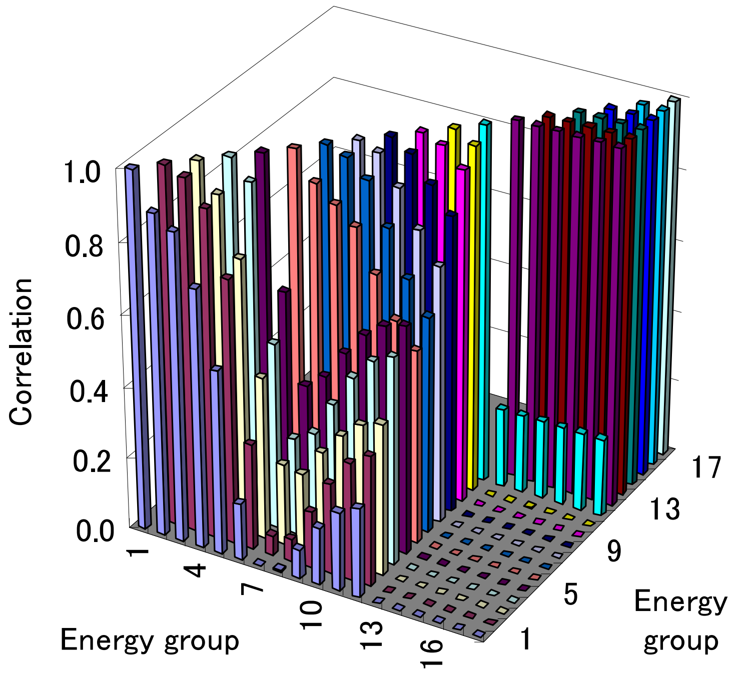

Fig. 2 Correlation matrix of Ru-101 of Low-Fi

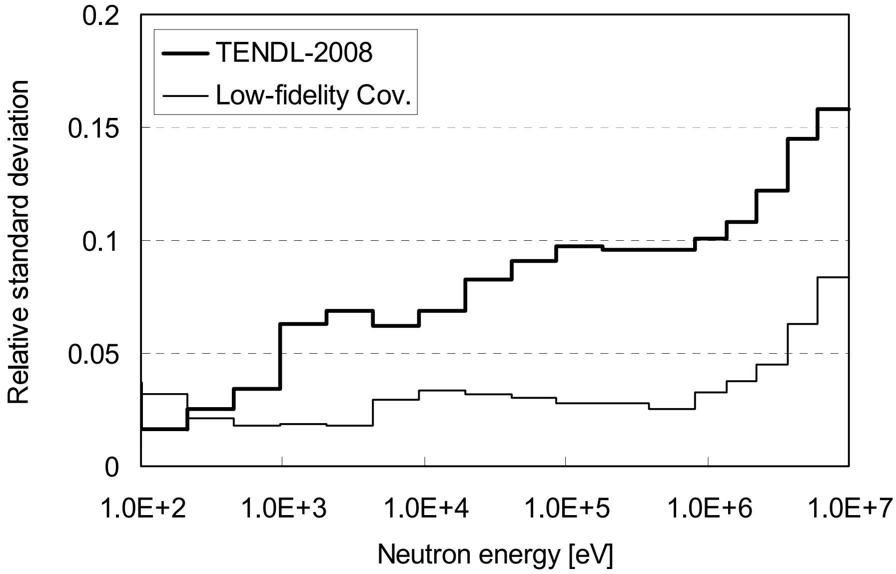

Fig. 3 Relative standard deviation of lumped FP nuclear data

10. Measurement of the spectral neutron flux at the ANITA facility at TSL

Yuuki Naitou[1], Yukinobu Watanabe[1], Shusuke Hirayama[1], Alexander Prokofiev[2], Anders Hjalmarsson[2], Pernilla Andersson[3], Riccardo Bevilacqua[3], Cecilia Gustavsson[3], Stephan Pomp[3], Vasily Simutkin[3], Henrik Sjöstrand[3], Michael Österlund[3], Milan Tesinsky[4], and Udomrat Tippawan[5]

[1]*Department of Advanced Energy Engineering Science, Kyushu University, Kasuga, Fukuoka 816-8580, Japan*
[2]*The Svedberg Laboratory, Uppsala University, Box 533, SE-751 21 Uppsala, Sweden*
[3]*Department of Physics and Astronomy, Uppsala University, Box 516, SE-751 20 Uppsala, Sweden*
[4]*Department of Nuclear and Reactor Physics, Royal Institute of Technology, 106 91 Stockholm, Sweden*
[5]*Plasma and Beam Physics Researcher Facility, P.O.Box 217, 50200, Thailand*
Email: watanabe@aees.kyushu-u.ac.jp

The ANITA spectral neutron flux at 0º was measured using a conventional recoil proton technique with a ΔE –E telescope consisting of two fully depleted ΔE silicon surface barrier detectors and a CsI(Tl) scintillator. The preliminary result shows good agreement with MCNPX simulation in both shape and magnitude.

1. Introduction

The ANITA (Atmospheric-like Neutrons from thIck TArget) facility [1] has been installed at The Svedberg Laboratory (TSL) in Uppsala, Sweden. The facility is intended mainly for accelerated testing of semiconductor devices for neutron-induced single event effects. The ANITA source produces neutron beams with “white” spectrum using proton-induced spallation reactions in a full-stop tungsten target. The neutron spectrum resembles that of neutrons in the Earth’s atmosphere and at the terrestrial level. This has the advantage to allow an easy deduction of the failure-in-time (FIT) rate for a component or a system tested with an atmospheric-like neutron source.

Up to now, beam characterization measurements [1] have been performed for the neutron spectrum, the energy-integrated neutron flux, the LANSCE-equivalent flux, spatial profiles of the neutron beam, etc. However, no measurement of the spectral neutron flux has been made to enable a direct comparison with the simulation of the ANITA neutron field which was performed with the MCNPX code [1]. In the present work, we have measured the spectral neutron flux at 0º using a conventional recoil proton method of measuring elastic *np*-scattering with the Medley setup [2,3,4] and then have compared the experimental result with the MCNPX simulation.

2. The ANITA facility

A schematic layout of the ANITA facility is illustrated in Fig. 1. Details of the facility are described elsewhere [1], and only a short summary is presented below.

The Gustaf Werner cyclotron is utilized for acceleration of the proton beam to the energy of approximately 180 MeV, and then the beam is guided to a full-stop tungsten target. The target is placed inside a massive bending magnet in a concrete cave. The neutron beam, generated by spallation reactions induced by incident protons in the target, is formed geometrically by a collimator aperture in a 1-m thick iron shielding wall. Collimator apertures of different sizes and shapes are available: e.g., cylindrical apertures in diameter in the 0 – 30 cm range, and a 1 cm x 1 cm square aperture.

Neutron monitor devices based on ionization chambers (IC) and thin-film breakdown counters

(TFBC) are placed downstream the aperture. Also the proton beam current on the tungsten target is monitored.

The user area extends from 250 cm to ≈ 15 m downstream the tungsten target. The energy-integrated neutron flux above 10 MeV amounts to ≈10^6 cm^{-2} s^{-1} for the standard ANITA neutron field, which is defined as the field at the Standard User Position (SUP) at the closest distance *L*= 250 cm for the standard incident proton beam current of 200 nA on the production target.

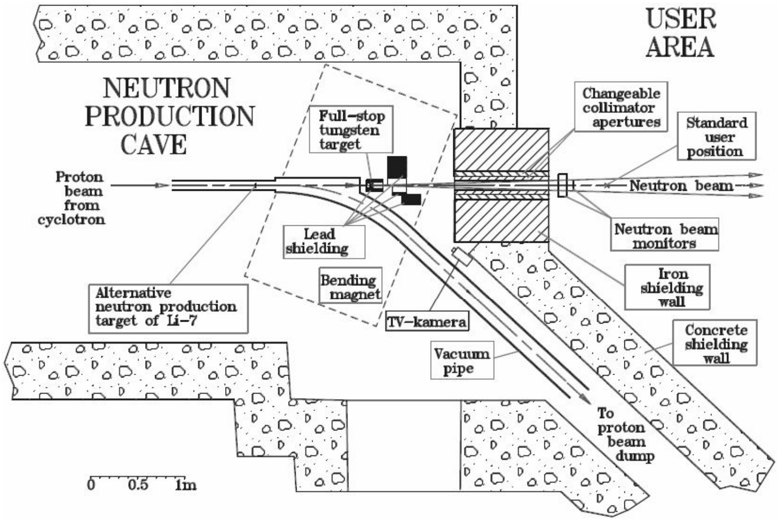

Fig. 1 A schematic layout of the ANITA facility

3. Experimental method

The spectral flux of the ANITA neutron beam was measured using a conventional proton recoil method with the MEDLEY setup which consists of eight three-element ΔE –E telescopes mounted inside a 90-cm-diam evacuated scattering chamber. The details are described in Refs.[2-5]. The MEDLEY setup was connected with the exit of the neutron beam collimator via a vacuum pipe in an additional 50-cm thick iron shielding wall as shown in Fig. 2. The distance between the ANITA target and the center of the MEDLEY setup was 338.3 cm. The collimator configuration used is also depicted in Fig. 2.

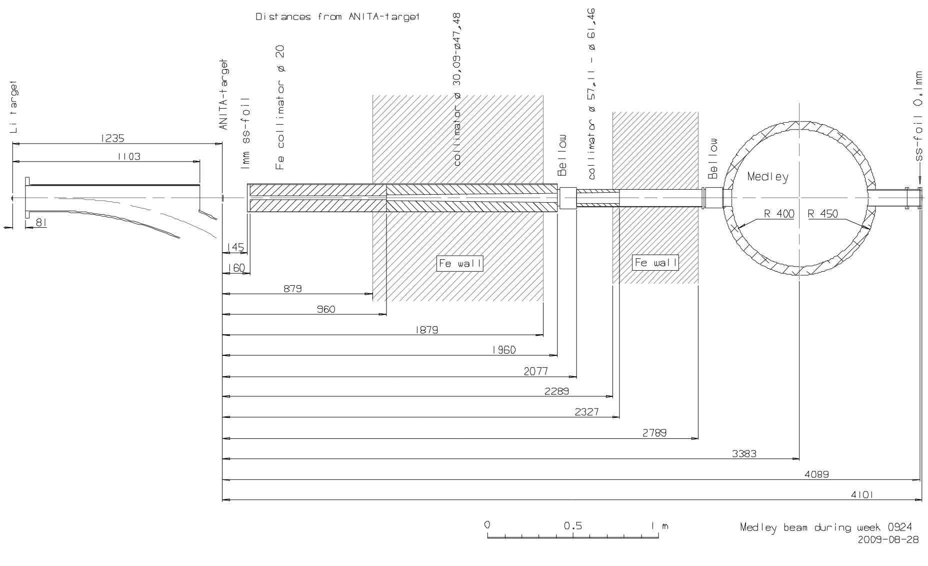

Fig. 2 A schematic drawing of the neutron beam line used in the measurement

The neutron beam irradiated a polyethylene (CH_2) target placed at the center of the MEDLEY setup, and protons recoiled elastically in the direction of 20º were detected using the ΔE–E telescope depicted in Fig. 3. It consists of two fully depleted ΔE silicon surface barrier detectors and a CsI(Tl) scintillator. The CH_2 targets of the following different sizes were used: 0.2-mm-thick and 26-mm-diam., 1-mm-thick and 25-mm-diam., 1-mm-thick and 35-mm-diam., and 5-mm-thick and 25-mm diam. In addition, runs with a 1-mm-thick and 22-mm-diam carbon target were carried out to subtract the contribution from (n,xp) reactions on C, and background runs with empty target were also performed.

The energy of the proton beam incident on the tungsten target was 176.6 MeV. The average proton beam current was 7.6 nA during the experiment.

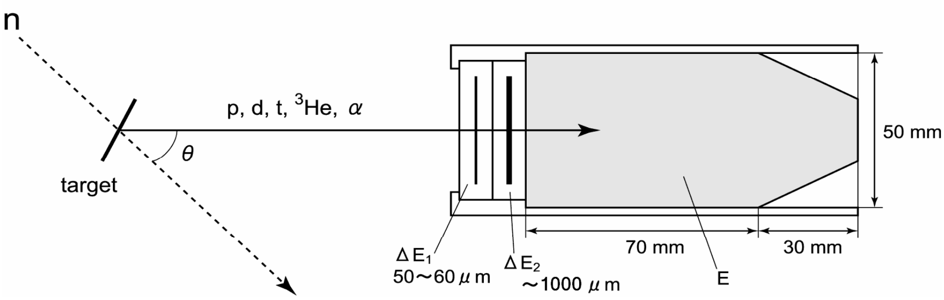

Fig. 3 Construction details of the ΔE–E telescope.

4. Data reduction procedure

Data reduction procedure on an event-by-event basis was similar to the previous MEDLEY experiments [2-5]. At first, proton events were selected using the ΔE-E particle identification. Energy calibration of all detectors was made in the same way as in Ref. [4]. Target-out and C(n,xp) background contributions were subtracted properly after normalization to the same neutron monitor counts and application of dead time corrections. A net recoil proton spectrum was derived after correction for incomplete detection efficiency of the CsI(Tl) scintillator. In Fig. 4, the resultant net proton spectrum is shown by open squares with the statistical error bar for the measurement with the 1-mm-thick and 35-mm-diam CH_2 target.

The thickness of the target causes a non-negligible energy loss and absorption of recoil protons. As a result, the measured spectra are distorted, particularly in the low-energy range. To make the thick-target correction, we use the TCORR code developed in the data analysis of light ion production measurements with the MEDELY setup [6]. The corrected spectrum is shown by closed circles in Fig. 4. Large enhancement of the proton yield after the correction is seen at proton energies below 10 MeV. The correction becomes negligible as the proton energy increases. To check the validity of the TCORR correction, we have performed a simulation using the PHITS code [7] which is a general-purpose three-dimensional Monte Carlo radiation transport code. In the simulation, recoil protons are generated uniformly in the target by sampling based on the corrected proton spectrum, and an energy spectrum of protons escaping from the target is obtained. The result of the PHITS simulation is shown by the solid histogram in Fig. 3, and is found to coincide with the measured proton spectrum plotted by the open squares. This demonstrates the reliability of the thick target correction with the TCORR code.

The threshold of proton detection is 1.2 MeV as shown in Fig. 4, The threshold is lower than the low-energy cutoff for particle identification, i.e., about 3 MeV for protons, because proton events stopped in the 50~60μm thick ΔE_1 detector can be included in the data analysis.

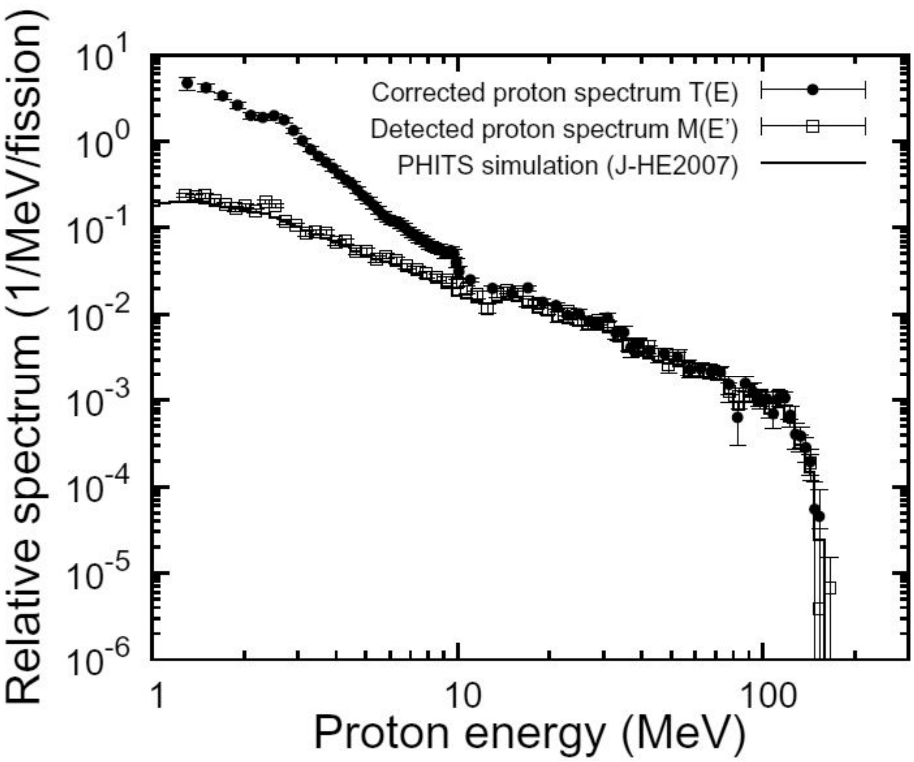

Fig. 4 Recoil proton spectra normalized to the counts of the IC neutron monitor. Open squares and closed circles denote measured recoil proton spectra without and with thick target correction, respectively. The solid histogram shows the result of energy loss simulation with the PHITS code.

Finally, the ANITA neutron spectrum $\Phi(E_n)$ per incident proton is determined using the following expression with the net recoil proton spectrum $S_{np}(E_p)$ per incident proton after the thick target correction:

$$\Phi(E_n)[1/(\mathrm{cm}^2 \cdot \mathrm{MeV} \cdot \mathrm{proton})] = \frac{S_{np}(E_p)}{\left(\left. \frac{d\sigma_H}{d\Omega} \right|_{\theta=20^\circ} \Delta\Omega \right) \times N_p}, \tag{1}$$

where $d\sigma_H/d\Omega$ is the differential *np* scattering cross section at 20 º laboratory angle [8], $\Delta\Omega$ is the solid angle, and N_p is the number of hydrogen atoms in the CH_2 target. The total number of incident protons is obtained by monitoring the beam current on the tungsten target.

4. Results and discussion

Figure 5 shows a preliminary ANITA neutron spectrum derived from the measurement with the 1-mm-thick and 35-mm-diam CH_2 target in comparison with the MCNPX simulation [1]. The magnitude of the experimental fluence is reduced to that at the standard user position (SUP) L=250 cm on the basis of the inverse square rule of the distance. Good agreement between the measurement and the simulation is obtained in shape and magnitude over the whole energy range.

Energy-integrated neutron flux above 10 MeV for proton beam current of 200 nA at SUP has been estimated using the present experimental data. It amounts to 8.5 x 10^5 cm^{-2} s^{-1}, which seems consistent with 9.3 x 10^5 cm^{-2} s^{-1} given in Ref. [1].

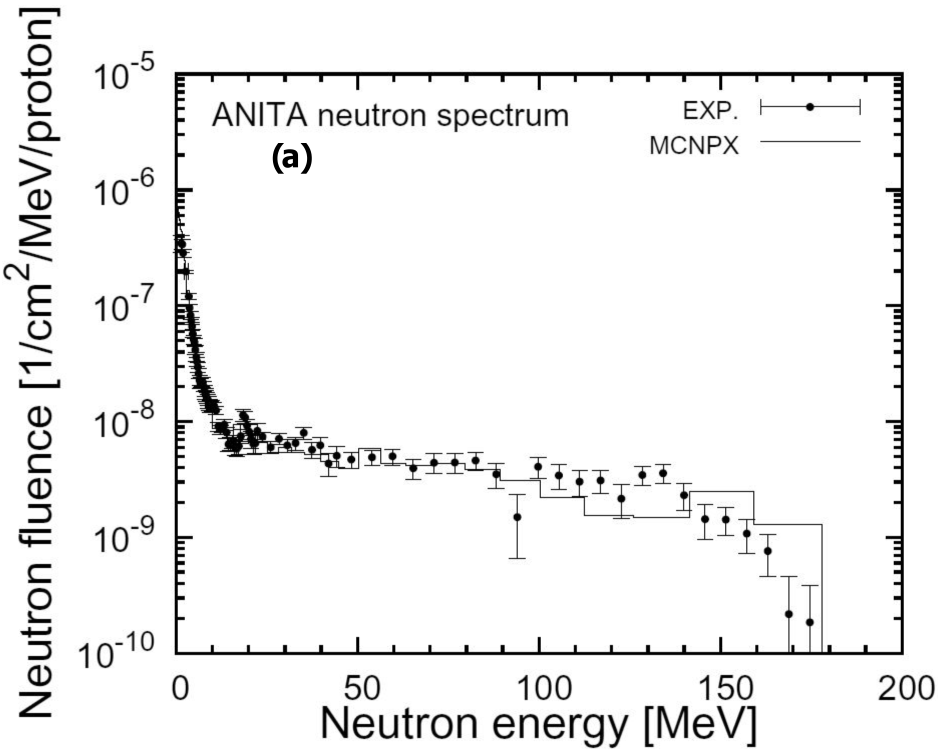

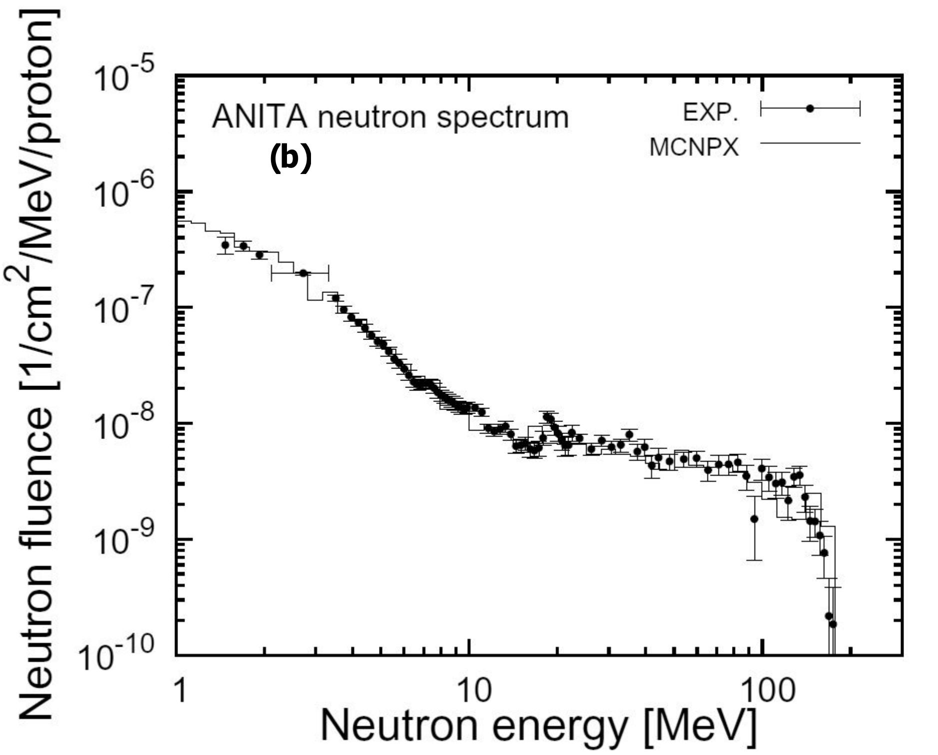

Fig. 5 Comparison between the measured spectral neutron fluence and the MCNPX simulation at the standard user position (SUP) in log-log scale (a) and linear-log scale (b). The experimental errors are only statistical ones.

5. Conclusions

The ANITA spectral neutron flux at 0º was measured using a conventional recoil proton method with the MEDLEY setup. The preliminary result shows good agreement with the MCNPX calculation in magnitude as well as in shape. We plan to carry out further data analyses for measurements using the CH_2 targets of different sizes. Also, the systematic errors should be estimated in the future.

Acknowledgements

The authors wish to thank the staff of the The Sverberg Laboratory for careful cyclotron operation during the experiment.

References

[1] A. V. Prokofiev, J. Blomgren, M. Majerle, et al., "Characterization of the ANITA Neutron Source for Accelerated SEE Testing at The Svedberg Laboratory", Nuclear and Space Radiation Effects Conference (NSREC'2009), 2009 IEEE Radiation Effects Data Workshop, Quebec, Canada, July 20-24, 2009, pp. 166-173, http://ieeexplore.ieee.org/stamp/stamp.jsp?arnumber=05336295, doi:10.1109/REDW.2009.5336295.

[2] S. Dangtip, A. Atac, B. Bergenwall *et al.*, "A facility for measurements of nuclear cross sections for fast neutron cancer therapy", *Nucl. Instr. Meth.* **A452**, 484-504 (2000).

[3] M. Hayashi, Y. Watanabe, R. Bevilacqua *et al.*, "Measurement of light-ion production at the new Uppsala neutron beam facility", in Proceedings of the International Conference on Nuclear Data for Science and Technology, April 22-27, 2007, Nice, France, EDP Sciences, pp.1091-1094 (2008).

[4] S. Hirayama, Y. Watanabe, Y. Naitou, et al., "Production of protons and deuterons from silicon bombarded by 175 MeV quasi mono-energetic neutrons", presented at this symposium (2009).

[5] U. Tippawan, S. Pomp, J. Blomgren et al., "Light-ion production in the interaction of 96 MeV neutrons with carbon" Phys. Rev. C79, 064611 (2009).

[6] S. Pomp and U. Tippawan, "An interative procedure to obtain inverse response functions for thick-target correction of measued charged-particle spectra", *Nucl. Instr. Meth.* **A 572** , 893-898 (2007).

[7] H. Iwase, K. Niita and T. Nakamura, "Development of General-Purpose Particle and Heavy Ion Transport Monte Carlo Code", *J. Nucl. Sci. and Technol.* **39**[11], 1142-1151 (2002).

[8] SAID Nucleon Nucleon scattering database. URL: http://gwdac.phys.gwu.edu.

11. Production of protons and deuterons from silicon bombarded by 175 MeV quasi mono-energetic neutrons

Shusuke HIRAYAMA[1], Yukinobu WATANABE[1], Yuuki NAITOU[1], Pernilla ANDERSSON[2], Riccardo BEBILACQUA[2], Cecilia GUSTAVSSON[2], Anders HJALMARSSON[3], Michael ÖSTERLUND[2], Stephan POMP[2], Alexander PROKOFIEV[3], Vasily SIMUTKIN[2], Henrik SJÖSTRAND[2], Milan TESINSKY[4] and Udomrat TIPPAWAN[5]

[1]*Department of Advanced Energy Engineering Science, Kyushu University, Kasuga, Fukuoka 816-8580, Japan*
[2]*Department of Physics and Astronomy, Uppsala University, Box 516, SE-751 20 Uppsala, Sweden*
[3]*The Svedberg Laboratory, Uppsala University, Box 533, SE-751 21 Uppsala, Sweden*
[4]*Department of Nuclear and Reactor Physics, Royal Institute of Technology, 106 91 Stockholm, Sweden*
[5]*Plasma and Beam Physics Researcher Facility, P.O.Box 217, 50200, Thailand*
Email: hirayama@aees.kyushu-u.ac.jp

We have measured double differential yields of protons and deuterons produced from silicon induced by 175 MeV quasi mono-energetic neutrons using the MEDLEY setup at the TSL neutron beam facility in Uppsala University. The measured data are used for benchmarking of a high-energy nuclear data file, JENDL/HE-2007, and intra-nuclear cascade (INC) model and quantum molecular dynamics (QMD) calculations.

1. Introduction

Recently, the importance of single event effects (SEEs) caused by cosmic-ray neutrons in logic and memory circuits have been increasing as one of the key reliability issues for advanced CMOS technology. When electronic memory circuits are exposed to neutron radiation, secondary ions can be produced by nuclear reactions on atomic nuclei in materials. The released charge can cause a flip of the memory information in a bit, which is called a single-event upset (SEU). To simulate accurately the SEEs including SEU, more reliable nuclear reaction models which can predict neutron induced light-ion production from silicon are strongly required. Since the validity of nuclear reaction models may be evaluated by comparison with measurements, a lot of experiment data over the wide incident energy range are needed for improvement of nuclear reaction models. However, there is no measurement for neutron induced light-ion production from silicon in the energy range of more than 100 MeV.

At the The Svedberg Laboratory (TSL)[1] in Uppsala, Sweden, quasi mono-energetic neutrons up to 175 MeV are available. Previous experiments using the MEDLEY spectrometer setup at TSL have been conducted to measure neutron induced light-ion production cross sections for Fe, Pb, U [2], Si [3], O [4], and C [5] at 96 MeV and for C [6,7], Fe and Bi [8] at 175 MeV. In the present work, we have measured double-differential production yields of light ions (p, d, t, ^{3}He, and α) from silicon bombarded by 175 MeV quasi mono-energetic neutrons. The experimental data are compared with the calculations using the PHITS code [9] with evaluated high-energy nuclear data and nuclear reaction models. The result of proton and deuteron production is reported in this paper.

2. Experimental method

Details of the experimental set up have been reported in Refs.[1,6]. Quasi mono-energetic neutrons generated by using the ^{7}Li(p,n)^{7}Be reaction irradiated a silicon target 1mm thick and 25mm in diameter. Energy and angular distributions of neutron-induced light-ion production yields from silicon were measured with the MEDLEY setup. The MEDLEY setup and construction details of each telescope are illustrated in Fig.1. The MEDLEY setup is composed of eight telescopes placed at angles from 20° to 160° in steps of 20°. Each telescope consists of two silicon surface barrier detectors as the ΔE detector and a CsI(Tl) detector as the E detector. Light ions produced from the silicon target placed at the center of the MEDLEY were detected by the eight telescopes. Moreover, the incident neutron spectrum was measured using the same setup with both 5mm-thick polyethylene (CH_2) target 25mm in diameter and 1mm-thick carbon target 22mm in diameter by means of a conventional proton recoil method.

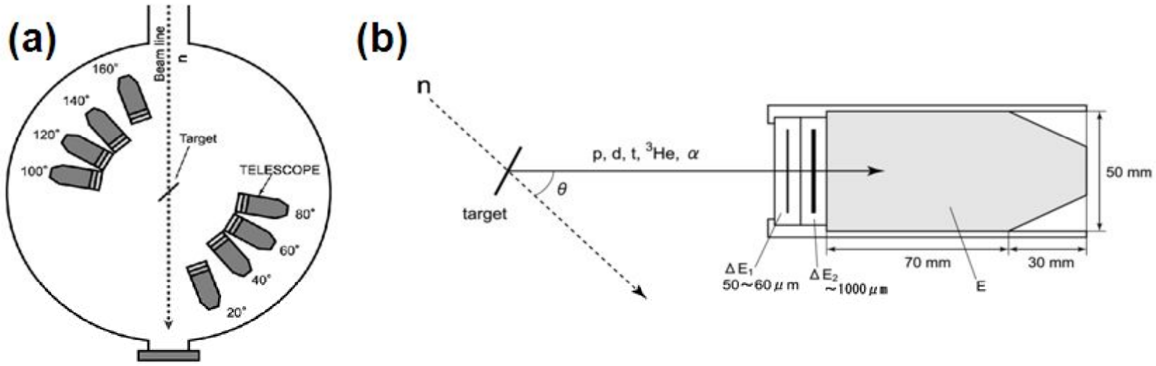

Fig. 1 MEDLEY setup: (a) arrangement of eight telescopes inside the MEDLEY chamber, (b) construction details of telescope.

3. Data analysis

Data analysis procedure based on ΔE-E particle identification technique is basically same as in the previous measurements at 96 MeV[3,4,6]. Figure 2 shows examples of two-dimensional scatter plots of pulse height signals for ΔE_1- ΔE_2 and ΔE_2-E located at 20°. Each light ion is found to be clearly separated.

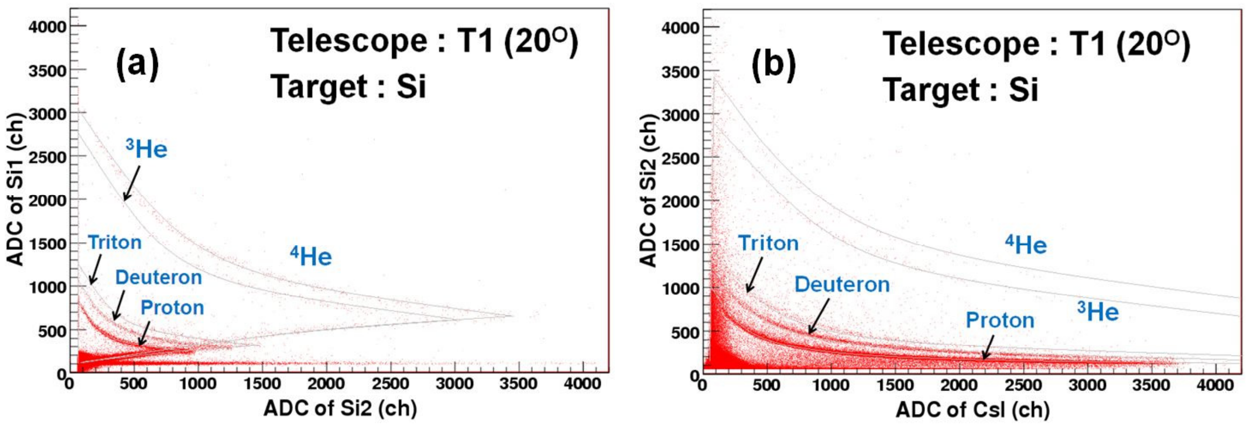

Fig. 2 Two-dimensional scatter plots of particle identification for (a) ΔE_1- ΔE_2 and (b) ΔE_2-E located at 20°. The solid lines are guided lines.

Energy calibration of all detectors was made using the data themselves. Events in the ΔE-E bands were fitted with respect to the energy deposition in the ΔE detectors, which was determined from the thickness and the energy loss calculated SRIM code[10]. For the energy calibration of the E detectors, the following approximate expression was applied to protons, deuterons, and tritons, which reflects a non-linear relationship between the light output and the energy deposition in the CsI(Tl) scintillator[11]:

$$E = a + bL + c(bL)^2 , \qquad (1)$$

where L is the light output, and a, b and c are the fitting parameters. The parameter c depends on the kind of charged particles.

The efficiency correction due to the reaction losses in the CsI(Tl) scintillator was implemented using the same method as reported in Ref.[7].

The incident neutron spectrum was obtained from the data analysis of recoil protons from np scattering in the measurement of CH_2 at 20°. By subtracting the contribution from C(n,xp) reaction using the measured data of C at 20°, we can derive the net recoil proton spectrum at 20°. Finally, it was converted into the source neutron spectrum by using efficiency correction and the np scattering cross section taken from NN-online[12]. Fig.3 (a) shows the result along with the source neutron spectrum calculated using an empirical formula[13]. Both the spectra are normalized by the number of the peak neutrons, and the calculated spectrum is smeared using a Gaussian function with the same experimental energy resolution. Fig.3 (b) shows the result of comparison with the past measurement[6]. The measured neutron spectrum shows good agreement with the past experimental data as well as the calculated one within the errors.

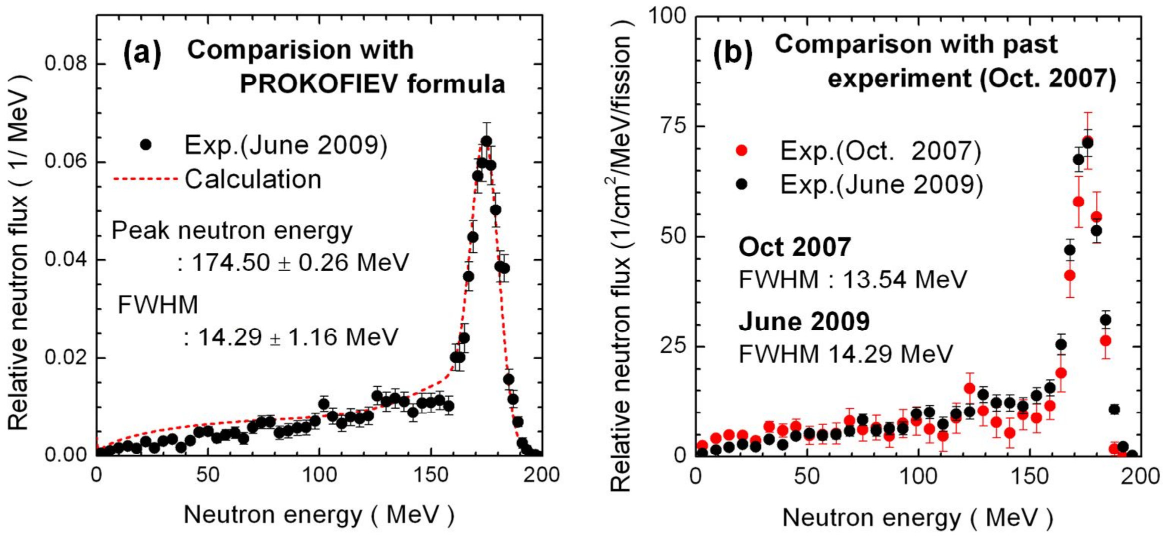

Fig. 3 Measured neutron spectra: (a) comparison with the neutron spectra calculated using empirical formula and (b) comparison with the past experimental data.

The measured double-differential production yields of protons and deuterons per incident neutron on the target were determined with using the following expression:

$$\left(\frac{d^2Y}{dEd\Omega}\right)_j = \frac{N_j(E,\theta)\times\dfrac{1}{f(E)}}{S_n\times\Delta E\times\Delta\Omega}, \tag{2}$$

where j denotes the kind of particles (p and d), $N_j(E,\theta)$ is the net counts in a certain energy bin ΔE, $f(E)$ is the effective efficiency which includes the energy loss effect in the CsI(Tl) scintillator, and S_n is the total number of incident neutrons on the target. In Eq. (2), the solid angle $\Delta\Omega$ was given under an assumption that the target is treated as a point source. It was confirmed that this assumption is valid by a comparison of the PHITS simulation between a point source and a plane source, in which the difference is only 1%.

Figure 4 shows the measured (n,xp) spectra from 20° to 140° by closed circles. Figure 5 shows the measured (n,xd) spectra from 20° to 60° in steps of 20°. For protons and deuterons, the measured double-differential yields show a strong angular dependence at high emission energies above 30 MeV.

4. Benchmark using PHITS code

The measured double-differential yields are compared with the PHITS calculations using three nuclear reaction options: the evaluated nuclear data library (JENDL/HE2007[14]), the quantum molecular dynamics(QMD) [15], and the intra-nuclear cascade model(INC) [16]. Note that INC is used for only proton, because INC cannot predict the dynamical process of complex particle production. The source neutron spectrum calculated using the empirical formula is used as an input of the PHITS calculation. It should be noted that the energy loss of charged particles generated by nuclear reactions in the silicon target is taken into account explicitly in the PHITS calculation.

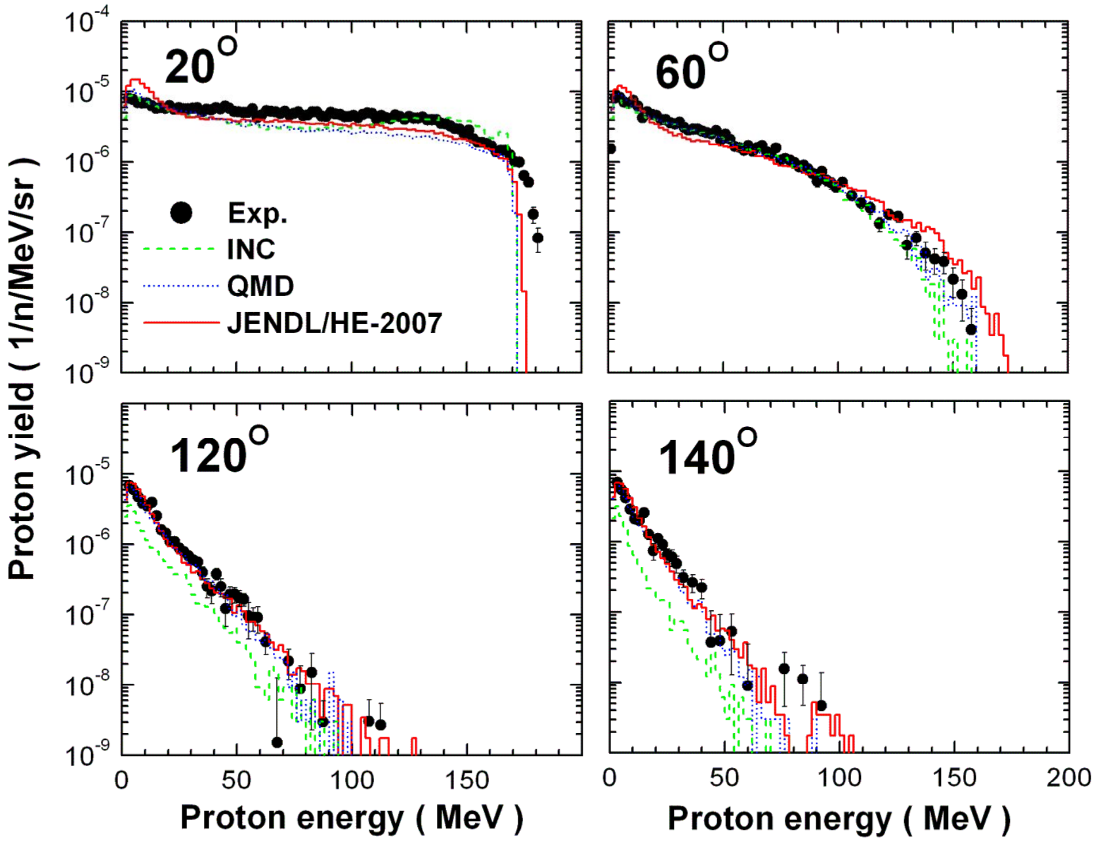

Fig. 4 Comparison between measured (n,xp) spectra at 20°, 60°, 120° and 140° and calculation results of JENDL/HE2007, QMD and INC.

Figure 4 shows the results of proton production yields. Three calculations show reasonably good agreement with the measured proton spectra at small angles except for 20°. The calculations with JENDL/HE2007 and QMD give fairly good descriptions of the spectra below 70 MeV at large angles. However, the INC calculations underestimate largely the measurement over the wide emission energy range at large angles.

The results of deuteron production are shown at angles from 20° to 60° in Fig. 5. There are obvious differences between both the calculations with JENDL/HE2007 and QMD. The calculations with JENDL/HE2007 show relatively good agreement with the measured deuteron yields at small and large angles. However, the QMD calculations underestimate the experimental data remarkably over the wide emission energy range.

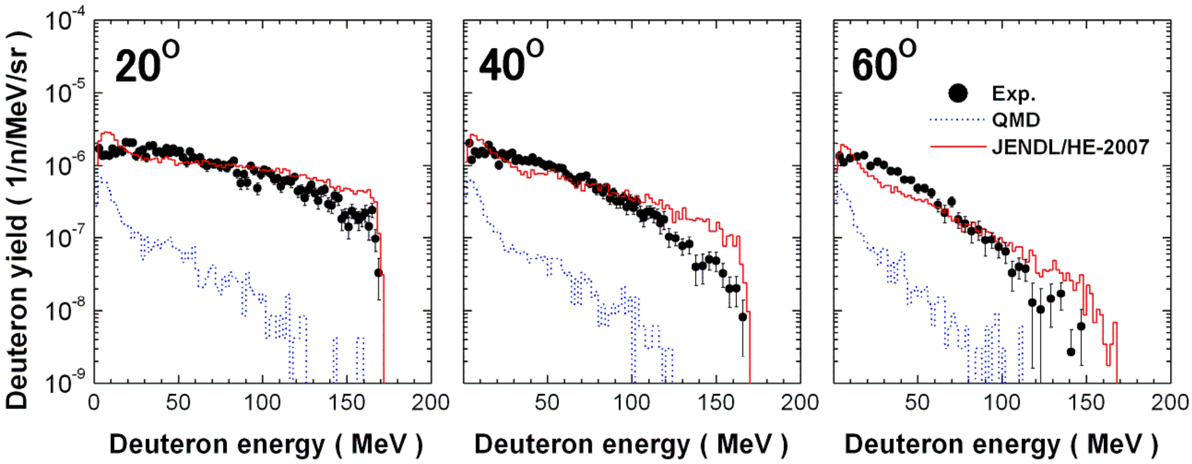

Fig. 5 Comparison between measured (n,xd) spectra from 20° to 60° in steps of 20° and calculation results of JENDL/HE2007 and QMD.

5. Summary and conclusions

The double-differential production yields of protons and deuterons from silicon were measured for bombardment of 175 MeV quasi mono-energetic neutrons at the The Svedberg Laboratory (TSL). The measured yields were compared with the PHITS calculations to benchmark evaluated high-energy nuclear data and nuclear reaction models. As a result of the proton production, the PHITS calculations with JENDL/HE2007 and QMD reproduce the measured yields better than the INC calculations at all angles except for 20º. For deuterons, the calculations with JENDL/HE2007 are in reasonably good agreement with the measurement at small and large angles. However, the QMD calculations underestimate experimental data remarkably over the wide emission energy range.

In the future, similar data analyses will be made for production yields of triton, ^{3}He and ^{4}He measured in the present experiment. We also aim at improving theoretical reaction models, such as QMD, used in the PHITS code and nuclear data evaluation, paying particular attention to the dynamical process in the production of complex particles.

Acknowledgements

We would like to thank the staff of the The Svedberg Laboratory for their assistance during the experiments. This work was supported in part by the STARC joint research program.

References

[1] S. Pomp, A. Prokofiev, J. Blomgren *et al.*, “The New Uppsala Neutron Beam Facility”, *Proc. Int. Conf. on Nuclear Data for Science and Technology*, Santa Fe, USA, Sept. 26-Oct. 1 AIP Conf. Proc. **769**, 780-783 (2005).

[2] V. Blideamu, F.-R.Lecolley, T. Lefort et al., “Nucleon-induced reactions at intermediate energies: New data at 96 MeV and theoretical status”, *Phys. Rev.* **C*70***, 014607 (2004).

[3] U. Tippawan, S. Pomp, A. Atac *et al.*, “Light-ion production in the interaction of 96 MeV neutrons with silicon” , *Phys. Rev.* **C69**, 064609 (2004).

[4] U. Tippawan, S. Pomp, A. Atac *et al.*, “Light-ion production in the interaction of 96 MeV neutrons with oxygen”, *Phys. Rev.* **C73**, 034611 (2006).

[5] U. Tippawan, S. Pomp, J. Blomgren *et al.*, “Light-ion production in the interaction of 96 MeV neutrons with carbon” *Phys. Rev.* **C79**, 064611 (2009).

[6] M. Hayashi, Y. Watanabe, R. Bevilacqua *et al.*, “Neutron induced proton production from carbon at 175 MeV”, *Proc. of 2007 Symp. on Nuclear Data*; JAEA-Conf 2008-008, 62-67 (2008).

[7] S. Hirayama, Y. Watanabe, Y. Naitou et al., *Proc. of the Fifth Int. Symp. on Radiation Safety and Detection Technology ISORD-5,* July 15-17, 2009, Kitakyushu, Japan, in press

[8] R. Bevilacqua, S. Pomp, V. Simutkin et al., "Neutron induced light-ion production from Iron and Bismuth at 175 MeV", *Proc. of the 2009 Int. Workshop on Compound-Nuclear Reactions and Related Topics CNR*2009*, October 5-8, 2009, Bordeaux, France, in press.

[9] H. Iwase, K. Niita and T. Nakamura, "Development of General-Purpose Particle and Heavy Ion Transport Monte Carlo Code", *J. Nucl. Sci. and Technol.* **39**[11], 1142-1151 (2002).

[10] SRIM-2008 , URL : http://www.srim.org/.

[11] S. Dangtip, A. Atac, B. Bergenwall *et al.*, "A facility for measurements of nuclear cross sections for fast neutron cancer therapy", *Nucl. Instr. Meth.* **A452**, 484-504 (2000).

[12] SAID Nucleon Nucleon scattering database. URL: http://gwdac.phys.gwu.edu.

[13] A. Prokofiev, private communication (2007); A. Prokofiev, M. Chadwick, S. Mashink *et al.* "Development and Validation of the ^{7}Li(p,n) Nuclear Data Library and Its Application in Monitoring of Intermediate Energy Neutrons", *J. Nucl. Sci. and Technol., Suppl.* **2**, 112-115 (2002).

[14] Y. Watanabe, T. Fukahori, K. Kosako *et al.*, "Nuclear Data Evaluations for JENDL High-Energy File", *Proc. Int. Conf. on Nuclear Data for Science and Technology*, Santa Fe, USA, Sept. 26-Oct. 1 AIP Conf. Proc. **769**, 326-331 (2005).

[15] K. Niita, S. Chiba, T. Maruyama *et al.*, "Analysis of the (*N,xN′*) reactions by quantum molecular dynamics plus statistical decay model", *Phys. Rev.*, ***C52*,** 2620-2635 (1995).

[16] H.W.Bertini, ORNL-3383, Oak Ridge National Laboratory (1963).

12. Resonance analysis of the ^{7}Li (p, p) reaction to estimate neutron yields by the ^{7}Li (d, n) reaction

Toru Murata
t.murata@ma.point.ne.jp
Former NAIG Nuclear Research Laboratory

As a step of estimation of neutron yields data by the ^{7}Li(d, n) reaction, spectroscopic factors of the DWBA process of the reaction were determined by the resonance analysis of the ^{7}Li(p, p) reaction and by analysis of some experimental data of the ^{7}Li(d, n) reaction with a combined model of resonance and DWBA reactions.

1. Introduction

Evaluation of neutron production data of the deuteron bombardment of ^{7}Li target are under-way in the deuteron energy region below 10 MeV. Compound nuclear states of the ^{7}Li+d reaction have been studied by analyzing experimental data of the ^{7}Li(d, p)^{8}Li reactions[1]. Present study is intended to estimate neutron production by the direct reaction of the ^{7}Li(d, n)^{8}Be reaction. The direct reaction cross sections are calculated with a DWBA code using spectroscopic factors of the final states of ^{8}Be. The spectroscopic factor of a final state is obtained as the ratio of transferred particle width to the single particle width, which is calculated in the optical model potential of the DWBA calculation. For ^{8}Be excited states below proton emission, some experimental data of the (d, n) reactions are available[2] and the evaluation can be made on the data. Above proton binding energy, transferred proton widths are obtained by resonance analysis of the experimental differential cross sections[3] of the ^{7}Li(p, p) reaction. Though resonance analyses of the (p, p) reaction were reported by several authors in some restricted energy region such as that by Brown et al.[4], for the present object, consistent analysis in the wide energy range is required.

As for the ^{7}Li(d, n) reaction, recently, Kyushu University group has analyzed inclusive neutron energy spectrum at Ed=40 MeV, successfully[5] using the Glauber model and so on.

2. Estimation Methods and Results

Nuclear data estimation methods of the ^{7}Li(d, n)^{8}Be reaction in the energy region below incident deuteron energy E_d =10 MeV were divided into the following two processes. Present analysis scheme is shown in Fig.1.

1) Resonance reaction via compound nucleus ^{9}Be

Resonance energies, deuteron widths and proton widths have been determined to reproduce the experimental data of the ^{7}Li(d, p)^{8}Li reaction with the combined model of resonance and DWBA. The proton widths were converted to neutron widths by theoretical calculation using emitted particle penetration factors. Above resonance region, statistical calculation will be applied with the Hauser-Feshbach model.

2) Direct reaction by DWBA calculation with DWUCK4 code[6]

DWBA absolute cross section is given by the following formula using calculated σ_{DW}^{lsj}

with DWUCK4 code for the A(d, n)B reaction; spin and orbital angular momentum relationship : $\left|\vec{I}_B - \vec{I}_A\right| = \vec{j} = \vec{l}_p + \vec{s}$, in the approximation of zero-range and Hulthen type D-wave function.

$$\sigma^{lsj} = \frac{(2I_B+1)}{(2I_A+1)} S_{jl} \frac{1.55}{(2j+1)} \sigma_{DW}^{lsj} \quad , \tag{1}$$

where S_{jl} is the spectroscopic factor of the (j, l) particle transfer reaction and given by the ratio of the particle width of the final state to the single particle width in the optical model potential to obtain distorted waves.

a) ^{8}Be excited states; Ex >17.25 MeV (proton unbound states)

Proton widths were obtained by the present analysis of the ^{7}Li(p, p) reaction using the approximated transition matrix $T_{\alpha l s, \alpha' s' l'}{}^{J}$ and the following differential cross section formula described in the summary paper of the R-matrix theory by Lane and Thomas[7].

$$d\sigma_{\alpha\alpha'}(\theta_{\alpha'}) = \left[(2I_1+1)(2I_2+1)\right]^{-1} \sum_{ss'} (2s+1) d\sigma_{\alpha s \alpha' s'}(\theta_{\alpha'}) , \tag{2}$$

where differential cross section $d\sigma_{\alpha s \alpha' s'}(\theta_{\alpha'})$ is given by the sum of Coulomb scattering amplitude C_α, nuclear scattering B_L term and their interference terms as ;

$$(2s+1)\sigma_{\alpha s \alpha' s'}(\theta_{\alpha'}) = \frac{\pi}{k_\alpha{}^2} \Bigg\{ (2s+1)\left|C_{\alpha'}(\theta_{\alpha'})\right|^2 \delta_{\alpha' s \alpha s'} + \frac{1}{\pi} \sum_L B_L(\alpha' s', \alpha s) P_L(\cos\theta_{\alpha'}) +$$
$$(4\pi)^{-\frac{1}{2}} \sum_{Jl} (2J+1) 2\,\mathrm{Re}\left[i T_{\alpha s' l' \alpha s l}{}^{J} \cdot C_{\alpha'}(\theta_{\alpha'})^* \delta_{\alpha' s' l' \alpha s l} P_{l'}(\cos\theta_{\alpha'}) \right] \Bigg\} d\Omega_{\alpha'} \tag{3}$$

where notations are the same as those defined in the paper by Lane and Thomas[7].

For the collision matrix calculation, sharp change of elastic scattering widths are assumed at the threshold energy of the ^{7}Li(p, n_0)^{7}Be reaction; E_p(Lab.)=1.880 MeV. Results of the present analysis is shown in Fig.2.

b) ^{8}Be excited states; Ex <17.25 MeV (proton bound states)

For the ground-state and the 1st excited state of ^{8}Be, differential cross sections were measured by Nussbaum with two scintillators TOF type spectrometer and by Johnson-Trail with proton recoil telescope type spectrometer, who reported that the experimental data of the 2nd excited state include some continuum neutron spectrum and intensity of the broad 2nd excited state is less than 10% of the ground-state intensity. For the 3rd excited state; Ex=16.64 MeV, using TOF method, Dietrich-Cranberg measured neutron intensity of the forward angle at several energies of incident deuteron energies from Ed= 3.59 to 7.25 MeV.

These data were analyzed with the combined model of resonance and DWBA. Results of the analysis are shown in Fig.3 and Fig.4.

Left side of Fig.3 shows the fittings for the incident energy E_d=1.05 MeV and the experimental data for the (d,n_0) reaction were reproduced with the DWBA calculation only, and the (d,n_1) reaction were reproduced with 60 % DWBA and 40% resonance reaction. Right side of Fig.3 shows the cases for Ed=1.98 MeV and the (d, n_0) data were reproduced with 70 % DWBA and 30 % resonance. The (d, n_1) data, reported to include some continuum neutrons, were reproduced with 50 % DWBA and 50 % resonance reactions. The spectroscopic factors based on the experimental data by Nussbaum and by Johnson-Trail were somewhat different and average values were adopted for the (d, n_0) and the (d, n_1) reactions.

For the 2nd excited state, upper limit of the spectroscopic factor was determined using the information given by Johnson-Trail. This broad level will be almost composed of 2·^{4}He and has very small amplitude of the ^{7}Li core + p configuration, So, very small spectroscopic factor will be expected for the ^{7}Li(d, n_2)^{8}Be reaction.

For the 3rd excited state, resonance contributions at forward angle is calculated using neutron widths estimated from the proton widths determined in the analysis of the ^{7}Li(d, p)^{8}Li reactions, and the contribution was about 20% as is shown in Fig.4. The 4th excited state has about same excitation energy and the same spin-parity as those of the 3rd excited state, so equal spectroscopic factor is adopted.

For these excited states, spectroscopic factors of ^{8}Be states are summarized in Table 1, along with the resonance parameters of the ^{7}Li(p, p) reaction. Single particle widths of transferred protons were given in the output file of the DWUCK4 code.

3. Discussion and Conclusion

Though the first step estimation of the spectroscopic factors of the direct ^{7}Li(d, n)^{8}Be reactions have been made, ambiguities of the factors will be large and adjustments should be made to reproduce some experimental data of bulk neutron productions measured with a flat response long counter, after estimation of neutron productions by other processes such as the ^{7}Li(d, p)^{8}Li→^{7}Li+n and the ^{7}Li(d, α)^{5}He→^{4}He+n reactions. For the ^{7}Li(d, p)^{8}Li→^{7}Li+n reactions, spectroscopic factors will be obtained using the well observed resonance parameters of the ^{7}Li+n reactions.

References

1) T. Murata, The 2008 Symposium on Nuclear Data; Poster 20
2) C. Nussbaum, Helv. Phys. Acta 42,361 (1969),
C. H. Johnson, C.C. Trail, Phys. Rev. 133, B1183 (1964),
F. S. Dietrich, L. Cranberg, Bull. Am. Phys. Soc. 5,493 (1960)
3) W. D. Warters et al., Phys.Rev.91,917(1953),
P. R. Malmberg, Phy.Rev.101,114(1956),
R. Gleyvod et al., Nuclear Physics 63,650(1965)
4) L. Brown et al., Nucl. Physics. A260,353(1973)
5) T. Ye, Y. Watanabe, K. Ogata, Phys.Rev.C80,014604 (2009)
6) P. D. Kunz, *Distorted Wave Code DWUCK4*, Univ. of Colorado (1974)
7) A. M. Lane, R. G. Thomas, Rev. Mod. Phys. 30,257(1958)

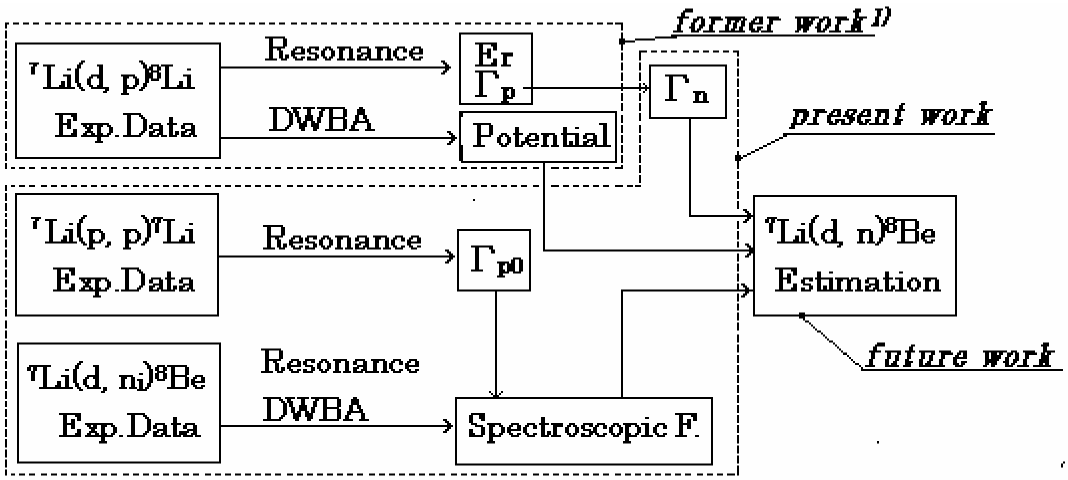

Fig.1 Present analysis scheme of the ^{7}Li(d, n)^{8}Be reaction (exclusive)

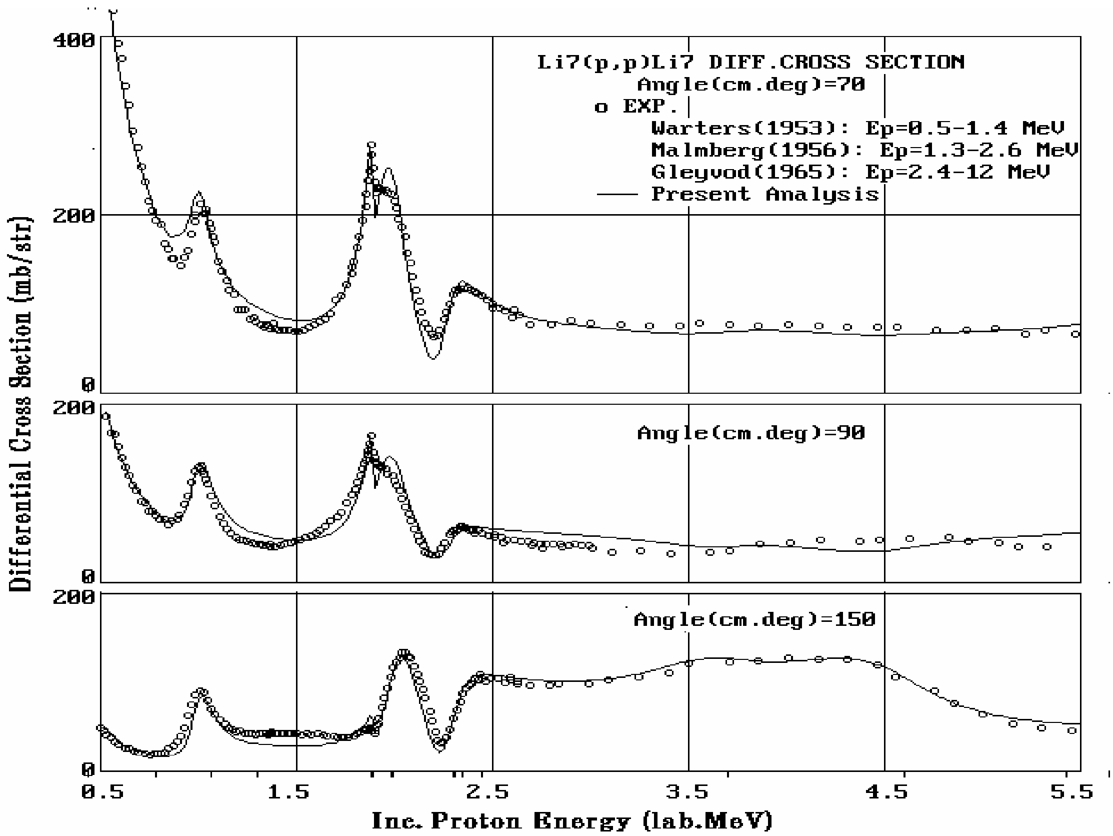

Fig.2 Results of resonance analysis of the ^{7}Li(p,p)^{7}Li reactions comparing with the experimental data[3] for scattering angles at 70, 90 and 150 degrees in center of mass system. Open circles represent experimental data and solid lines shows analysis results. Small lines below horizontal axis represent the resonance energies

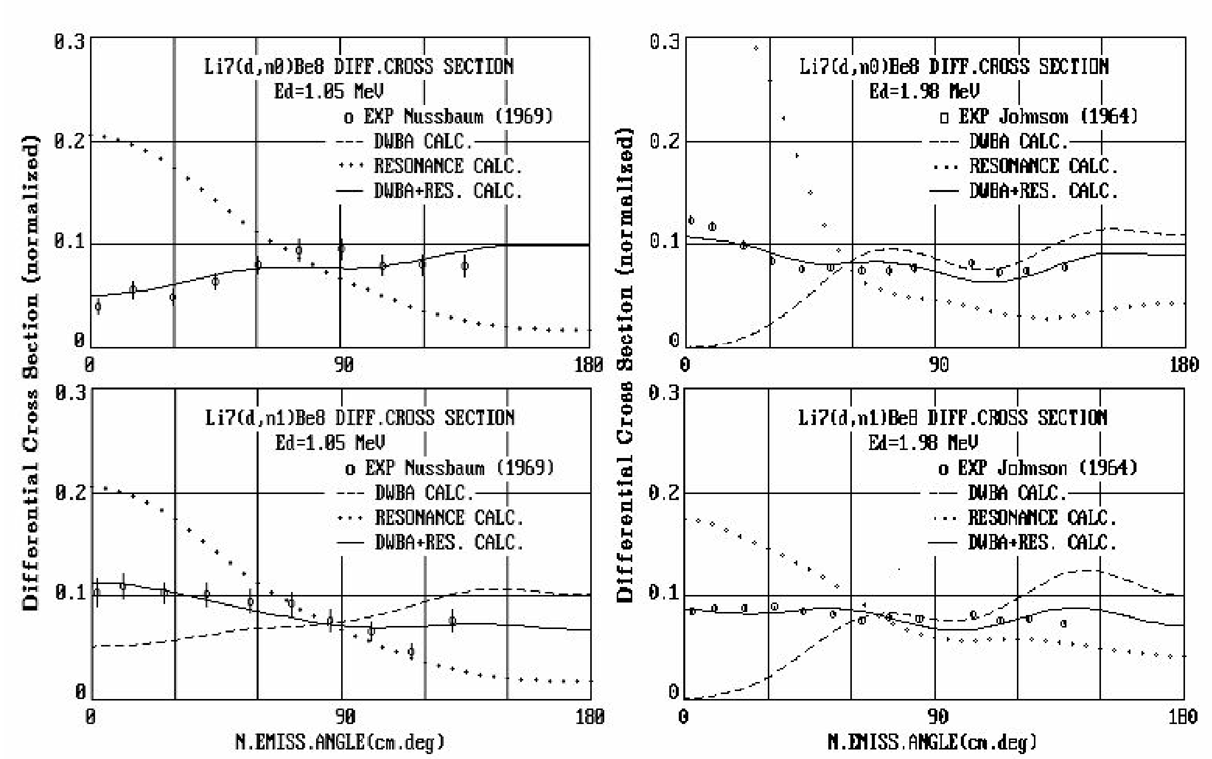

Fig.3 Experimental differential cross section fittings with a combined model of resonance and DWBA to determine the normalization factors of the DWBA calculation of the ^{7}Li(d,n$_0$) and ^{7}Li(d,n$_1$) reactions. Left side figures for E_d=1.07 MeV and right side for E_d=1.98 MeV

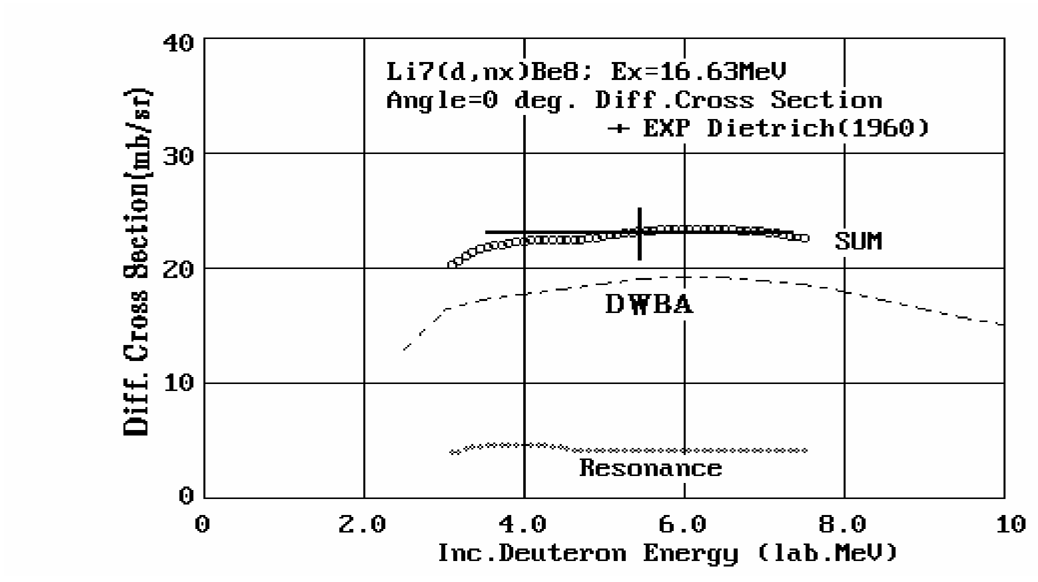

Fig.4 Forward angle (0 deg.) differential cross section of the ^{7}Li(d,nx)^{8}Be reaction. for ; Ex=16.63 MeV state Experimental data are measured by Dietrich and Cranberg in the incident energy region Ed(lab.)=3.59-7.25 MeV. The DWBA calculation was made with DWUCK4 code and shown by dashed line. Dotted line shows the results of the resonance calculation. Sum of these results are shown in circled line.

Table 1 Fitting parameters of resonance structures of the $^{7}Li(p,p)^{7}Li$ reaction and spectroscopic factors

Er	Ex	J^{π}	L_p	S	Γ_t	Γ_p	Γ_{sp}	SF.
—	0	0+	1	—	—	—	—	0.59
—	3.04	2+	1	—	—	—	—	0.37
—	11.4	4+	3	—	—	—	—	<6E−03
—	16.63	2+	1	—	—	—	—	0.35
—	16.92	2+	1	—	—	—	—	(0.35)
0.44	17.64	1+	1	2	5.25E−03	2.62E−03	3.52E−02	7.44E−02
0.78	17.94	1+	1	2	1.31E−01	1.31E−04	3.02E−01	4.34E−04
1.06	18.18	1+	1	2	1.97E−01	7.08E−02	3.27E−01	2.17E−01
1.30	18.39	1−	0	1	7.87E−01	1.42E−01	1.07E+01	1.33E−02
1.88	18.90	2−	0	2	1.75E−01	8.22E−02	2.79E+01	2.95E−03
1.89	18.91	2−	0	2	5.25E−02	5.25E−04	2.74E+01	1.92E−05
1.98	18.99	3+	1	2	1.75E−01	7.00E−02	1.42E+00	4.93E−02
1.99	19.00	2+	1	2	2.19E−01	3.94E−02	1.42E+00	2.78E−02
2.30	19.27	2−	0	2	1.92E−01	4.81E−02	1.21E+01	3.98E−03
2.31	19.27	3+	1	2	1.75E−01	3.15E−02	4.20E+00	7.50E−03
2.35	19.31	2+	1	2	2.62E−01	7.87E−02	4.43E+00	1.78E−02
2.45	19.40	1−	0	1	5.68E−01	7.96E−02	1.49E+01	5.34E−03
3.70	20.49	3−	2	1	7.00E−01	1.12E−01	7.78E−01	1.44E−01
4.60	21.28	4−	2	2	8.74E−01	2.19E−01	1.42E+00	1.54E−01
5.43	22.00	1−	0	1	2.62E+00	3.94E−01	1.27E+01	3.10E−02
5.65	22.20	2+	1	1	8.74E−01	1.75E−01	3.30E+01	5.30E−03

Er: Resonance energy (lab.MeV), Ex: Excitation energy of ^{8}Be (MeV)

J^{π}: Spin-parity of the excited state, L_p: Orbital angular momentum of transferred proton

S: Channel spin of the reaction, Γ_t: Total width of the resonance (cm.MeV)

Γ_p; Proton elastic width of the resonance (cm.MeV), Γ_{sp}: Single particle width of the state (cm.MeV)

SF: Spectroscopic factor of the state

13. Development of Web-based User Interface for Evaluated Covariance Data Files

Tomoaki TOGASHI[1], Kiyoshi KATŌ[1], Ryusuke SUZUKI[2], Naohiko OTUKA[3]

[1]Division of Physics, Graduate School of Science, Hokkaido University, Sapporo 060-0810, Japan

[2]Department of Medical Physics, Hokkaido University Hospital, Sapporo 060-8648, Japan

[3]Nuclear Data Section, Department of Nuclear Sciences and Applications, International Atomic Energy Agency, A-1400 Wien, Austria

e-mail: toga@nucl.sci.hokudai.ac.jp

We develop a web-based interface which visualizes cross sections with their covariance compiled in the ENDF format in order to support evaluated covariance data users who do not have experience of NJOY calculation. A package of programs has been constructed without aid of any existing program libraries.

1. Introduction

One can estimate uncertainties in various reactor characteristics by using error propagation calculation on the basis of sensitivity coefficients and evaluated nuclear reaction cross section covariances, which are now intensively evaluated for general-purpose data libraries and compiled in the ENDF format. However, the ENDF format for covariance data is too complicated for users who do not have experience of utility codes for the covariances in the ENDF format (e.g. ERRORJ). Therefore, we are developing a web-based interface which visualizes cross sections with their covariances in the resolved resonance region (MF=2 and 32) and above the region (MF=3 and 33) compiled in the ENDF formats in order to support evaluated covariance data users who do not have experience of NJOY calculation. For this purpose, we construct a package of programs to process and display covariance data compiled in the ENDF format without aid of any existing program libraries.

2. Formulation

In the resonance region, the cross section covariances are not compiled in the ENDF format [1]. Alternatively, the resonance parameter covariances $COV(P,P')$ are compiled in MF = 32. Therefore, one must calculate the cross section covariances in the resonance region $COV(\sigma_m(E),\sigma_l(E'))$ as

$$COV(\sigma_m(E), \sigma_l(E')) = \sum_{P,P'} \frac{\partial \sigma_m(E)}{\partial P} COV(P,P') \frac{\partial \sigma_l(E')}{\partial P'},$$

where $\sigma_m(E)$ denotes the cross section of the reaction type m (e.g. elastic, capture) and

$$\frac{\partial \sigma_m(E)}{\partial P}$$

is the sensitivities to the resonance parameters *P*. In the above equation, we calculate the cross sections $\sigma_m(E)$ by using the resonance parameters *P* and the resonance formula compiled in MF = 2, and the sensitivities are calculated as the perturbation to *P*: $(\sigma_m(P+\Delta P) - \sigma_m(P))/\Delta P$. In general, the covariances between the cross sections of different reaction types $\sigma_m(E)$ and $\sigma_l(E')$ are defined, however, the current version of our system covers only the covariances for the same reaction type ($m = l$). The cross sections and covariances above the resonance region or as the backgrounds of the resonances are compiled in MF = 3 and 33, respectively. If the backgrounds in the resonance region exist, the data in MF = 3 and 33 are added to the cross sections and covariances of the resonances, respectively. The current version of our system can process the data of NI-type subsection and NC-type subsection with the flag LTY = 0 in MF = 3 and 33.

In calculating the group-wise cross sections, one integrates the cross sections $\sigma(E)$ over each energy region *I* defined by the group structure with the weighting function $w(E)$ as

$$\frac{1}{w_I} \int_I w(E)\, \sigma(E)\, dE\,,$$

where

$$w_I \equiv \int_I w(E)\, dE\,.$$

And then, the group-wise covariances are calculated as the matrix for the energy regions *I* and *J*:

$$\frac{1}{w_I w_J} \int_I dE \int_J dE'\, w(E)\, w(E')\, COV(\sigma_m(E), \sigma_l(E'))\,.$$

In the resonance region, the above equation becomes

$$\sum_{P,P'} D_m^I(P) COV(P,P') D_l^J(P')\,,$$

where one must calculate the followings:

$$D_m^I(P) \equiv \int_I dE\, w(E) \frac{\partial \sigma_m(E)}{\partial P}\,.$$

In the calculation of the group-wised quantities, we adopt 44 groups [2] as the energy group structure with the weighting function $w(E)$ described in Ref. [3].

3. System and Applications

In our interface, a Fortran program reads data in the ENDF format and calculates cross sections, their standard deviations and covariances. And then, the obtained physical quantities are displayed on web browsers by connecting this Fortran program with a CGI script written in Perl. In addition, the function to display group-wise cross sections with their covariances is also attached to this interface. Note that all modules used in this system are constructed by us and therefore there is no restriction due to licenses of other libraries.

In Fig.1, the initial screen of the interface is shown. All users may input library name (“Library”), target nucleus (“Target”), reaction type (“Reaction”), neutron incident energy range (“E(min)[eV]” and “E(max)[eV]”), and quantity (“Physical Quantity”) in this screen. In this interface, one can select JENDL-3.3 [4], ENDF/B-VII.0 [5], or JEFF-3.1 [6] for “Library”, and total, elastic, fission, or capture for “Reaction”. “Accuracy” means the allowed uncertainty due to interpolation [%] and determines the intervals of mesh δE to draw the graphs and to calculate the integrations in the group-wise quantities in this case:

$$\frac{|\sigma(E+\delta E)-\sigma(E)|}{\sigma(E)}\times 100,\quad \frac{|\sigma(E+\delta E)-\sigma(E)|}{\sigma(E+\delta E)}\times 100\,.$$

Users select moderate (5%) or high accurate (0.1%) precision in “Accuracy”, which will accept any accuracy values in future versions.

As the “Physical Quantity”, this interface can visualize the cross sections, the cross sections with their standard deviation, the group-wised cross sections and standard deviations, and the group-wised covariances. The standard deviation can be calculated by the covariance as $\sqrt{COV(\sigma(E),\sigma(E))}$. The diagonal elements of group-wised covariances are normalized to 1 (0 in the unevaluated regions) to form correlation matrices. After providing all information and submission the request by the “plot” button (or the “next” button in the case of the covariance), data are plotted on web browsers.

In Figs. 2-5, the applications for the ^{156}Gd(n,total) reaction are shown as examples.

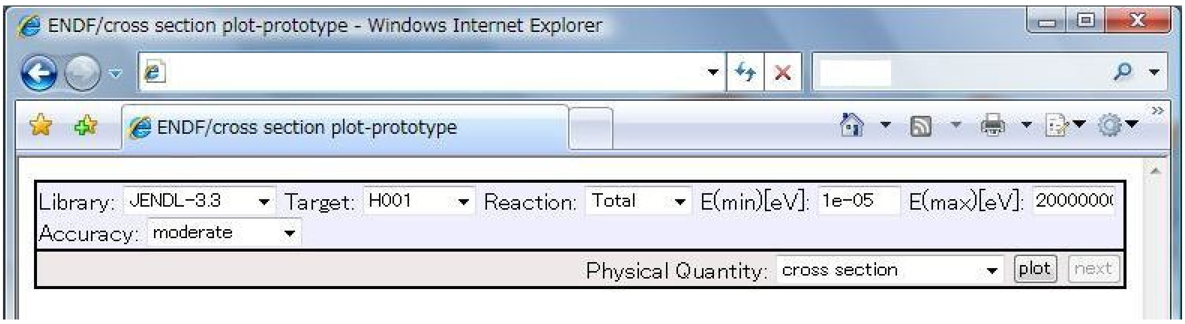

Fig.1. The initial screen in the interface.

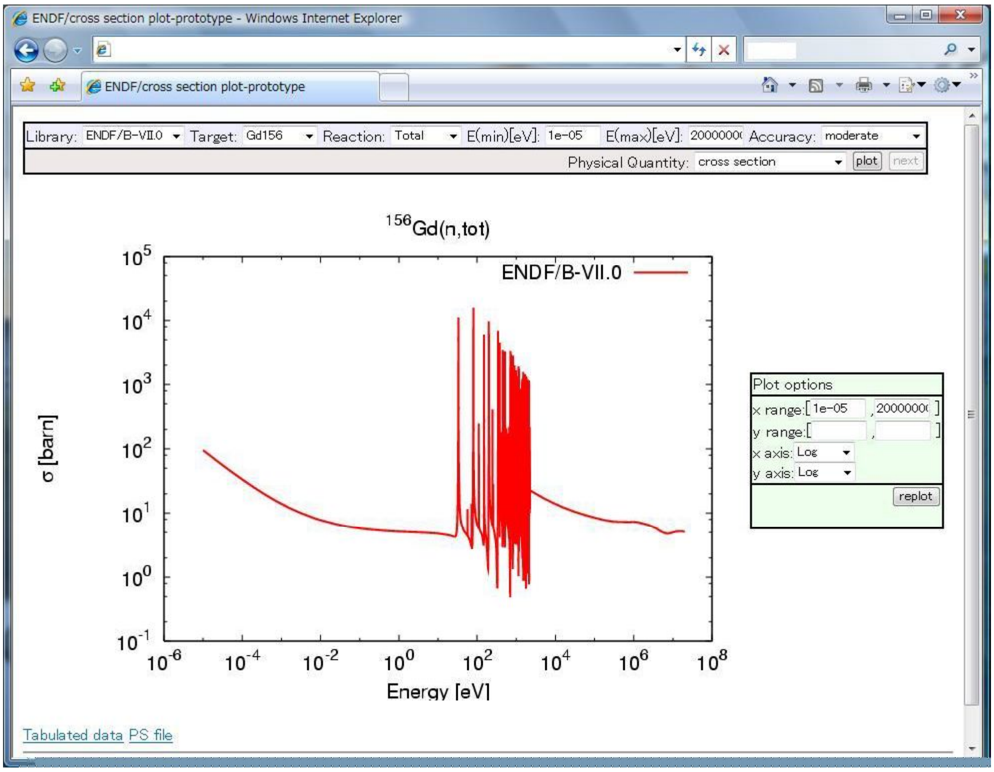

Fig.2. Output of the cross sections in the ^{156}Gd(n,total) in the interface.

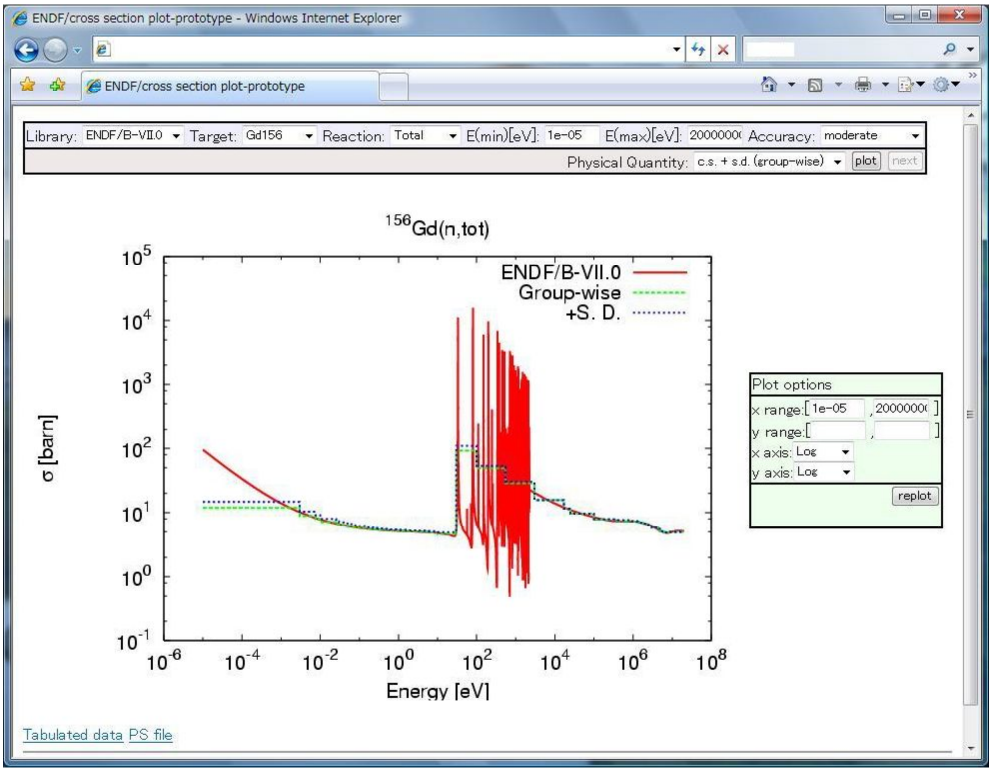

Fig.3. Output of the group-wised cross sections with their standard deviation in the ^{156}Gd(n,total) in the interface.

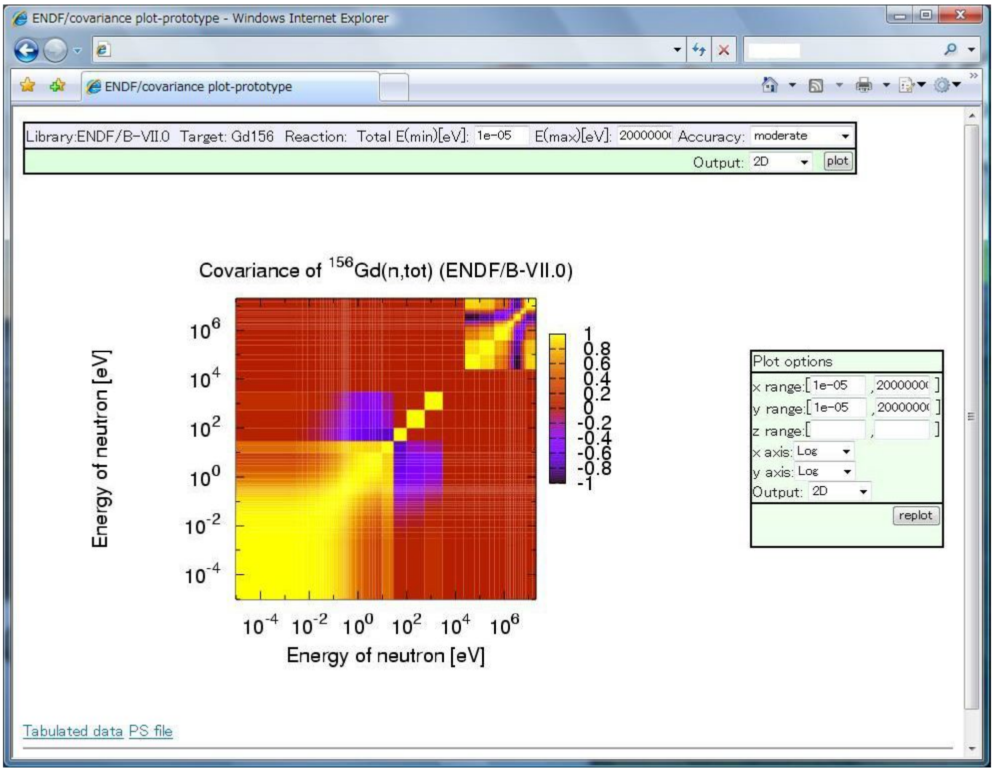

Fig.4. 2-dimesions output of the group-wised covariance in the ^{156}Gd(n,total) in the interface.

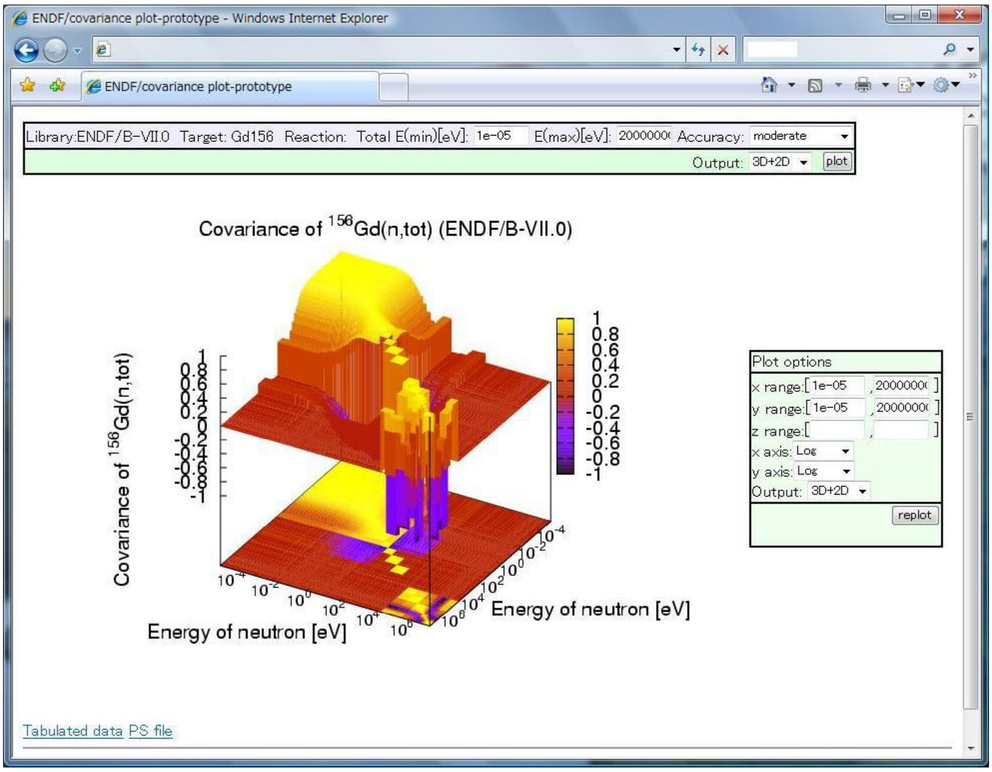

Fig.5. 3-dimesions output of the group-wised covariance in the ^{156}Gd(n,total) in the interface.

4. Summary

We developed a web-based interface which visualizes cross sections with their covariances in the resolved resonance region (MF=2 and 32) and above the region (MF=3 and 33) compiled in the ENDF formats. We constructed a package of programs free to be used without use of any existing program libraries to support general users who have no experience of NJOY calculation.

Acknowledgement

Present study is the result of "Study on nuclear data by using a high intensity pulsed neutron source for advanced nuclear system" entrusted to Hokkaido University by the Ministry of Education, Culture, Sports, Science and Technology of Japan (MEXT).

References

[1] *ENDF-102 Data Formats and Procedures for the Evaluated Nuclear Data File ENDF/B-VI and ENDF/B-VII*, BNL-NCS-44945-05-Rev., Brookhaven National Laboratory, June 2005.

[2] K. Ivanov, M. Avramova, I. Kodeli and E. Sartori, NEA/NSC/DOC(2007)23 JT03238980, p.77.

[3] t2.lanl.gov/njoy/grou02.html.

[4] K. Shibata, T. Kawano, T. Nakagawa, O. Iwamoto, J. Katakura, T. Fukahori, S. Chiba, A. Hasegawa, T. Murata, H. Matsunobu, T. Ohsawa, Y. Nakajima, T. Yoshida, A. Zukeran, M. Kawai, M. Baba, M. Ishikawa, T. Asami, T. Watanabe, Y. Watanabe, M. Igashira, N. Yamamuro, H. Kitazawa, N. Yamano, and H. Takano: "Japanese Evaluated Nuclear Data Library Version 3 Revision-3: JENDL-3.3", J. Nucl. Sci. Technol. **39**, 1125 (2002).

[5] M.B. Chadwick, P. Oblozinsky, M. Herman, N.M. Greene, R.D. McKnight, D.L. Smith, P.G. Young, R.E. MacFarlane, G.M. Hale, S.C. Frankle, A.C. Kahler, T. Kawano, R.C. Little, D.G. Madland, P. Moller, R.D. Mosteller, P.R. Page, P. Talou, H. Trellue, M.C. White, W.B. Wilson, R. Arcilla, C.L. Dunford, S.F. Mughabghab, B. Pritychenko, D. Rochman, A.A. Sonzogni, C.R. Lubitz, T.H. Trumbull, J.P. Weinman, D.A. Brown, D.E. Cullen, D.P. Heinrichs, D.P. McNabb, H. Derrien, M.E. Dunn, N.M. Larson, L.C. Leal, A.D. Carlson, R.C. Block, J.B. Briggs, E.T. Cheng, H.C. Huria, M.L. Zerkle, K.S. Kozier, A. Courcelle, V. Pronyaev, and S.C. van der Marck: "ENDF/B-VII.0: Next Generation Evaluated Nuclear Data Library for Nuclear Science and Technology", Nucl. Data Sheets **102**, 2931 (2006).

[6] A. Koning, R. Forrest, M. Kellett, R. Mills, H. Henriksson and Y. Rugama: "The JEFF-3.1 Nuclear Data Library", JEFF Report 21 (2006).

14. Development of CdTe detector for BNCT-SPECT

Taiki Mukai*, Isao Murata, Masao Ito, Hiroyuki Miyamaru
Division of Electrical, Electronic and Information Engineering, Osaka University
Yamada-oka 2-1, Suita, Osaka, 565-0871 Japan
*E-mail: tmukai@ef.eie.eng.osaka-u.ac.jp

Abstract

Boron neutron capture therapy (BNCT) is a radiation therapy which can destroy tumor cells, simultaneously suppressing influence against healthy cells. However, at present its treatment effect is just estimated numerically by the currently used treatment protocol. Since the actual treatment effect cannot be known directly now, we are developing a SPECT device for measuring the treatment effect of BNCT in real time. In the present study, we examined the feasibility of BNCT-SPECT when a CdTe detector was used.

Ⅰ. Introduction

Boron neutron capture therapy (BNCT) is a radiation therapy which can destroy tumor cells, simultaneously suppressing influence against healthy cells. The principle of BNCT is as follows. At first, ^{10}B is locally concentrated in tumor cells. Then, low-energy neutrons such as thermal neutrons are irradiated from outside. As the result, only the tumor cells including boron are selectively destroyed by charged particles emitted from ^{10}B(n,α)^{7}Li reaction. Produced α particle and ^{7}Li have path lengths of about 8 and 4 μm, respectively. Since these lengths are comparable to a cell diameter, only the tumor cells are killed and the effect to normal tissues can be suppressed substantially.

The actual treatment effect of BNCT is estimated by making product of ^{10}B concentration and thermal neutron flux intensity. The distribution of ^{10}B concentration can be estimated by using positron emission tomography (PET) just before an actual BNCT, for instance. However, the ^{10}B concentration is changing gradually, meaning the estimated distribution by the PET is just a reference. The thermal neutron flux intensity can be estimated by JCDS developed by JAEA, for example. Under these predicted conditions, the irradiation schedule is made prior to BNCT. After starting irradiation, with help of supplemented means like activation foils, small neutron detectors and so on, the ending time of irradiation is determined. However, by this procedure it was reported that the convalescence did not follow the expectation before. Also, there were different convalescences observed at KUR and JRR-4 even with an equal protocol. This fact indicates that it is not clear whether the expected treatment effect is really obtained with the current BNCT procedure mentioned above. Therefore it is necessary to establish a new method that could measure the treatment effect especially in real time.

As is well known, in principle, three-dimensional treatment effect of BNCT can be estimated by measuring 478keV gamma-rays emitted from the exited state of ^{7}Li nucleus created by ^{10}B(n,α)^{7}Li reaction. In addition, it could be realized by using a SPECT device. In the present study, we examined the feasibility of BNCT-SPECT when a CdTe detector was used together with a quite narrow tungsten collimator.

Ⅱ. Measurement

A. Principle of Measurement

The principle of the present real-time measuring technique is as follows. As well known, $^{10}B(n,\alpha)^7Li$ reaction as in the next two equations is utilized for BNCT.

$$^{10}\mathbf{B} + \mathbf{n} \rightarrow \alpha + {}^{7}\mathbf{Li} + \mathbf{2.79\ MeV} \qquad \mathbf{(6.1\%)}$$

$$\rightarrow \alpha + {}^{7}\mathbf{Li}^{*} + \mathbf{2.31\ MeV} + \gamma\ \mathbf{(478\ keV)} \qquad \mathbf{(93.9\%)}$$

Out of produced ^7Li, 94 % of it is in an excited state, from which 478 keV gamma-ray is emitted by a transition from the first excited state to the ground state in about 10^{-14} s. The attenuation coefficient of this photon in tissue is about 0.1 cm^{-1}. Thus, this gamma-ray escapes from the body to a large extent. If the position and intensity of the gamma-ray emission are measured, the information is equivalent to the reaction rate distribution of $^{10}B(n,\alpha)^7Li$ reaction, which can be regarded as the three-dimensional BNCT effect. The measurement could be realized by a so-called SPECT system as shown in Fig.1 schematically. And using one-by-one estimation based on the Bayes' theorem, three-dimensional visualization of the BNCT effect would become possible in real time.

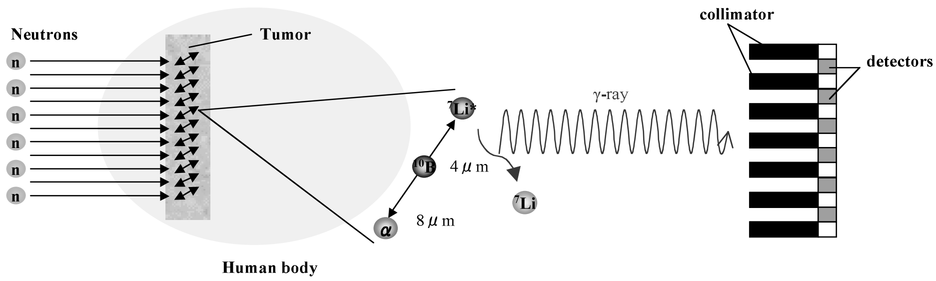

Fig.1 Conceptual figure of BNCT-SPECT

B. Present status of BNCT-SPECT development

In reality, however, it is not so straightforward to realize the 478 keV gamma-ray measurement in BNCT. In case of a normal SPECT measurement, no radiations exist except those used for acquiring a tomography image. However, in the case of BNCT-SPECT, the thermal neutron intensity used reaches ~10^9n/sec/cm^2 around the tumor. The cross section of $^{10}B(n,\alpha)^7Li$ reaction is quite large, i.e., about 3840 barns. However the ^{10}B concentration is quite low, i.e., about 10 ppm in the tumor. Hence, the intensity of 478 keV gamma-rays emitted from $^{10}B(n,\alpha)^7Li$ reaction becomes much smaller than that of secondary gamma-rays emitted by various (n,γ) reactions and direct signals in the CdTe detector directly produced by incident neutrons. Thus it becomes quite hard for a conventional SPECT to selectively measure 478 keV gamma-rays in a strong radiation field including a lot of background gamma-rays.

Backgrounds to be removed in the present measurement include as in the following.

(1) 2223 keV gamma-rays produced by $^1H(n,\gamma)^2H$ reaction at around the tumor.

(2) Direct signal due to neutrons produced by scattering of incident neutrons at around the tumor and capture

gamma-rays except from ^1H produced there.

(3) Direct signal due to neutrons produced by scattering of incident neutrons at around the structural materials and wall surrounding the target and capture gamma-rays produced there.

Especially, contribution (1) becomes a large background. The point is to accurately measure the photopeak of 478 keV gamma-ray even in a very bad S/N-ratio field, i.e., the peak might be hiding in or be overlapped with a dominantly existing Compton continuum. On the other hand, direct contribution from neutrons of (2) and (3) is not high in case of using nuclear reactors as a neutron source.

The above discussion shows the reason why the presently proven techniques could not be applied to this measurement the past. Kobayashi et al.[1)] studied possibility of SPECT for BNCT with HpGe and CdTe semiconductor detectors. These detectors have an enough ability to measure gamma-rays of interest. However, in case of HpGe, the system becomes too large and requires cooling. In case of CdTe, the detector can be used at room temperature. But the detector efficiency is rather low. They stated that one detector must measure gamma-rays of about 100 counts from 1 cm^3 tumor located in the deepest place.

According to our preliminary research, however, one must consider that the background intensity becomes quite large. And even in this case one detector should acquire around 1000 counts to achieve an acceptable statistical accuracy. This is however not so easy task especially in order to realize a good spatial resolution of about mm order.

C. Requirements for BNCT-SPECT

The requirements to achieve BNCT-SPECT are summarized as follows:

(1) Measuring time should be around 30 minutes, because most clinical irradiations are completed in less than 1 hour.

(2) Spatial resolution should be less than several mm.

(3) Statistical accuracy should be less than several %, meaning one detector should measure about 1000 counts under conditions of (1) and (2).

For the above requirements, the detector should be small and should have an enough large sensitivity. We thus employed a CdTe device as an elemental detector for the BNCT-SPECT. However, it is difficult to meet these requirements with a marketed CdTe. A good idea that could improve the spatial resolution and count rate of the detector is necessarily found.

D. Proposed technique

The presently proposed measuring technique is shown in Fig.2. Generally, CdTe detectors available on the market have a large area perpendicular to the radiation incidence direction, and the thickness of the incidence direction is small. Therefore, if the CdTe detector is arranged so that gamma-rays are incident to the CdTe detector from the side surface, the spatial resolution and count rate are improved simultaneously.

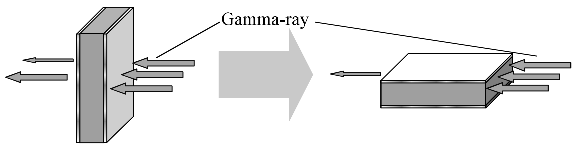

Fig.2 Proposed technique to improve detector efficiency and spatial resolution

Ⅲ. Analysis

A. Calculation

Simulation calculations were performed with MCNP-4C[2)] and JENDL-3.3 as a cross section library. The calculation model is shown in Fig.3. The tumor is modeled as a cylindrical phantom of 2 cm in diameter and 2 cm long, filled with boric acid solution including 10~100 ppm ^{10}B. The thermal neutron flux intensity is 10^9n/sec/cm^2 for 10 ppm and 10^8n/sec/cm^2 for 100 ppm, because it is assumed in the present study that the irradiation time is fixed to be 30 min. The distance between the tumor and the front edge of the collimator is 21 cm considering the position of treatable tumors in human brain. The pulse height spectra were calculated with F8 tally of MCNP. We adopted two steps calculations as follows. In the first step, the gamma-ray source term was calculated with the tumor phantom to which neutrons are incident. In the second step, with the obtained gamma-ray source of the phantom, gamma-ray transport calculations were carried out with the phantom and detector model with a tungsten collimator of 2 mm in diameter. Also, separate calculations for 478 and 2222 keV gamma-rays were performed and the results are summed up to make the real spectrum to be observed in an actual BNCT.

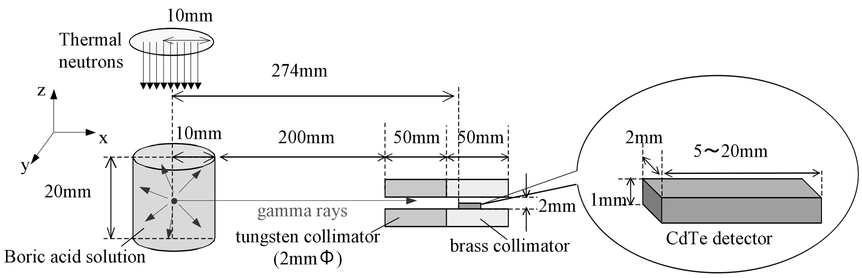

Fig.3 Calculation model by MCNP

B. Discussion

Table 1 shows the calculation results. The count rate for the case of 5 mm thickness seems to be a little small. On the other hand, it is enhanced up to 0.58 cps if using a thicker one of 20 mm, as shown in Fig.4. One thousand counts per 30 minutes could be accomplished. In this case, the spatial resolution is less than 8 mm, as shown in Fig.5 and Fig.6. And the statistical error is suppressed within 5%. It means that the detector could meet the requirement for realization of the BNCT-SPECT. However, a problem remains that in actual case there exist a lot of other backgrounds caused by incident neutrons as mentioned earlier in Sec. II .B. We need to check up the background contribution in a real BNCT case.

Table1. Calculation results for 5 cases

Case.	^{10}B [ppm]	Neutron flux [/cm^2/sec]	Detector thickness [mm]	0.478MeV (^{10}B(n, α)^{7}Li) [cps]	Statistical error [%]
1	10	10^9	5	0.221	7.84
2	10	10^9	10	0.387	5.94
3	10	10^9	15	0.499	5.33
4	10	10^9	20	0.580	4.89
5	100	10^8	20	0.569	3.34

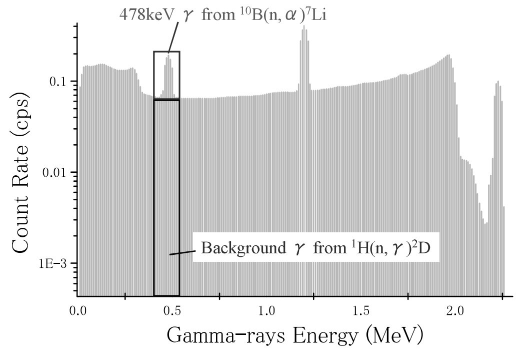

Fig.4 Pulse height spectrum for the case of 20 mm thick CdTe detector

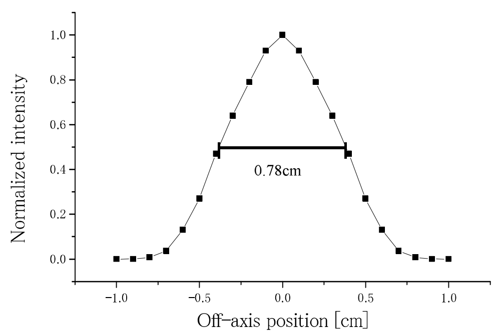

Fig.5 Spatial resolution of detector (y-axis)

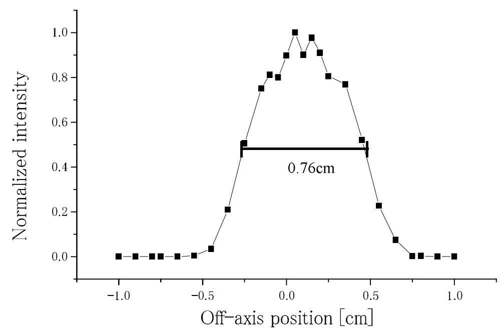

Fig.6 Spatial resolution of detector (z-axis)

C. Hemagglutinating virus of Japan envelope (HVJ-E)

Recently a new boron agent with an empty virus named HVJ-E has been proposed by Kaneda et al. of Osaka University[3)]. By using it, the concentration of ^{10}B in the tumor would become 10 times or more higher than conventional agents[4)]. In this case, the neutron flux intensity can be decreased down to 1/10, and the gamma-ray background of 2.22MeV hence becomes 1/10. As shown in Table1 (Case 5), the statistical error is improved down to 3.3 %.

IV. Future work

We are carrying out basic research & development for the BNCT-SPECT with a radiation line sensor. This line sensor consists of 64 CdTe detectors as shown in Fig.7. A tungsten collimator having 32 holes, each diameter of which is 0.5 mm, is used together. Researches are underway by using this sensor and CdTe detectors of 1×2 mm^2 and 20 mm in thickness (Fig.8) in order to confirm the feasibility of the BNCT-SPECT. It is planned to do test measurements in a hospital to confirm the background level and the intactness of the CdTe detector in such a high background field.

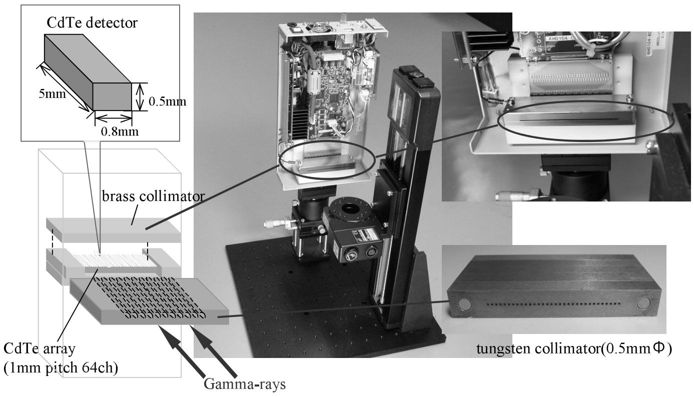

Fig.7 A line sensor with 64 CdTe detector array device

Fig.8 CdTe detector 1×2×20 mm thick

Ⅴ. Conclusion

In present study, we have carried out the feasibility study of BNCT-SPECT. We employed thick CdTe detectors with a quite narrow collimator and performed calculations to obtain basic data for realization of BNCT-SPECT image keeping a good spatial resolution. From the detector response calculations, it was confirmed that the sufficient number of 478keV prompt gamma-rays (more than 1000 counts for a statistical error of within 5%) could be measured in 30 minutes in the case of 1×2×20 mm thick CdTe detector with the collimator of 2 mm in diameter. It means that the detector could meet the requirement for realization of the BNCT-SPECT. Now we are developing two detector systems for examination of the BNCT-SPECT. One is a line sensor with 64 CdTe detector array device. The other one is very thick CdTe detectors of 1×2 mm^2 and 20 mm in thickness. After test measurements, we will carry out gamma-ray spectrum measurement in a real clinical situation including all the possible backgrounds to confirm the applicability of the presently proposed CdTe decvice to the BNCT-SPECT.

References

1) T. Kobayashi et al. “A noninvasive dose estimation system for clinical BNCT based on PG-SPECT—Conceptual study and fundamental experiments using HPGe and CdTe semiconductor detectors,” Med. Phys.27 (9), 2124-2131 (2000)

2) J. F. Briesmeister, (Ed): “MCNP-A general Monte Carlo N-particle transport code, Version 4C, LA-13709, Los Alamos National Laboratory

3) Y. Kaneda et al. “Hemagglutination virus of Japan (HVJ) envelope vector as a versatile gene delivery system,” Mol. Ther. 6, 219-226 (2002)

4) M. Sakai et al “Thermal neutron field with D-T neutron source for BNCT”, Proc. Fifth Int. Sym. on Radiation Detection Technol. (ISORD-5), July 15-17, 2009, Kitakyushu, Japan, to be published

15. Analysis of proton-induced reactions by using simulation

Hiroki IWAMOTO[1*], Yosuke IWAMOTO[2], Yuichi HIRATA[3], Naohiko OTUKA[4], and Koji NIITA[5]
[1] *Department of Applied Quantum Physics and Nuclear Engineering, Kyushu University, Motooka 744, Nishi-ku, Fukuoka 819-0395, Japan*
[2]*Japan Atomic Energy Agency, Tokai-mura, Naka-gun, Ibraki 319-1195, Japan*
[3]*RADONET, Kokubunji, Tokyo 185-0001, Japan*
[4]*Nuclear Data Section, Department of Nuclear Sciences and Applications, International Atomic Energy Agency, A-1400 Wien, Austria*
[5]*Research Organization for Information Science and Technology, Tokai-mura, Naka-gun, Ibaraki 319-1106, Japan*
*E-mail: iwamoto.hiroki@jaea.go.jp

Energy spectrum of proton, neutron, composite particles (deuteron, triton, ^{3}He, ^{4}He) for p(175 MeV) + ^{58}Ni and p(62.9 MeV) + ^{208}Pb reactions are analyzed by using the Bertini and ISOBAR models implemented in PHITS and the INC-FRG model.

1. Introduction

Spallation reactions are nuclear reactions playing an important role in a wide domain of applications ranging from neutron sources for condensed matter and material studies, transmutation of nuclear waste and rare isotope production to astrophysics, simulation of detector set-ups in nuclear and particle physics experiments, and radiation protection near accelerators or in space.

The simulation tools developed for these domains use nuclear model codes to compute the production yields and characteristics of all the particles and nuclei generated in these reactions. The codes are generally Monte-Carlo implementations of Intra-Nuclear Cascade (INC) or Quantum Molecular Dynamics (QMD) models followed by de-excitation (principally evaporation/fission) models.

The International Atomic Energy Agency (IAEA) and the Abdus Salam International Centre for Theoretical Physics (ICTP) have recently organized an expert meeting on model codes for spallation reactions. The experts have discussed in depth the physics bases and ingredients of the different models in order to understand their strengths and weaknesses. Since it is of great importance to validate on selected experimental data the abilities of the various codes to predict reliably the different quantities relevant for applications, it has been agreed to organize an international benchmark of the different models developed by different groups in the world [1]. The specifications of the benchmark, including the set of selected experimental data to be compared to models, have been fixed during the workshop.

In this work, we analyze energy spectrum of proton, neutron, composite particles (deuteron, triton, ^{3}He, ^{4}He) for p(175 MeV) + ^{58}Ni [2] and p(62.9 MeV) + ^{208}Pb [3] reactions using INC-FRG model and PHITS code.

2. Simulation models

2.1 PHITS

PHITS[4] calculations were done using implement theoretical models, Bertini and ISOBAR models.

2.1.1 Bertini model [5]

The nuclear reaction is treated classically as a sequence of a two body collision of free nucleons in a generated Fermi sea in which the Pauli-blocking is taken into account. The collision probability is calculated with the free or in-medium nucleon-nucleon (*NN*) cross sections.

2.1.2 Isobar model [6,7]

Isobar code is an extend version of VEGAS to supplement the isobar capture and the isobar-nucleon exchange and so on to the treatment of the isobar-nucleon interaction. VEGAS traces the evolution of the cascade process by a time interval base. VEGAS also treats the *NN* collision in a target in the same manner as the Bertini model.

2.2 INC-FRG

The INC-FRG model is a nuclear reaction model [8] developed for describing cluster productions in the framework of the intranuclear cascade model [9]. The cluster production model of INC-FRG is composed of two models; the surface coalescence [10] and the knockout models. In INC-FRG, INC is combined with de-excitation (evaporation/fission) model.

2.2.1 The surface coalescence model

Within the framework of the INC model, when a nucleon traverses the nuclear surface and is going to be emitted, it is tested whether it produces a preliminary cluster. The preliminary cluster production is judged whether the relative distance in phase space is close or not. The condition is given by

$$r_{ij}\,p_{ij} \leq h_0 \tag{1}$$

where h_0 is the adjustable parameter reproduce experimental data. The candidate cluster is checked whether it can be raised to a realistic cluster from the isospin of the constituent nucleons. The order of priority is ^{4}He > (^{3}He or triton) > deuteron. The kinetic energy of the emitted cluster is given by

$$T_c = \sum_i^{A_c} t_i + V_0 - B_c \tag{2}$$

where t_i is the kinetic energy of constituent nucleons i, V_0 denotes the depth of the square-shaped nuclear potential with −45 MeV. B_c is the binding energy of the cluster.

2.2.2 The knockout model

Cluster productions by the knockout model are performed according to the following procedure.

When two particles collide with each other, we search for nucleons around the bombarded particle in *r*-space. If there are nucleons in the vicinity of the nucleon, which are under Fermi momentum, we consider the group of nucleons as a preliminary cluster. The condition is simply given by

$$r_{ij} \leq r_0 \tag{3}$$

where r_0 is the free parameter corresponding to the candidate cluster radius. The candidate cluster is checked whether it can be raised to a realistic cluster in the same method as the surface coalescence. In the knock out model, kinematics of the collision follows the *N-AN* elastic scattering. In order to avoid complexity of the calculation, the cluster is produced in the knockout process, we do not collide the cluster with other particles any more.

3. Results

PHITS calculations were done using implement theoretical models, Bertini and ISOBAR models. ISOBAR treated reflection and refraction, parameterized in-medium nucleon-nucleon (*NN*) cross sections and the threshold energy for (p,n) and (n,p) reactions. The de-excitation calculation following the cascade calculations was done with the GEM code implemented in PHITS.

Figures 1-3 show double-differential proton, deuteron, triton, ^{3}He, and α particle cross-sections for proton induced reactions on ^{58}Ni at 175 MeV. Although both PHITS and INC-FRG calculations are much too peaked at very forward angles (16º) on proton production spectra (See **Fig. 1**), we found that they provide results in overall good agreement with the proton experimental data. As shown in Figs. 3 and 4, the INC-FRG model gives reasonable overall agreement for not only protons but composite particles (deuteron, triton, and ^{3}He) except for α particles, especially at energies above 100 MeV.

Figures 4-6 show energy differential neutron, proton, deuteron, ^{3}He, and α particle cross-sections for proton induced reactions on ^{208}Pb at 62.9 MeV. The Bertini model gives good agreement with experimental data in the case of neutron spectra. However it can be seen that the calculated proton, deuteron, ^{3}He, and α particles spectra disagree with the data. The significant underestimation of the composite particles is attributed to the lack of description of composite particle productions of the traditional intranuclear cascade model such as Bertini and ISOBAR.

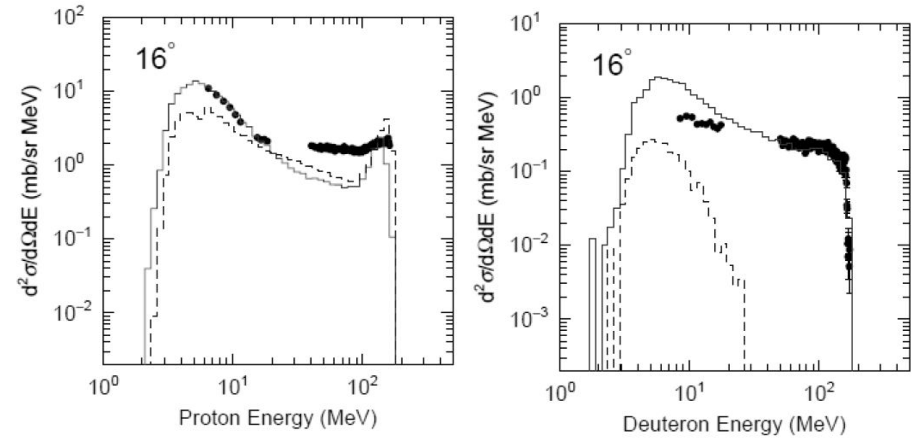

Fig. 1. Double differential proton (left panel) and deuteron (right panel) cross sections for proton induced reactions on ^{58}Ni at 175 MeV. The dashed and solid histograms show the results of PHITS(Bertini) and INC-FRG, respectively.

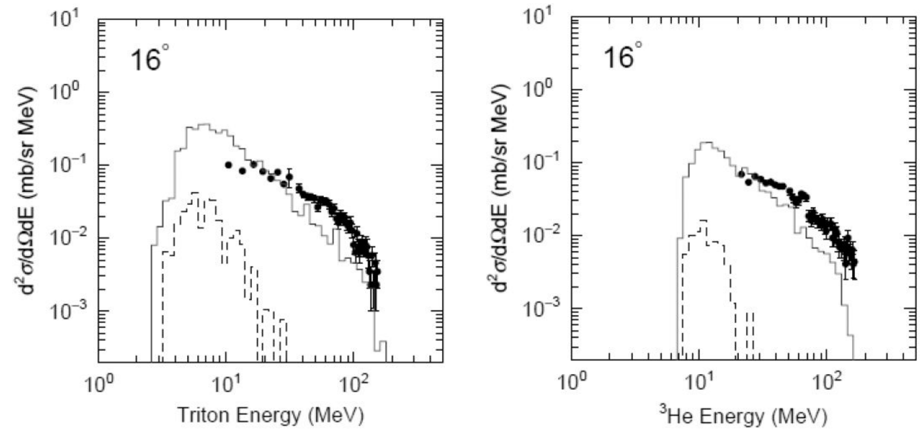

Fig. 2. Same as Fig. 1 but for triton (left panel) and ^{3}He (right panel)

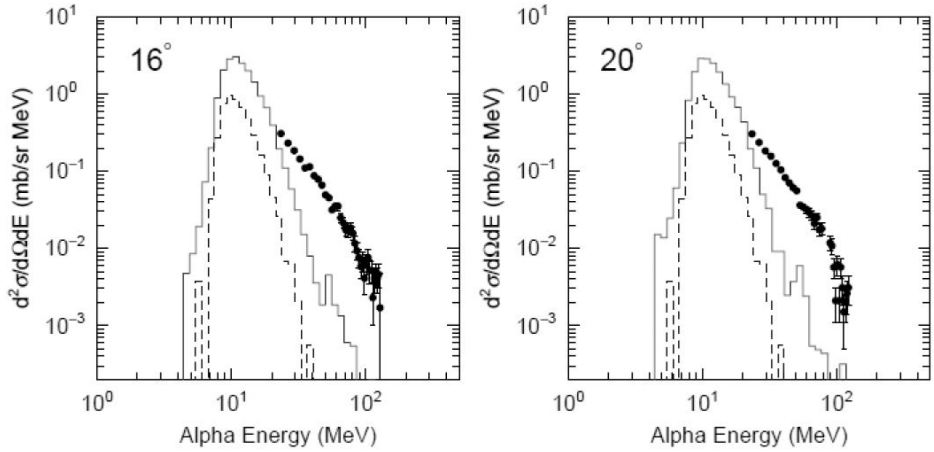

Fig. 3. Same as Fig. 1 but for α particle.

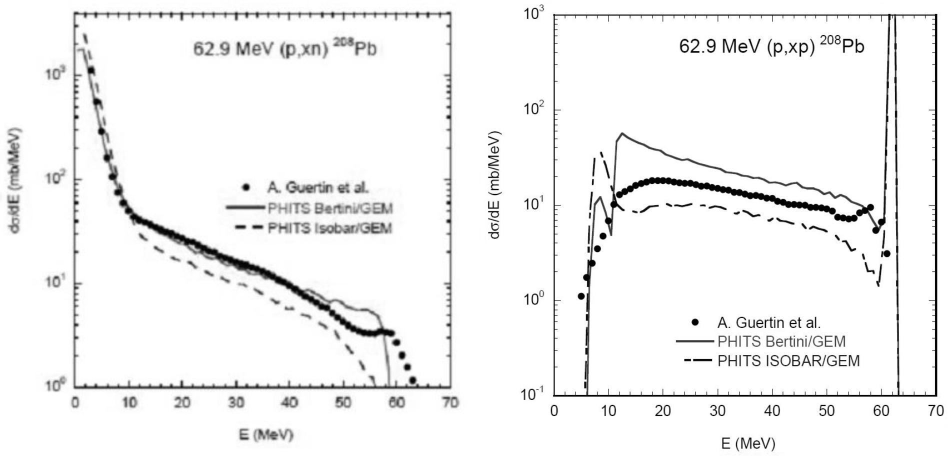

Fig. 4. Energy differential neutron (left panel) and proton (right panel) cross-section for proton-induced reactions on ^{208}Pb at 62.9 MeV. The solid and dashed lines show the results of PHITS(Bertini) and PHITS(ISOBAR), respectively.

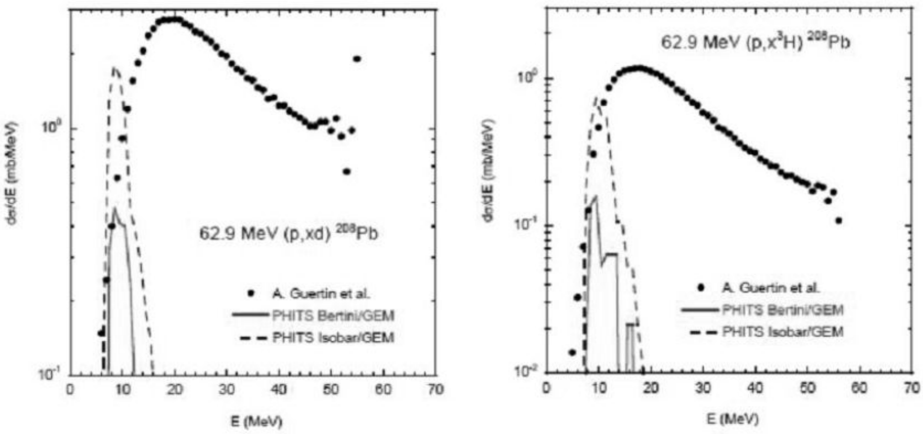

Fig. 5. Same as Fig. 4 but for deuteron (left panel) and ^{3}He (right panel).

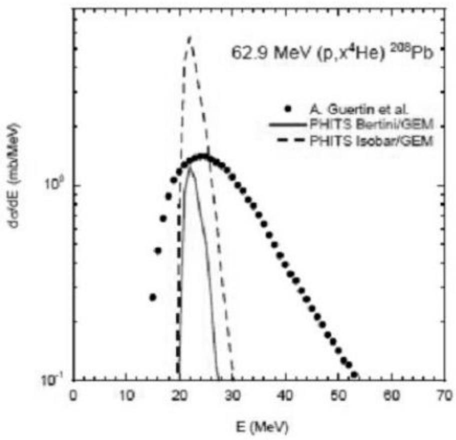

Fig. 6. Same as Fig. 4 but for α particles

.

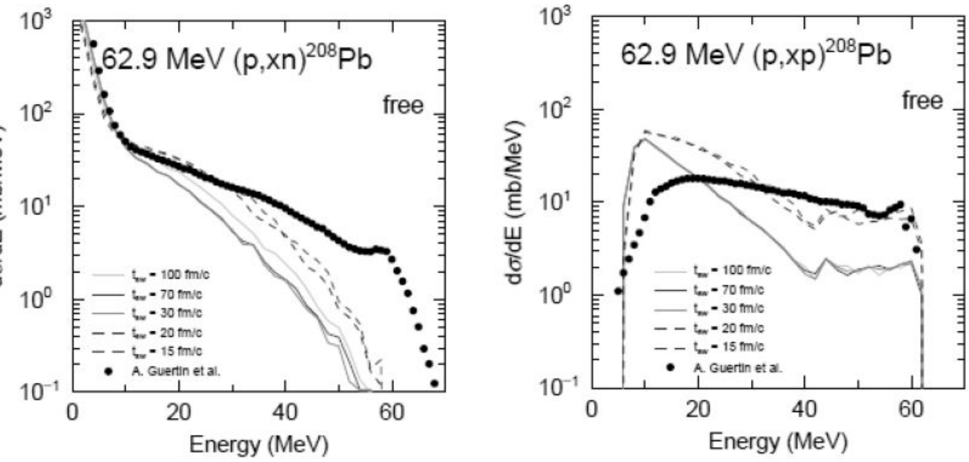

Fig. 7. Energy differential neutron (left panel) and proton (right panel) cross-section for proton-induced reactions on ^{208}Pb at 62.9 MeV. The lines show the results of INC-FRG.

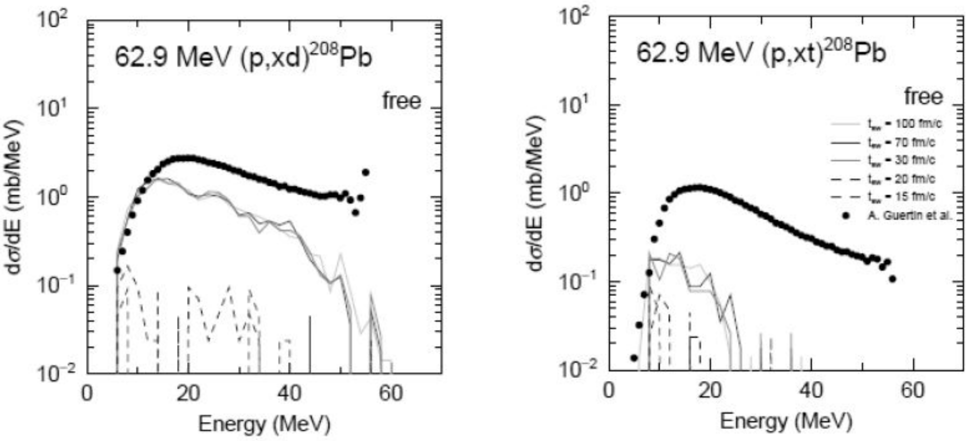

Fig. 8. Same as Fig. 5 but for deuteron (left panel) and triton (right panel).

Figures 7-8 show the results of INC-FRG (t_{sw} (switching time from INC to de-excitation (evaporation/fission) model) = 15 fm/*c*, 20 fm/*c*, 30 fm/*c*, 70 fm/c, 100 fm/*c*). Although the INC-FRG model allows us to treat composite particles emissions during the cascade stage and allows us to change value of t_{sw} in the simulation, unfortunately the INC-FRG calculations do not agree with experimental data. This indicates that nuclear reactions at lower incident energies may be more sensitive to the model parameters than those at higher incident energies.

4. Conclusion

We analyzed energy spectrum of proton, neutron, composite particles (deuteron, triton, ^{3}He, ^{4}He) for p(175 MeV) + ^{58}Ni and p(62.9 MeV) + ^{208}Pb reactions using the Bertini and ISOBAR model implemented in PHITS and the INC-FRG model. We found that it is necessary to improve the existing intranuclear cascade model so as to reproduce composite particle in spallation reactions with incident energy under 200 MeV.

References

[1] http://www-nds.iaea.org/spallations/

[2] B.Piskor-Ignatowicz and F.Goldenbaum, To be submitted as the thesis of B.Piskor-Ignatowicz to Jagellonian University, Krakow, Poland, (2009).

[3] A. Guertin et al., Eur. Phys. J. A23, pp.49-60, (2005).

[4] H. Iwase et al., J. Nucl. Sci. Technol., 39, p. 1142-1151, (2002).

[5] Bertini, H.W.: Phys. Rev., 188, 1711 (1969).

[6] Harp, G.D., Chen, K., Friedlander, G., Frankel, Z., Miller, M.: Phys. Rev., C8, 581 (1973).

[7] H. Takada, Journal of Nuclear Science and Technology, Vol.33, No.4, p.275-282 (1996).

[8] H. Iwamoto and Y. Uozumi, Proceedings of the 2007 International Workshop on Compound-Nuclear Reactions and Related Topics (CNR*2007), AIP Conference Proceedings 1005, pp.140-143, Sep. (2008).

[9] J. Cugnon et al., Nucl. Instr. and Methods in Phys. Res. B 111, p.215-220 (1996).

[10] A. Boudard et al., Nucl. Phys. A 740, p.195-210 (2004).

16. Measurement of fragment production DDX of 72 and 144 MeV ^{12}C beam induced reaction on carbon using Bragg Curve Counter

T.Sanami, M.Hagiwara, M.Takada[1] and M.Baba[2]

High Energy Accelerator Research Organization (KEK)
[1]National Institute of Radiological Science
[2]Cyclotron Radioisotope Center, Tohoku University
email: toshiya.sanami@kek.jp

Double differential cross section (DDX) data of fragment production for 72 (6 MeV/nucleon) and 144 MeV (12 MeV/nucleon) ^{12}C beam induced reaction on carbon were measured using a Bragg Curve Counter (BCC). The DDX data were obtained for fragments of He, Li, Be, B, C, N and O at 30 degree emission angle. Theoretical calculation using PHITS code with QMD+GEM model represents the DDX well except for components from reactions of direct process and α particle clustering process.

1. Introduction

Applications of high energy ion beam have developed in last decades, especially tumor treatment using ion beam have been intensively studied since it has possibility to improve quality of life for patient after the treatment. High energy carbon beam is one of a candidate for the treatment since it has large tissue peak dose ratio in comparison with the other radiation. The program of the treatment for each patient is developed with consideration of biological effects on tumor and organ using high energy multi-particle transport code [1]. To obtain relevant estimation, the nuclear reaction model involved in the code should be maintained to reproduce secondary particles from the interaction of ion beam. For nuclear reaction of ion, Quantum Molecular Dynamics (QMD) model is one of popular models to describe the reaction in medium-high energy region, however applicability of the model for low energy should be confirmed experimentally since clustering effect would become to dominant instead of nucleon-nucleon interaction [2].

We have been conducting a series of experiment to measure double differential cross section of fragment productions from tens of MeV proton induced reactions[3,4,5]. For this experiment, we developed Bragg curve counter (BCC) with advantages of large solid angle, insensitivity for light charged particle, thin entrance window, and, particle identification without transmission part. The measureable energy range of the BCC is enhanced using a particle identification method using range-energy relationship [3] and an energy compensation analysis for punch-through fragment [4]. In this study, we measure fragment production DDXs from $^{12}C + {}^{12}C$ reaction for 72 (6MeV/nucleon) and 144 MeV (12MeV/nucleon) incident energy, which provides reaction energy below and near nucleon binding energy of carbon on center of mass system, using the BCC. The experimental data were compared with results obtained from theoretical model calculated by QMD+GEM model implemented in PHITS code[1].

2. Experimental

The series of the experiment were performed using the NIRS 930 cyclotron in National Institute of Radiological Science (NIRS). The detail of the system employing the BCC was described in references [3,4]. In this section, outline of this system is described. Figure 1 shows schematic view of the experimental setup. Full strip carbon ($^{12}C^{6+}$) beam (20 nA) enters to the scattering chamber. A thin graphite target foil, 206 μg/cm^2, is mounted on the center of the chamber. The intensity of the beam is measured by the Faraday Cup placed downstream of the target. Beam profile of the carbon is adjusted to fit into 5 mm square region on target using beam transport devices of the cyclotron.

The BCC is mounted on the 30-degree port of the scattering chamber. The BCC is a parallel plate ionization chamber with a grid, the structure of which is contained in a stainless steel cylindrical chamber. The distances between cathode and grid, and, grid and anode are 300 mm and 5 mm, respectively. High voltage is applied to the cathode and grid electrode to form electric field for electron drift. The field shaping rings maintain uniformity of the electric field. The cylindrical chamber is sealed using O-rings to keep low-pressure counting gas, 400 Torr Ar+10% CH_4 gas, inside. The cathode side of the chamber has a hole covered with a thin entrance window (2.5 μm thick Mylar) to introduce fragments from the target.

The fragment entered to the chamber stops and produces electrons through ionization process due to energy deposition. The distribution of the electrons along its trajectory is proportional to energy loss of the fragment, i.e, Bragg curve. The electrons drift toward to the grid with keeping their distribution due to the electric field by the cathode, grid and anode. The grid potential is chosen to allow that all electrons reach to the anode with passing through the grid. Under this condition, time distribution of the anode signal

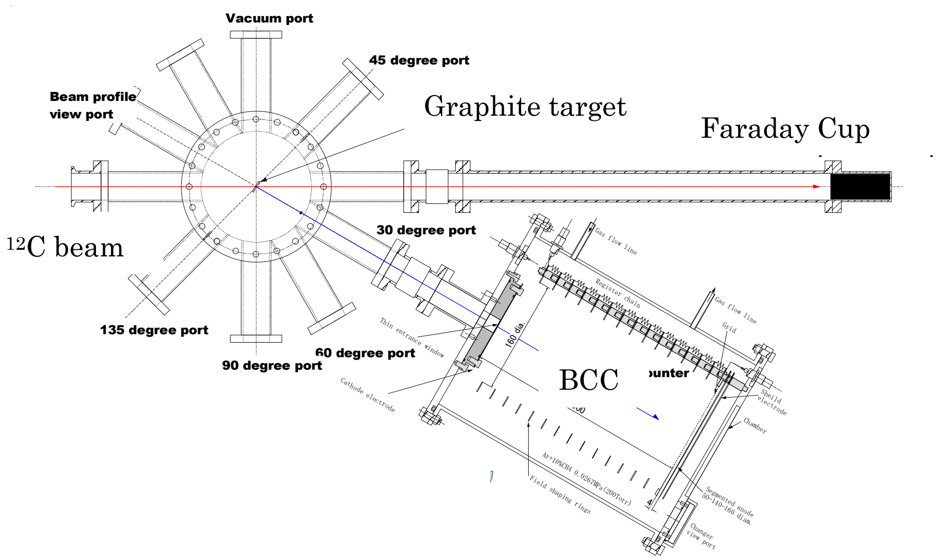

Fig. 1: Schematic drawing of experimental setup using the Bragg curve counter.

has inverse shape of the original distribution of electrons that equal to Bragg curve. Thus, the energy and atomic number of the fragment can be deduced from integral and peak height of the anode signal.

Two dimensional plots of events at 30 degree from 72 and 144 MeV ^{12}C induced reaction on carbon are shown in figs 2 and 3, respectively. The vertical and horizontal axes correspond to fragment Z and energy. The events in dotted circle A on the both figures have too low energy to indentify using Bragg curve vs energy plot. The part of the events can be indentified through range-energy plot[2]. The events in dotted circle B have too high energy to measure their energy. The missed energy can be compensated through off-line analysis [3]. Thus, the energy spectrum for each fragments up to hundred MeV can be obtained from these data.

3. Results and discussions

For carbon production from 72 MeV carbon beam reaction (Fig.2), we can observe several peaks that correspond to ground and excitation levels of ^{12}C nuclei. It indicates that these carbons are emitted through elastic and inelastic scattering process, such as $^{12}C+^{12}C \rightarrow ^{12}C+^{12}C_{0,1,2}$. The other peak can be observed for boron and nitrogen production. It indicates the boron would be produced through a two-body reaction, such as $^{12}C+^{12}C \rightarrow ^{x+1}N+^{x-1}B$, which correspond to proton exchange reaction. In comparison between oxygen and nitrogen production, both maximum energy and production rate of oxygen are larger than these of nitrogen. Oxygen can be generated from combination of carbon and helium, such as $^{12}C+^{12}C \rightarrow ^{16}O+^{8}Be$, which correspond to α-particle exchanging reaction. The production rate of beryllium, which corresponds to carbon minus α-particle, is low in comparison with oxygen since ^{8}Be decays two α-particles immediately[6]. Thus, the facts indicate that α-particle exchange reaction has larger production rate than proton exchange reaction on $^{12}C+^{12}C$ reaction below binding energy region. This result intends importance

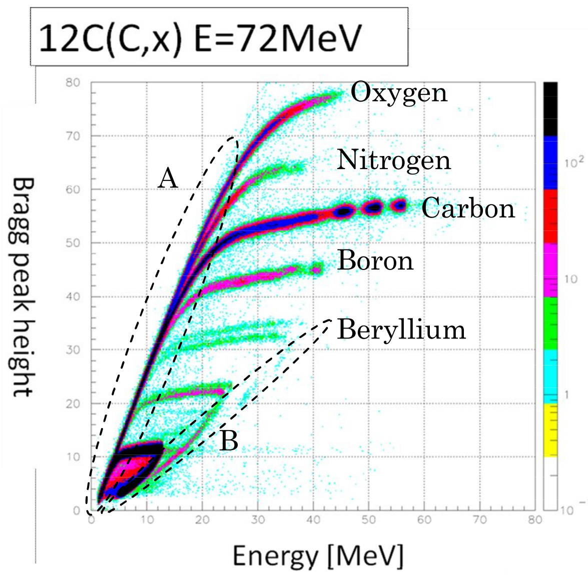

Fig.2: Two dimensional plots of events at 30 degree from 6 MeV/nucleon ^{12}C induced reaction on carbon

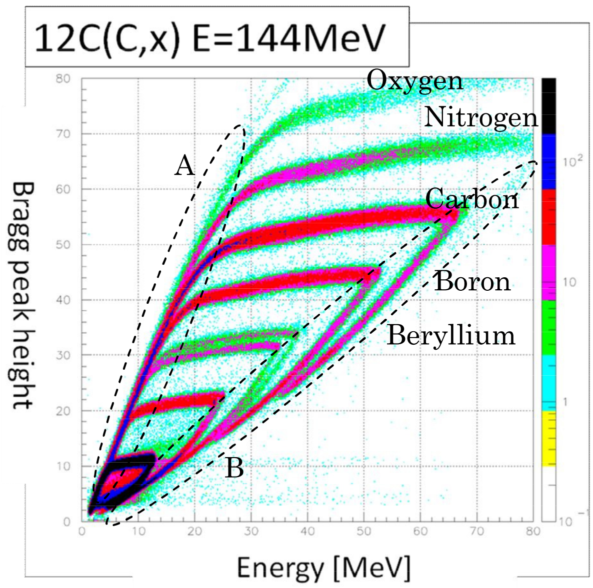

Fig.3: Two dimensional plots of events at 30 degree from 12 MeV/nucleon ^{12}C induced reaction on carbon

of α-particle cluster effect for nuclear reaction on ^{12}C nuclei .

In contrast, 144 MeV result of figure 3 shows remarkable difference concerning the features observed in the 72 MeV result, i.e, peak structure of carbon, large production of oxygen and unbalance of oxygen and beryllium production, are completely disappear. The fact intend dramatically change of reaction mechanism on ^{12}C+^{12}C reaction up to the binding energy.

Figures 4 and 5 shows double differential cross section of He, Li, Be, B, C, N and O production at 30 degree from 72 and 144 MeV ^{12}C induced reaction. The dots and lines describe experimental data and calculation results, respectively. The calculation results are obtained using PHITS code [1] with QMD + GEM models. From these plots, the calculations represent experimental data generally well. In detail comparison, underestimation of direct reaction component can be observed for 72 MeV results of C production. In particular, peaks of elastic and inelastic reaction cannot be reproduced since no adequate model is implemented. The underestimation for C production is mitigated for 144 MeV results. It is easy to understand if the direct component reduces with increasing incident energy. The calculation results also lack components from clustering effect that can be seen as oxygen emission of 72 MeV results, as expected. The component disappears completely with increasing incident energy, as shown in 144 MeV result.

4. Conclusion

Double differential cross section for fragment production from 72 and 144 MeV ^{12}C induced reaction on carbon were measured using BCC. The experimental results indicate significant contribution for reaction product from direct reaction and α-particle clustering reaction for 72 MeV ^{12}C induced reaction. The contribution of the components is mitigated with increasing incident energy to 144 MeV. QMD +GEM model reproduces fragment production generally well except for the components. The models having information of low lying excitation levels and clustering of nuclei would be required to describe fragment production in this energy range.

References

1. H.Iwase, K.Niita and T.Nakamura, *J.Nucl.Sci.Technol.*, **39** (2002) 1142
2. T.Maruyama, K.Niita, and A.Iwamoto, *Phys.Rev.C* **53** (1996) 297
3. T.Sanami, M.Hagiwara, T.Oishi, M.Baba, M.Takada, *Nucl. Instrm. Meth.* **A 589/2** (2008) 193
4. M. Hagiwara, T. Sanami, T. Oishi, M. Baba, M. Takada, *Nucl. Instrm. Meth.* **A 592** (2008) 73
5. M. Hagiwara, T. Oishi, S. Kamada, M. Baba, T. Sanami, M. Takada and N. Miyahara, “Measurements of Double Differential Fragment Production Cross Sections of Silicon for 70 MeV Protons”, Proceedings of the 2005 Symposium on Nuclear Data (JAEA-Conf 2006-009)
6. B.Antolkovic, G.Dietze and H.Klein, *Nucl.Sci.Eng.* **107** (1991) 1

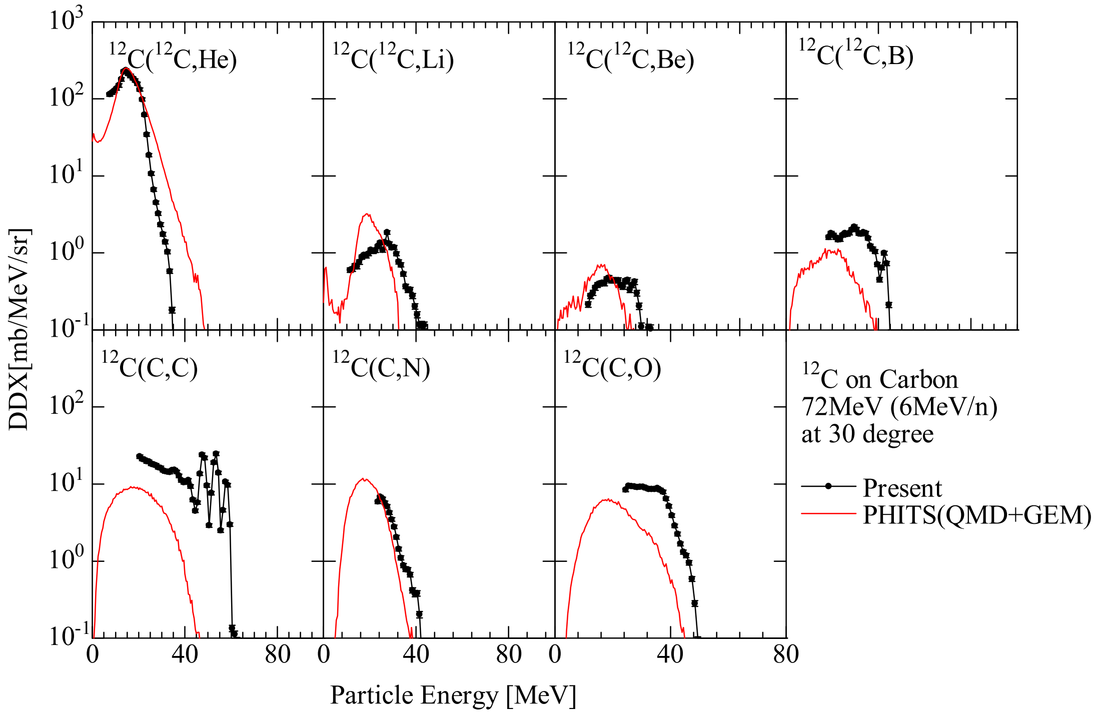

Fig. 4: Double differential cross section of fragment production at 30 degree from 72 MeV ^{12}C induced reaction on carbon

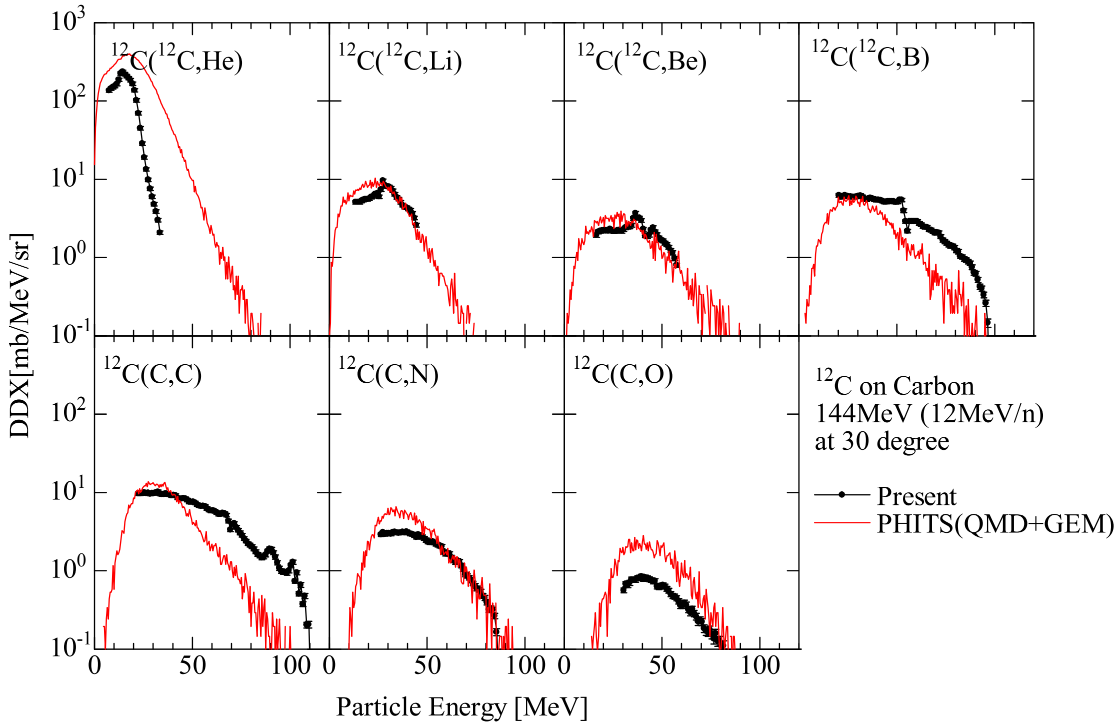

Fig. 5: Double differential cross section of fragment production at 30 degree from 144 MeV ^{12}C induced reaction on carbon

17. Prompt γ-rays emitted in the $^{74}Ge(n,\gamma)^{75}Ge$ reaction

K.Y. Hara, T. Kin, M. Oshima, S. Nakamura, A. Kimura, M. Koizumi, and Y. Toh
Japan Atomic Energy Agency (JAEA)
2-4 Shirakata-Shirane, Tokai-mura, Naka-gun, Ibaraki 319-1195, Japan
e-mail: hara.kaoru@jaea.go.jp

The prompt γ-rays emitted in the $^{74}Ge(n_{cold},\gamma)^{75}Ge$ reaction were studied with the cold neutron at the Japan Research Reactor (JRR-3M) of JAEA. Many new γ-ray transitions and new levels of ^{75}Ge were proposed.

1. Introduction

Neutron capture cross sections of radioactive nuclei, such as long-lived fission products (LLFP's) and minor actinides (MA's), are important for deign of nuclear transmutation systems based on fast breeder reactor or accelerator driven system. However, accuracy of the data is not sufficient at present, because of the experimental difficulties. It is not easy to prepare a sufficient amount of enriched target for radioactive nucleus. The measurement was accompanied by a background arise from radioactivity of target.

The experimental methods for the neutron capture cross sections are roughly categorized to neutron activation method and prompt γ-ray detection method. While the former allows one to obtain the reliable results even for the nuclei with small cross sections, it is limited to the case of the unstable daughter nuclei. On the contrary, the latter can be applied to all nuclei. Since, in the concept of the nuclear transmutation, the long-lived radioactive nuclei are changed to the stable (or short-lived) by utilizing the neutron capture reaction, the prompt γ-ray detection method is effective to measure the cross sections.

In order to accurately determine neutron capture cross sections for nuclear transmutation study, we have been developing experimental and analysis methods with the prompt γ-ray detection technique and the neutron time-of-flight method [1-7]. Since the neutron capture cross sections are derived by summing all the intensities of primary or ground-state transition γ-rays [1,2], the information of level structures and γ-ray transitions in the compound nuclei are required for the developed method.

As a part of these developments with the target of the stable nucleus, we found a level scheme in the $^{74}Ge(n,\gamma)^{75}Ge$ reaction. As shown in Fig. 1, the decay from/to excited state above 2 MeV is unknown in ^{75}Ge, where the neutron separation energy is 6.5 MeV. The γ-ray transitions of ^{75}Ge in the energy of 3-4 MeV have not been assigned to the decay scheme, although these transitions were previously reported [8].

For the determination of the neutron capture cross section of ^{74}Ge with the prompt γ-ray detection method, the prompt γ-rays emitted from the $^{74}Ge(n_{cold},\gamma)^{75}Ge$ reaction were measured with a 4π Ge spectrometer and the coincidence event data were analyzed to identify the level scheme in ^{75}Ge. We report the results in this paper.

2. Experiments

The experiments were performed at the beam line (C2-3-2) of JRR-3M of JAEA. A target was irradiated by the cold neutron beam with the typical intensity of ~10^7 n/s/cm^2. For the ^{74}Ge target, the germanium oxide powder (GeO_2) highly enriched in ^{74}Ge to 99% was used. The GeO_2 powder of 860 mg was packed in a 25μm-thick FEP film and mounted on a Teflon frame. The geometry was chosen that the cross-sectional area of the neutron beam covered the target, while it fell within the inside of frame.

The multiple prompt γ-rays emitted from the $^{74}Ge(n,\gamma)^{75}Ge$ reaction were measured by using a gamma-ray spectrometer, STELLA, which consists of eight clover-type Ge detectors and BGO Compton-suppressors [4,5]. The clover-type Ge detector surrounded with the BGO detector was placed at the position of 90° with respect to the beam axis (See [4,5] about the detail for the setup). The distance from the target to each clover-type Ge detector was about 5 cm.

The coincidence event data from these detectors were acquired with a data acquisition (DAQ) system based on the advanced digital processing technique [6,7]. The DAQ system mainly divided to 3 parts: main ADC modules, fast timing modules, and coincidence modules. The preamplifier signals for Ge and BGO detectors were pulse-shaped, discriminated, and digitized by the fast timing modules. In order to obtain the trigger signals, the digitized outputs were sent from the fast timing modules to the coincidence modules. When the digitized pattern matched the coincidence condition, the preamplifier signals for Ge detectors were processed to obtain the pulse heights by the main ADC modules.

The multiple prompt γ-rays emitted from the $^{14}N(n,\gamma)^{15}N$ reaction and the $^{50,53}Cr(n,\gamma)^{51,54}Cr$ reaction were also measured for the energy calibration, where the melamine powder (498 mg, natural) and the grain of metallic chromium (152 mg, natural) were used.

3. Event Data Sorting

Since a clover-type Ge detector was composed of four crystals, the pulse-heights were recorded every crystals. The pulse-heights were calibrated with the intense γ-rays peaks emitted from the $^{14}N(n,\gamma)^{15}N$ and $^{50,53}Cr(n,\gamma)^{51,54}Cr$ reactions. After the energy calibration, the pulse-heights of four crystals in a clover-type Ge detector were assembled by each event. Since the four crystals in a clover-type Ge detector are very closely packed, Compton-scattered γ-ray is often absorbed by one of the other three crystals. Therefore, this procedure could improve photo-peak efficiency and the peak-to-total ratio.

In addition to the above procedure, the energies of all γ-rays which coincidentally detected with the clover-type Ge detectors were summed to derive the total energy. The total energy (E_{tot}) should be nearly equal to the neutron separation energy of ^{75}Ge (S_n=6505 keV), if all prompt γ-rays in a cascade from a given compound state were ideally detected. To discriminate the background, the event data adapted to this condition were used in the present analysis, where the gate region for E_{tot} was from S_n-15 keV to S_n+15 keV.

4. Analysis and Results

The so-called “single gamma energy spectrum” is shown in Fig. 2. All energy spectra for a clover-type Ge detector were summed into the single gamma energy spectrum. Many unknown γ-ray transitions, in addition to the known one, were seen in the energy spectrum. The solid arrows in Fig. 2 indicate only the prominent unknown peaks. The dashed arrow indicates the position of the neutron separation energy.

The combination for the coincident γ-rays was given by the following procedures. The pairs of γ-ray energies coincidentally detected with the clover-type Ge detectors were plotted on the 2-dimentional spectrum (Fig. 3(a)). The portion of Fig. 3(a) is magnified and presented on Fig. 3(b), where both axis stand for the γ-ray energies. The pair of the numbers indicates the coordinate (x, y) on Fig. 3(b). The spots located on the bold line (x+y=S_n) mean two-step cascade. The other spots (x+y<S_n) relate to three-step or more cascade. (For example, 6 pairs would be plotted on Fig. 3 for the triple coincidence. Since Fig. 3 has a symmetrical distribution, the half region of the figure was analyzed.) The γ-γ coincidence analysis was performed with the present data to identify the γ-ray transitions and the levels of ^{75}Ge.

As shown in Fig. 1, more than half of the consecutive transitions (secondarily or ground-state transitions) have not been researched, while 17 primary transitions are known. First, therefore, we analyzed two-step cascade with the known primary transitions as shown in Fig. 4(a). When a known primary transition (A) with the energy E_A and a unknown transition (B) with the energy E_B(=S_n-E_A) were observed at once, the transition B was assigned as the ground-state transition in the two-step cascade. Second, three-step cascade (A, C, and D in turn) was analyzed by using 3 observed pairs (E_A,E_C), (E_C,E_D), and (E_D,E_A), where the γ-ray energies for the transition A, C, and D are E_A, E_C, and E_D, respectively (S_n=E_A+E_B=E_A+E_C+E_D). When the transition A and D were known as primary and ground-state transition, respectively, the unknown transition C was assigned as the secondarily transition in the three-step cascade. Finally, the combination of two-step cascade and three step cascades as shown in Fig. 4(b) were treated as the similar manner for Fig. 4(a). The only difference between Fig. 4(a) and Fig. 4(b) is that the transition A is unknown. Although both transition of two-step cascade are unknown, these transitions were assigned base on the energy information of three-step cascade.

As a result, the candidates of new γ-ray transitions (~100) and new levels (~20) were found in the ^{74}Ge(n,γ)^{75}Ge reaction. The γ-ray transitions of ^{75}Ge in the energy of 3-4 MeV have not been assigned to the level scheme, although these transitions were previously reported [8]. These transitions were almost assigned as the primary transitions in this analysis. The candidates of new levels were at the energy region from 2 to 3 MeV.

5. Conclusion

The multi prompt γ-rays emitted in the ^{74}Ge(n,γ)^{75}Ge reaction were measured with the STELLA at JRR-3. The level scheme of ^{75}Ge was constructed with the measured energies of γ-rays. The candidates of new γ-ray transitions and new levels in ^{75}Ge were found in the ^{74}Ge(n,γ)^{75}Ge reaction. The present results will be used to determine the neutron capture cross section of ^{74}Ge.

References

[1] K. Furutaka, H. Harada, and S. Raman, "Prompt Gamma Rays Emitted in Thermal-neutron Capture Reaction by ^{99}Tc and Its Reaction Cross Section", *J. Nucl. Sci. and Tech.* ***41***, 1033 (2004).

[2] M. Oshima, J. Hori, H. Harada *et al., Proceedings of the 2007 International Conference on Nuclear Data for Science and Technology*, pp. 603-606 (2008).

[3] T. Kin *et al., AIP Conf.* Proc. 1090 (2009) pp.575-576.

[4] Y. Toh, M. Oshima, K. Furutaka *et al*., "Development of a neutron beam line and detector system for multiple prompt gamma-ray analysis", *J. Radioanal. Nucl. Chem.* ***278***, 703 (2008).

[5] T. Kin, M. Oshima, K. Furutaka *et al., Proceedings of 2nd International Conference on Frontiers in Nuclear Structure, Astrophysics and Reactions (FINUSTAR2),* Crete, Greece, Sep. 10-14, 2007, p.374 (2008).

[6] A. Kimura, Y. Toh, M. Koizumi *et al*., "Performance of a High Speed and High Density Data Acquisition System for Multiple Gamma-ray Detection", *Conference Record of IEEE NSS/MIC/RTDS*, Dresden, Germany, Oct. 19-25, 2008, Article Number: N30-68 (2008).

[7] M. Koizumi, A. Osa, Y. Toh *et al*., "Minor actinide neutron capture cross-section measurements with a 4π Ge spectrometer", *Nucl. Instr. Meth.*, **A562**, 767 (2006).

[8] ENSDF, http://www.nndc.bnl.gov/ensdf/

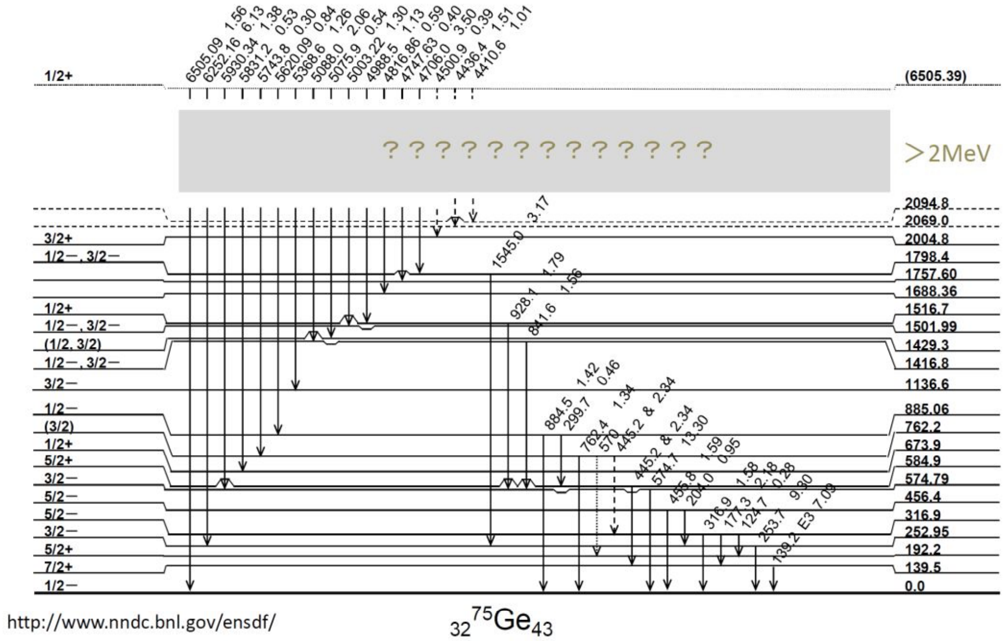

Fig. 1: Level scheme in the excited states of ^{75}Ge.

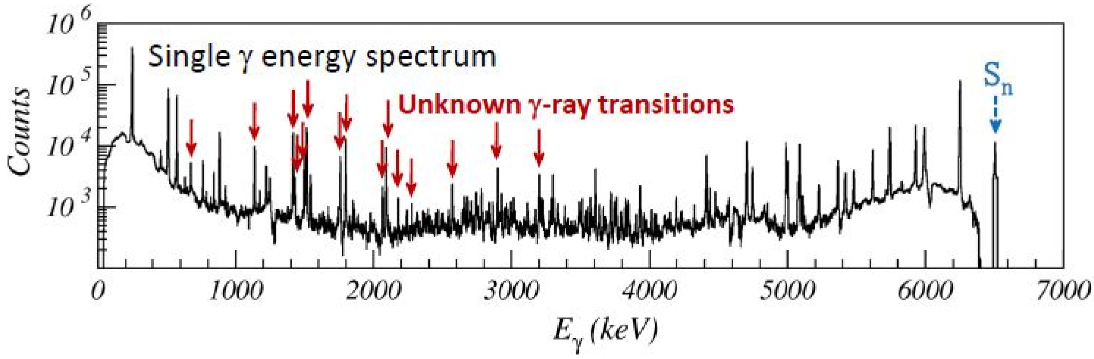

Fig2: Single gamma energy spectrum.

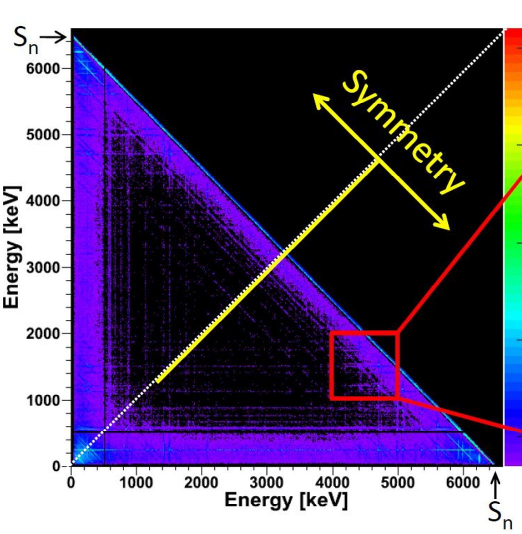

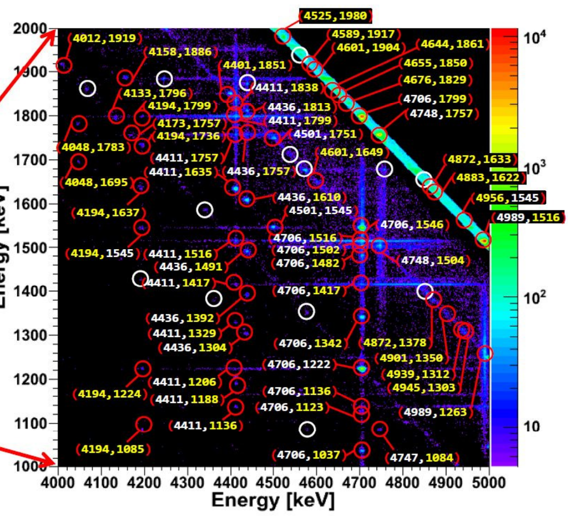

Fig. 3(a): 2-dimensional spectrum.

Fig. 3(b): Magnified view for the portion of Fig. 3(a).

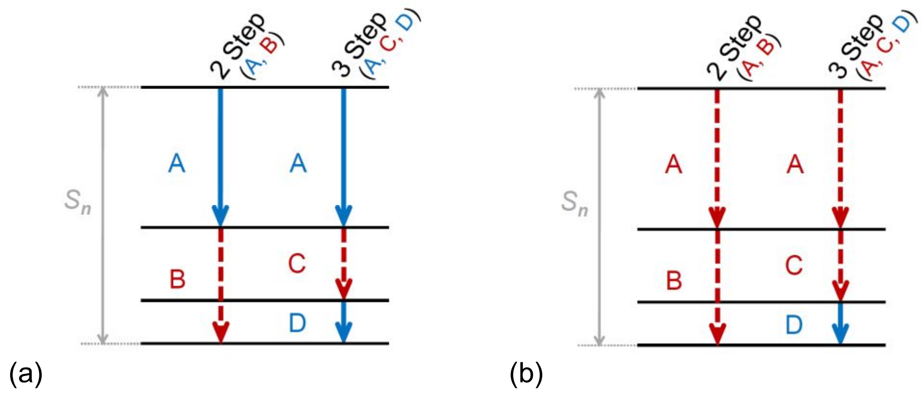

Fig.4: Identification of level and γ-ray transition.

The solid and dashed arrows stand for the known and unknown γ-rays transitions, respectively.

18. Measurements of Neutron Yields for 9 MeV Deuteron Incidence on Cu

Kosuke HIDAKA
Department of Applied Quantum Physics and Nuclear Engineering,
Kyushu University 744 Motooka, Nishi-ku, Fukuoka 819-0395 Japan
e-mail:k-hidaka@kune2a.nucl.kyushu-u.ac.jp

The thick target neutron yields on Cu for 9 MeV deuteron incidence were measured. The experiment was performed at the Kyushu University Tandem Accelerator Laboraotory. We adopted 0.2 mm thick Cu foil. An NE213 liquid organic scintillator 2” in diameter and 2” in thickness was employed to detect neutrons emitted from targets. The measurement angles were 0°, 30°, 60°, 90°, 120° and 140°. To consider the contribution of scattered neutrons from the floor, we also measured neutron yields with an Fe shadow bar located in front of the scintillator. Because incident deuteron beam was not pulsed and the Time-of-Flight method was not applied, the energy spectrum was derived from unfolding the light output spectrum using the FORIST code. The detection efficiency was calculated with the SCINFUL-QMD code. To validate this analysis method, we measured neutrons from an Am-Be and a ^{252}Cf neutron sources. The experimental results are compared with calculations.

1 Introduction

Neutron yields from low energy deuteron incidence have been discussed for the realization of Boron Neutron Capture Therapy (BNCT), International Fusion Material Irradiation Facility-Engineering Validation and Engineering Design Activity (IFMIF-EVEDA) and so on. IFMIF[1] is the international scientific research program designed to test materials for suitability for use in a fusion reactor. The 9 MeV deuteron accelerator facility is under construction at Rokkasho village in Aomori Prefecture, Japan. The accurate nuclear data are required to design the target or beam dump for the examination of safety. Because the experimental data of deuteron-incident neutron yields are scarce below 10 MeV, the prediction accuracy of the calculation codes has not been verifieds.

The purpose of this study is the measurements of neutron thick target yields for 9 MeV deuteron incidence on copper. The neutron spectra were measured with the unfolding method at 0°, 30°, 60°, 90°, 120° and 140°. The Experimental data results are compared with calculations.

2 Experiment

The experiment was carried out using the Tandem Accelerator Laboratory at Kyushu University. The schematic diagram of the Tandem accelerator is given in **Figure 1**[2]. We measured the thick target neutron yields of the Cu(d,xn) reaction for 9 MeV deuterons. The average intensity of the accelerator was 12.5 nA.

The experimental setup is shown in **Figure 2**. Neutrons emitted from the target were detected with an NE213 scintillation detector. The data were obtained at seven angles (0°, 30°, 60°, 90°, 120° and 140°). The detector 2” in diameter and 2” in thickness is cylindrical and is connected with a photomultiplier optically. The detector was placed at ∼2.1 m from the target. To consider the contribution of scattered neutrons from the floor, we also measured neutron yields with an iron shadow bar 30 cm thick located in front of the NE213 scintillator. We adopted 0.2 mm thick Cu foil which are enough for a deuteron to stop in the foils. The target was placed perpendicular to the deuteron beam in the stainless chamber cm in diameter, but the target was rotated 45° in 90° measurement.

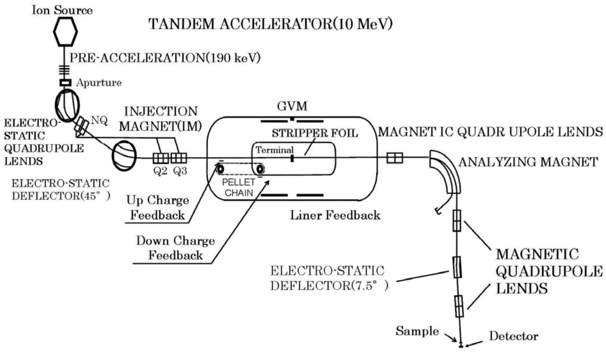

Fig. 1 Illustration of the Kyushu University Tandem Accelerator.

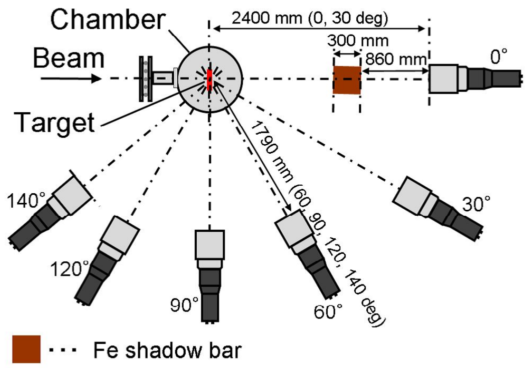

Fig. 2 Illustration of the experimental setup.

3 Analysis

3.1 Elimination of the gamma-ray events

The NE213 scintillation detector detects not only neutrons but also gamma-rays. To obtain neutron energy spectra, the neutron events were separated from the gamma-ray events by the gate integration method[3]. Figure 3 stands for a schematic view of the gate integration method. Comparison between charge spectrum with the fast-gate and that with the slow-gate enables to discriminate between neutron events and gamma-ray ones. An example of the two-dimensional plot of the charge spectra with the fast gate and the slow one obtained by the gate integration method is shown in Figure 4.

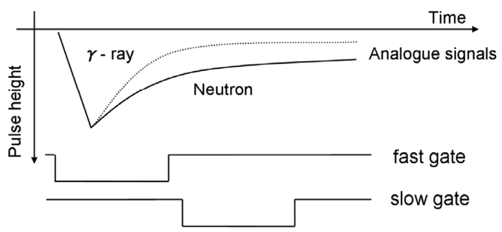

Fig. 3 Schematic view of the gate integration method.

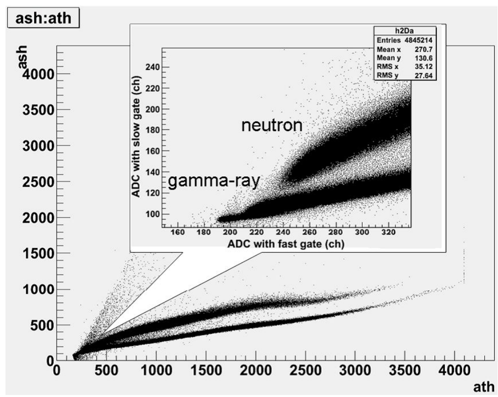

Fig. 4 Discrimination between neutrons and gamma-rays.

3.2 Calibration

Charge-integration spectra were calibrated to get corresponding electron-equivalent light-output for the NE213 scintillation detector. For the calibrations, the maximum energy of neutrons emitted from Am-Be neutron source and the gamma-ray Compton edges of ^{60}Co, ^{137}Cs and ^{133}Ba sealed sources were converted into light-unit with the semi-empirical formula by Dietze et al.[4]. The relationship between charge-integrations and electron-equivalent light-outputs for the NE213 scintillation detector is shown in **Figure 5**.

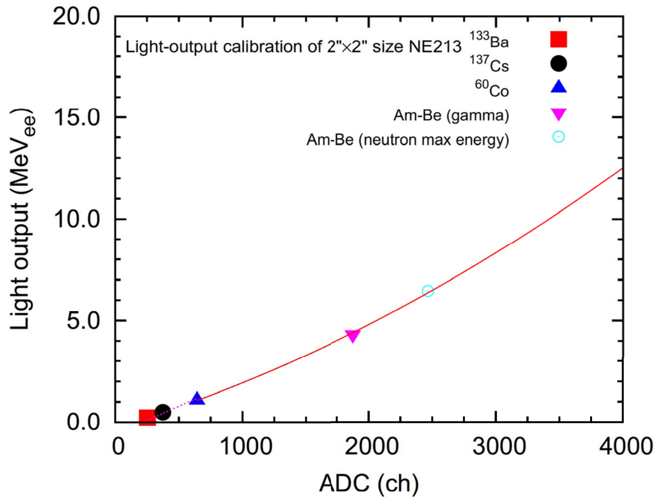

Fig. 5 Relationship between integrated charge and light out-put.

3.3 Unfolding

In this experiment, incident deuteron beam was not pulsed and the time-of-flight (TOF) method was not applied, so the energy spectrum was derived from unfolding the light output spectrum with the FORIST[5] code. The detection efficiency of the NE213 scintillation detector shown in **Figure 6** was calculated with the SCINFUL-QMD[6] code. We got the number of incident deuterons by dividing the current value over measurement time by 1.6×10^{-19} because the deuteron charge was +1.

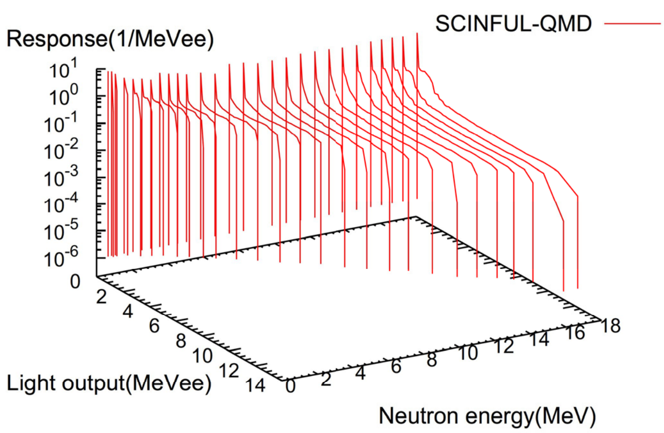

Fig. 6 Calculation of detector response functions by SCINFUL-QMD.

3.4 Validation of analysis

To validate this analysis method, we measured neutrons from the ^{252}Cf and Am-Be neutron sources. The present results are shown in **Figures 7** and **8**. The present data are consistent with the experimental data by Johnson et al.[7], the one by Knitter et al.[8], the one by Kotel et al.[9], the one by Statrostov et al.[10], the one by Werle et al.[11], the one by Marsh et al.[12] and the data by JIS[13]. Therefore, the validity was confirmed.

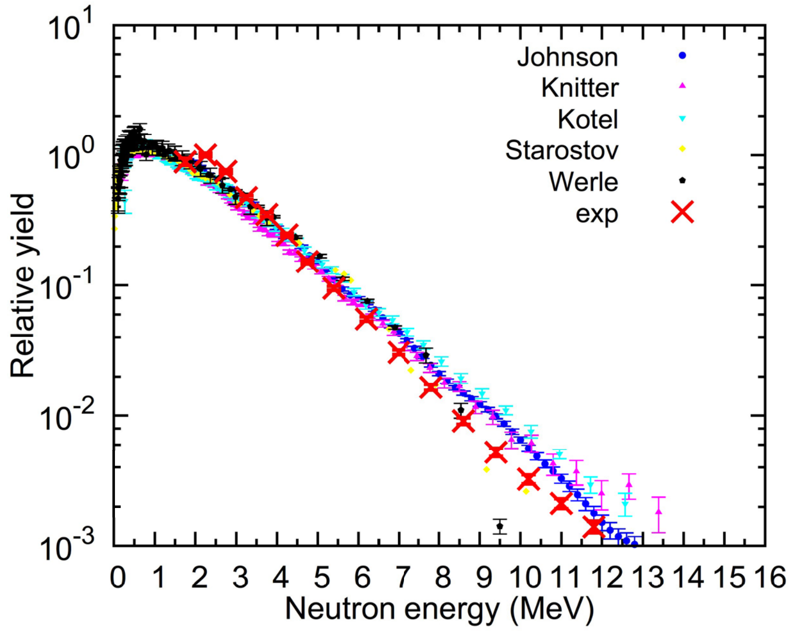

Fig. 7 Relative neutron energy spectra from the Californium source.

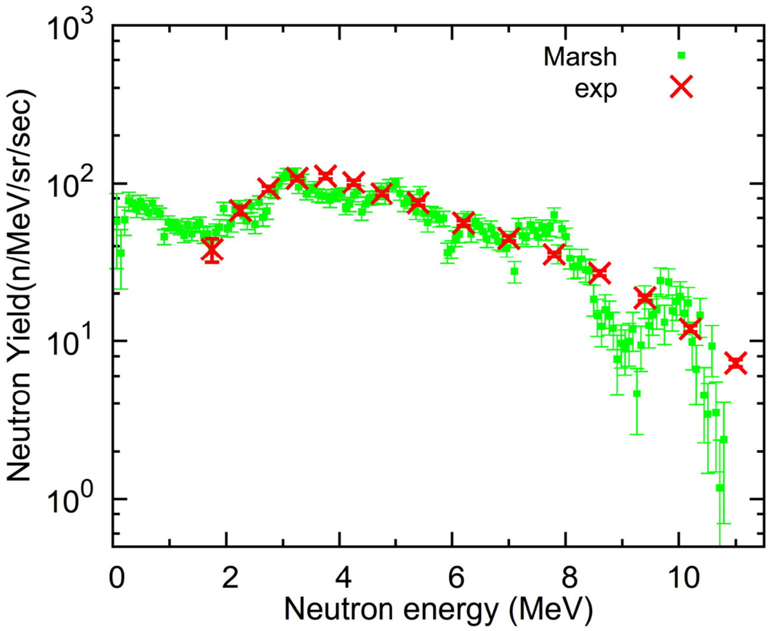

Fig. 8 Neutron energy spectra from the americium-beryllium source.

4 Result

The present results for the Cu(d,xn) thick target neutron yield (TTNY) for 9 MeV deuterons are shown in **Figure 9**. The present data are compared with the calculations using the TALYS[14)] code. TALYS calculation considered dE/dx in targets.

The caluculations do not fully reproduce the absolute yield, however the present results and the calculations show a similar tendency. Therefore, the present results are reliable.

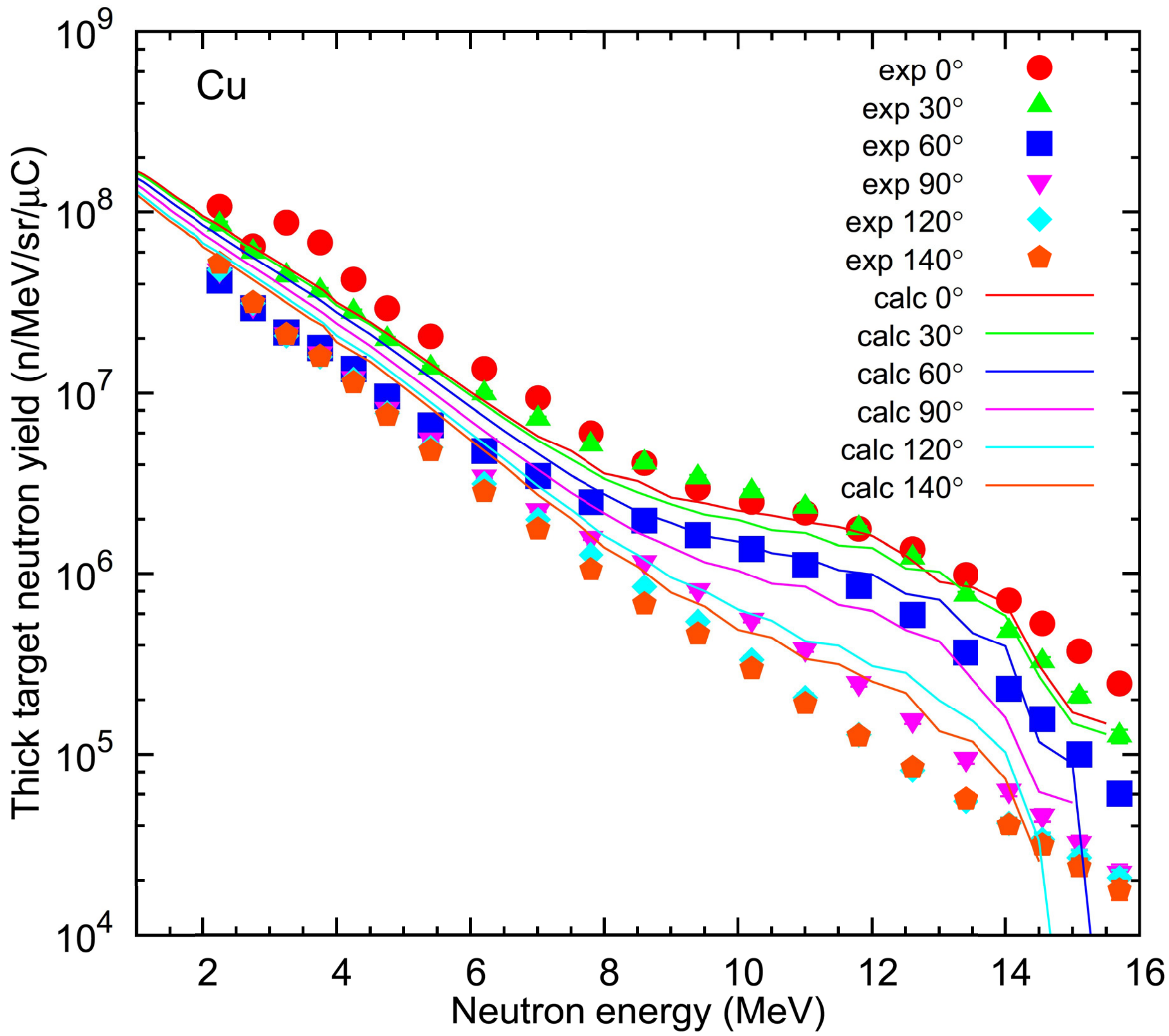

Fig. 9 Neutron thick target yield from copper targets with our experimental data.

5 Summary

We measured the thick target neutron yields from copper target bombarded by 9 MeV deuterons using the Tandem accelerator at Kyushu University. The detection efficiency of the NE213 scintillation detector was calculated using the SCINFUL-QMD code. The thick target neutron yield were derived by unfolding using the FORIST code. To validate this analysis method, we also measured energy spectra from the ^{252}Cf and Am-Be neutron sources and compared with the experimental data by Johnson et al., Knitter et al., Kotel et al., Statrostov, Werle et al., Marsh et al. and the data by JIS. The measured results are compared with calculations using the TALYS code. The measured results is consistent with calculations, so it turned out that there was no problem in the experiment method.

References

1) IFMIF CDA TEAM, "IFMIF Conceptual Design Activity Final Report," Report 96.11, M. Martone, Ed., ENEA, Dipartimento Energia, Frascati (1996).

2) S.Mitarai, Y.Kanegae, K.Tanaka, H.Morikawa, T.Maeda, T.Noro and S.Morinobu, *Nucl. Instr. and Meth. in Phys. Res.*, B**223**, 135 (2004).

3) M.Moszynski, G.J.Costa, G.Guillaume, *et al.*., *Nucl. Instr. and Meth. in Phys. Res.*, A**336**, 226 (1993).

4) G.Dietze and H.Klein, *Nucl. Instr. Meth.*, **193**, 549 (1982).

5) R.Koohi-Fayegh, S.Green and M.C.Scotto, *Nucl. Instr. and Meth. in Phys. Res.*, A**460**, 391 (2001).

6) D. Satoh,T. Sato,N. Shigyo and K. Ishibashi, JAEA-**Data**/Code 2006-023 (2006).

7) R. H. Johnson, D. T. Ingersoll, B. W. Whering and J. J. Dorning *Nucl Inst. and Meth. Phys. Res.*, Vol.145, 337 (1977).

8) H. H. Knitter, A. Paulsen, H. Liskien, M. M. Islam *Atomkernenergie*, Vol.22, 84 (1973).

9) G.V.Kote.Kotel'nikova, B.D.Kuz'minov, G.N.Lovchikova, et al. *Fiz.-Eng Institut. Obninsk Reports*, No.575 (1975).

10) B.I.Starostov, A.F.Semjonov and V.N.Nefjodov *Inst. Atomnykh Reaktorov Melekess Reports*, No.1, 360 (1979).

11) H.Werle and H.Bluhm *Nucl. Eng.*, Vol.26, 165 (1972).

12) J.W.Marsh, D.J.Thomas and M.Burke *Nucl. Inst. and Meth. Phys. Res.*, A**366**, 340 (1995).

13) Reference neutron radiations. characteristics and methods of production, (2001). BS ISO 8529-1:2001.

14) A. J. Koning, S. Hilaire and M. Duijvestijn, *Proc. Int. Conf. Nucl. Data. Sci. Technol*, Santa Fe, USA, 1154 (2005).

国際単位系（SI）

表１．SI 基本単位

基本量	SI 基本単位	
	名称	記号
長さ	メートル	m
質量	キログラム	kg
時間	秒	s
電流	アンペア	A
熱力学温度	ケルビン	K
物質量	モル	mol
光度	カンデラ	cd

表２．基本単位を用いて表されるSI組立単位の例

組立量	SI 基本単位	
	名称	記号
面積	平方メートル	m^2
体積	立法メートル	m^3
速さ，速度	メートル毎秒	m/s
加速度	メートル毎秒毎秒	m/s^2
波数	毎メートル	m^{-1}
密度，質量密度	キログラム毎立方メートル	kg/m^3
面積密度	キログラム毎平方メートル	kg/m^2
比体積	立方メートル毎キログラム	m^3/kg
電流密度	アンペア毎平方メートル	A/m^2
磁界の強さ	アンペア毎メートル	A/m
量濃度[(a)]，濃度	モル毎立方メートル	mol/m^3
質量濃度	キログラム毎立法メートル	kg/m^3
輝度	カンデラ毎平方メートル	cd/m^2
屈折率[(b)]	（数字の） 1	1
比透磁率[(b)]	（数字の） 1	1

(a) 量濃度（amount concentration）は臨床化学の分野では物質濃度（substance concentration）ともよばれる。
(b) これらは無次元量あるいは次元１をもつ量であるが、そのことを表す単位記号である数字の１は通常は表記しない。

表３．固有の名称と記号で表されるSI組立単位

組立量	SI 組立単位			
	名称	記号	他のSI単位による表し方	SI基本単位による表し方
平面角	ラジアン[(b)]	rad	1[(b)]	m/m
立体角	ステラジアン[(b)]	sr[(c)]	1[(b)]	m^2/m^2
周波数	ヘルツ[(d)]	Hz		s^{-1}
力	ニュートン	N		m kg s^{-2}
圧力，応力	パスカル	Pa	N/m^2	m^{-1} kg s^{-2}
エネルギー，仕事，熱量	ジュール	J	N m	m^2 kg s^{-2}
仕事率，工率，放射束	ワット	W	J/s	m^2 kg s^{-3}
電荷，電気量	クーロン	C		s A
電位差（電圧），起電力	ボルト	V	W/A	m^2 kg s^{-3} A^{-1}
静電容量	ファラド	F	C/V	m^{-2} kg^{-1} s^4 A^2
電気抵抗	オーム	Ω	V/A	m^2 kg s^{-3} A^{-2}
コンダクタンス	ジーメンス	S	A/V	m^{-2} kg^{-1} s^3 A^2
磁束	ウエーバ	Wb	Vs	m^2 kg s^{-2} A^{-1}
磁束密度	テスラ	T	Wb/m^2	kg s^{-2} A^{-1}
インダクタンス	ヘンリー	H	Wb/A	m^2 kg s^{-2} A^{-2}
セルシウス温度	セルシウス度[(e)]	℃		K
光束	ルーメン	lm	cd sr[(c)]	cd
照度	ルクス	lx	lm/m^2	m^{-2} cd
放射性核種の放射能[(f)]	ベクレル[(d)]	Bq		s^{-1}
吸収線量, 比エネルギー分与, カーマ	グレイ	Gy	J/kg	m^2 s^{-2}
線量当量, 周辺線量当量, 方向性線量当量, 個人線量当量	シーベルト[(g)]	Sv	J/kg	m^2 s^{-2}
酸素活性	カタール	kat		s^{-1} mol

(a)SI接頭語は固有の名称と記号を持つ組立単位と組み合わせても使用できる。しかし接頭語を付した単位はもはやコヒーレントではない。
(b)ラジアンとステラジアンは数字の１に対する単位の特別な名称で、量についての情報をつたえるために使われる。実際には、使用する時には記号rad及びsrが用いられるが、習慣として組立単位としての記号である数字の１は明示されない。
(c)測光学ではステラジアンという名称と記号srを単位の表し方の中に、そのまま維持している。
(d)ヘルツは周期現象についてのみ、ベクレルは放射性核種の統計的過程についてのみ使用される。
(e)セルシウス度はケルビンの特別な名称で、セルシウス温度を表すために使用される。セルシウス度とケルビンの単位の大きさは同一である。したがって、温度差や温度間隔を表す数値はどちらの単位で表しても同じである。
(f)放射性核種の放射能（activity referred to a radionuclide）は、しばしば誤った用語で”radioactivity”と記される。
(g)単位シーベルト（PV,2002,70,205）についてはCIPM勧告2（CI-2002）を参照。

表４．単位の中に固有の名称と記号を含むSI組立単位の例

組立量	SI 組立単位		
	名称	記号	SI 基本単位による表し方
粘度	パスカル秒	Pa s	m^{-1} kg s^{-1}
力のモーメント	ニュートンメートル	N m	m^2 kg s^{-2}
表面張力	ニュートン毎メートル	N/m	kg s^{-2}
角速度	ラジアン毎秒	rad/s	m m^{-1} s^{-1}=s^{-1}
角加速度	ラジアン毎秒毎秒	rad/s^2	m m^{-1} s^{-2}=s^{-2}
熱流密度，放射照度	ワット毎平方メートル	W/m^2	kg s^{-3}
熱容量，エントロピー	ジュール毎ケルビン	J/K	m^2 kg s^{-2} K^{-1}
比熱容量，比エントロピー	ジュール毎キログラム毎ケルビン	J/(kg K)	m^2 s^{-2} K^{-1}
比エネルギー	ジュール毎キログラム	J/kg	m^2 s^{-2}
熱伝導率	ワット毎メートル毎ケルビン	W/(m K)	m kg s^{-3} K^{-1}
体積エネルギー	ジュール毎立方メートル	J/m^3	m^{-1} kg s^{-2}
電界の強さ	ボルト毎メートル	V/m	m kg s^{-3} A^{-1}
電荷密度	クーロン毎立方メートル	C/m^3	m^{-3} sA
表面電荷	クーロン毎平方メートル	C/m^2	m^{-2} sA
電束密度，電気変位	クーロン毎平方メートル	C/m^2	m^{-2} sA
誘電率	ファラド毎メートル	F/m	m^{-3} kg^{-1} s^4 A^2
透磁率	ヘンリー毎メートル	H/m	m kg s^{-2} A^{-2}
モルエネルギー	ジュール毎モル	J/mol	m^2 kg s^{-2} mol^{-1}
モルエントロピー, モル熱容量	ジュール毎モル毎ケルビン	J/(mol K)	m^2 kg s^{-2} K^{-1} mol^{-1}
照射線量（Ｘ線及びγ線）	クーロン毎キログラム	C/kg	kg^{-1} sA
吸収線量率	グレイ毎秒	Gy/s	m^2 s^{-3}
放射強度	ワット毎ステラジアン	W/sr	m^4 m^{-2} kg s^{-3}=m^2 kg s^{-3}
放射輝度	ワット毎平方メートル毎ステラジアン	W/(m^2 sr)	m^2 m^{-2} kg s^{-3}=kg s^{-3}
酵素活性濃度	カタール毎立方メートル	kat/m^3	m^{-3} s^{-1} mol

表５．SI 接頭語

乗数	接頭語	記号	乗数	接頭語	記号
10^{24}	ヨタ	Y	10^{-1}	デシ	d
10^{21}	ゼタ	Z	10^{-2}	センチ	c
10^{18}	エクサ	E	10^{-3}	ミリ	m
10^{15}	ペタ	P	10^{-6}	マイクロ	µ
10^{12}	テラ	T	10^{-9}	ナノ	n
10^{9}	ギガ	G	10^{-12}	ピコ	p
10^{6}	メガ	M	10^{-15}	フェムト	f
10^{3}	キロ	k	10^{-18}	アト	a
10^{2}	ヘクト	h	10^{-21}	ゼプト	z
10^{1}	デカ	da	10^{-24}	ヨクト	y

表６．SIに属さないが、SIと併用される単位

名称	記号	SI 単位による値
分	min	1 min=60s
時	h	1h =60 min=3600 s
日	d	1 d=24 h=86 400 s
度	°	1°=(π/180) rad
分	’	1’=(1/60)°=(π/10800) rad
秒	”	1”=(1/60)’=(π/648000) rad
ヘクタール	ha	1ha=1hm^2=10^{4}m^2
リットル	L，l	1L=11=1dm^3=10^{3}cm^3=10^{-3}m^3
トン	t	1t=10^3 kg

表７．SIに属さないが、SIと併用される単位で、SI単位で表される数値が実験的に得られるもの

名称	記号	SI 単位で表される数値
電子ボルト	eV	1eV=1.602 176 53(14)×10^{-19}J
ダルトン	Da	1Da=1.660 538 86(28)×10^{-27}kg
統一原子質量単位	u	1u=1 Da
天文単位	ua	1ua=1.495 978 706 91(6)×10^{11}m

表８．SIに属さないが、SIと併用されるその他の単位

名称	記号	SI 単位で表される数値
バール	bar	1 bar=0.1MPa=100kPa=10^{5}Pa
水銀柱ミリメートル	mmHg	1mmHg=133.322Pa
オングストローム	Å	1 Å=0.1nm=100pm=10^{-10}m
海里	M	1 M=1852m
バーン	b	1 b=100fm^2=(10^{-12}cm)2=10^{-28}m^2
ノット	kn	1 kn=(1852/3600)m/s
ネーパ	Np	SI単位との数値的な関係は、対数量の定義に依存。
ベル	B	
デジベル	dB	

表９．固有の名称をもつCGS組立単位

名称	記号	SI 単位で表される数値
エルグ	erg	1 erg=10^{-7} J
ダイン	dyn	1 dyn=10^{-5}N
ポアズ	P	1 P=1 dyn s cm^{-2}=0.1Pa s
ストークス	St	1 St =1cm^2 s^{-1}=10^{-4}m^2 s^{-1}
スチルブ	sb	1 sb =1cd cm^{-2}=10^{4}cd m^{-2}
フォト	ph	1 ph=1cd sr cm^{-2} 10^{4}lx
ガル	Gal	1 Gal =1cm s^{-2}=10^{-2}ms^{-2}
マクスウェル	Mx	1 Mx = 1G cm^2=10^{-8}Wb
ガウス	G	1 G =1Mx cm^{-2} =10^{-4}T
エルステッド[(c)]	Oe	1 Oe ≙ (10^3/4π)A m^{-1}

(c) ３元系のCGS単位系とSIでは直接比較できないため、等号「 ≙ 」は対応関係を示すものである。

表10．SIに属さないその他の単位の例

名称	記号	SI 単位で表される数値
キュリー	Ci	1 Ci=3.7×10^{10}Bq
レントゲン	R	1 R = 2.58×10^{-4}C/kg
ラド	rad	1 rad=1cGy=10^{-2}Gy
レム	rem	1 rem=1 cSv=10^{-2}Sv
ガンマ	γ	1 γ =1 nT=10-9T
フェルミ		1フェルミ=1 fm=10-15m
メートル系カラット		1メートル系カラット = 200 mg = 2×10-4kg
トル	Torr	1 Torr = (101 325/760) Pa
標準大気圧	atm	1 atm = 101 325 Pa
カロリー	cal	1cal=4.1858J（｢15℃｣カロリー），4.1868J（｢IT｣カロリー）4.184J（｢熱化学｣カロリー）
ミクロン	µ	1 µ =1µm=10^{-6}m

（第8版，2006年改訂）

この印刷物は再生紙を使用しています